UNCLASSIFIED
SECURITY CLASSIFICATION OF THIS PAGE

AD-A265 159

(2)

REPORT DO

Form Approved
OMB No. 0704-0188

DTIC ELECTE S D A

1a. REPORT SECURITY CLASSIFICATION Unclassified	1b. RESTRICTIVE MARKINGS
2a. SECURITY CLASSIFICATION AUTHO	3. DISTRIBUTION/AVAILABILITY OF REPORT Approved for public release, distribution unlimited
2b. DECLASSIFICATION/DOWNGRADI SCHEDULE	
4. PERFORMING ORGANIZATION REP UMBER(S) FMRL TR-8	5. MONITORING ORGANIZATION REPORT NUMBER(S) AFOSR-TR-
6a. NAME OF PERFORMING ORGANIZATION Florida A&M University Dept. of Mechanical Engineer.	6b. OFFICE SYMBOL (If applicable)
7a. NAME OF MONITORING ORGANIZATION Air Force Office of Scientific Research Division of Aerospace Sciences.	
6c. ADDRESS (City, State, and ZIP Code) P.O. Box 2175 Tallahassee, Florida 32316-2175	7b. ADDRESS (City, State, and ZIP Code) Bolling AFB Washington, DC 20332-6448
8a. NAME OF FUNDING/SPONSORING ORGANIZATION AFOSR/NA Bolling AFB DC 20332-6448	8b. OFFICE SYMBOL (If applicable) NA
9. PROCUREMENT INSTRUMENT IDENTIFICATION NUMBER F49629-89-C-0014	
8c. ADDRESS (City, State, and ZIP Code) AFOSR/NA Bolling AFB DC [illegible]	10. SOURCE OF FUNDING NUMBERS PROGRAM ELEMENT NO. 61102F; PROJECT NO. 2307; TASK NO CS; WORK UNIT ACCESSION NO.

11. TITLE (Include Security Classification)

Unsteady Flow Past a NACA 0012 Airfoil Pitching at Constant Rates

12. PERSONAL AUTHOR(S)
L. Lourenco, A. Krothapalli, L. Van Dommelen, and C. Shih

13a. TYPE OF REPORT	13b. TIME COVERED	14. DATE OF REPORT (Year, Month, Day)	15. PAGE COUNT
Final	FROM 88/11/0 TO 92/10/3	93/04/13	79

16. SUPPLEMENTARY NOTATION

17. COSATI CODES		
FIELD	GROUP	SUB-GROUP

18. SUBJECT TERMS (Continue on reverse if necessary and identify by block number)

19. ABSTRACT (Continue on reverse if necessary and identify by block number)

The dynamic stall process of a NACA 0012 airfoil undergoing a constant-rate pitching up motion is studied experimentally in a water towing tank facility. This study focuses on the detailed measurement of the unsteady separated flow in the vicinity of the leading and trailing edges of the airfoil. The measurements are carried out using the Particle Image Velocimity (PIV) technique. This technique provides the two-dimensional velocity and associated vorticity fields, at various instants in time, in the mid-span of the airfoil. Near the leading edge, large vortical structures emerge as a consequence of Van Dommelen and Shen type separation and a local vorticity accumulation. The interaction of these vortices with the reversing boundary layer vorticity initiates a secondary flow separation and the formation of a secondary vortex. The mutual induction of this counter-rotating vortex pair eventually leads to the ejection process of the dynamic stall vortex from the leading edge region.

20. DISTRIBUTION/AVAILABILITY OF ABSTRACT ☐ UNCLASSIFIED/UNLIMITED ☐ SAME AS RPT ☐ DTIC USERS	21. ABSTRACT SECURITY CLASSIFICATION
22a. NAME OF RESPONSIBLE INDIVIDUAL Major Daniel FANT	22b. TELEPHONE (Include Area Code) 202-767-0471
	22c. OFFICE SYMBOL AFOSR/NA

DD Form 1473, JUN 86 — Previous editions are obsolete. — SECURITY CLASSIFICATION OF THIS PAGE

UNCLASSIFIED

UNSTEADY FLOW PAST A NACA 0012 AIRFOIL PITCHING AT CONSTANT RATES

Department of Mechanical Engineering
FAMU/FSU College of Engineering
Florida A & M University and Florida State University
P.O. Box 2175
Tallahassee, FL 32316-2175

Contract # F49620-89-C-0014

Prepared for

Air Force Office of Scientific Research
Bolling Air Force Base, Washington D.C., 20332
Final Report for the Period November 1, 1989 - October 31, 1992

Principal Investigator

Professor Luiz M. Lourenco

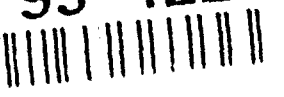

TABLE OF CONTENTS

UNSTEADY FLOW PAST A NACA 0012 AIRFOIL PITCHING AT CONSTANT RATES

ABSTRACT

The dynamic stall process of a NACA 0012 airfoil undergoing a constant-rate pitching up motion is studied experimentally in a water towing tank facility. This study focuses on the detailed measurement of the unsteady separated flow in the vicinity of the leading and trailing edges of the airfoil. The measurements are carried out using the Particle Image Velocimetry (PIV) technique. This technique provides the two-dimensional velocity and associated vorticity fields, at various instants in time, in the mid-span of the airfoil. Near the leading edge, large vortical structures emerge as a consequence of Van Dommelen and Shen type separation and a local vorticity accumulation. The interaction of these vortices with the reversing boundary layer vorticity initiates a secondary flow separation and the formation of a secondary vortex. The mutual induction of this counter-rotating vortex pair eventually leads to the ejection process of the dynamic stall vortex from the leading edge region.

1. INTRODUCTION

Modern combat aircraft frequently operate at high angles-of-attack with rapid maneuvering motions beyond the limit of the conventional flight envelope. Under these conditions, the character of the unsteady flow over a wing can be significantly different from that of a wing under a quasi-steady state motion. The departure is mainly due to the initiation of a local, unsteady boundary layer separation and its subsequent interaction with the external flow. This strong inviscid/viscous interaction eventually leads to the massive boundary layer separation and the formation of large scale vortical structures. These structures dominate the unsteady flow behavior over the wing. Since these vortices induce large suction forces on the upper surface of the wing, they are critical to the aerodynamic performance of the wing [1,2,3]. A careful management of these energetic structures can result in an effective control scheme to improve the flight envelope [4].

Having recognized these features of unsteady separation, several investigations have studied various aspects of these flows, including Visbal [5], Acharya and Metwally [6], and Lorber and Carta [7]. However, due to the lack of effective experimental and computational tools

for the study of this unsteady separated flow field, a fundamental understanding of the problem is still not available. To date, except in a few instances [8,9], most of the unsteady separated flow field measurements have employed traditional techniques, such as hot-wire, LDA, and surface pressure techniques. These single-point measurement techniques have difficulty in capturing with the required detail the overall field that evolves both in space and time, and show the interaction between the large scale vortices and the local boundary layer. In view of this, a new velocity measurement technique, the particle Image Velocimetry (PIV), has been developed in our laboratory. This whole-field technique can provide instantaneously the two-dimensional velocity and the associated vorticity fields in a selected plane of the flowfield. This technique has been successfully used in describing the dynamic stall process over a pitching-up airfoil (Shih et al. [10]). A detailed description of the PIV technique can bc found in Lourenco et al [11] and Adrian [12].

A detailed description of the unsteady flow behavior at the leading and trailing edges of an NACA 0012 airfoil undergoing a pitching-up motion is given in this paper. The instantaneous flow field was studied using the PIV technique. Experiments are conducted at different dimensionless pitch rates, α^+, normalized with the airfoil's chord and the free-stream velocity, ranging from 0.04 to 0.131. Two different Reynolds numbers, based on the chord of the airfoil, of 5,000 and 25,000 are investigated.

1.1 Unsteady Separation -- The Van Dommelen/Shen Structure

It is well known that the dynamic stall process is initiated by the unsteady boundary layer separation near the airfoil's leading edge. During rapid pitching up motion, vorticity production is greatly enhanced by the favorable pressure gradient at the leading edge. Local vorticity accumulation is accelerated by the slowdown of downstream convection process because of the local boundary layer flow reversal. This accumulation process is eventually interrupted by the sudden emergence of unsteady flow separation, which immediately releases the accumulated vorticity into the outer flow. This eruption of boundary layer vorticity triggers a sequence of spontaneous events such as the local viscous/inviscid boundary layer interaction, the formation and convection of large energetic vortices and, finally, the "stall". Therefore, in order to understand the dynamic stall process, a better physical understanding of the unsteady boundary layer separation is necessary.

A significant advance in the understanding of the unsteady separation process was made by Van Dommelen & Shen [13] who used an innovative Lagrangian approach (it will be referred to as

VDS model hereafter) to study the boundary layer separation over an impulsively started cylinder. They found no evidence of the emergence of singular behavior near the separation point as usually encountered by the traditional boundary layer analysis. This allowed them to examine in detail the evolution of the unsteady separation structure. They concluded that the strong adverse pressure gradient is the initial trigger of the onset of flow reversal along the surface. However, as the fluid particles approach the separation point, the convective terms become dominant compared to the viscous and pressure gradient terms. As a result, along the zero vorticity line, Burgers' equation dominates immediately before separation. Burgers' equation is well known because it provides a simple model of singularity formation through "wave steepening" in non-linear equation. Physically, the fastest reversing fluid particles quickly approach the slower-moving particles and create a local particle collision. Due to the restraint of the solid surface, the particles will be propelled away from the wall as a consequence of the rapid compression along the wall and "separation" occurs. Under inviscid assumption, the particles conserve vorticity, and the separation of the particles away from the wall signifies the outward distortion of the zero vorticity line. Based on the experimental results to be discussed below, we speculate that this distortion provides a **deterministic perturbation** to de-stablize the local vorticity distribution. This distortion leads to the emergence of very large vortical structures in the shear layer and a local secondary separation induced by the growing vortices. Strong inviscid/viscous interaction quickly evolves into the formation and ejection of a primary vortex from the airfoil's leading edge, and the the dynamic stall process begins.

1.2 Reynolds Number Effect

Like most boundary layer formulation, the VDS model implicitly assumes infinitely high Reynolds number for their theoretical formulation. However, the present water towing tank experiments were performed at relatively low Reynolds numbers of 5,000 and 25,000. Therefore, it is necessary to consider the effect of Reynolds number on the evolution of unsteady separation. According to VDS model, the unsteady separation is initiated by local adverse pressure gradient and later governed by the inertial effect as modelled by the Burger's equation. In other words, the onset of the unsteady separation structure is virtually inviscid and independent of the Reynolds number. As a matter of fact, it has been speculated that the generic characteristics of an unsteady separated flow are fairly universal, and independent of the Reynolds number and external flow conditions. Therefore, the results from a low Reynolds number experiment can be applied to higher Reynolds number flow conditions with confidence. On the other hand, because the effect of the Reynolds number, appreciable differences on the time and length scales of the separation structure are expected. For example, the separation structure of a low Reynolds number flow

evolves faster as compared to a high Reynolds number case (Peridier et.al [14]). Moreover, the stronger viscous diffusion of a low Reynolds number flow will thicken the boundary layer, thereby, attenuate the explosive nature of the unsteady separation. However, none of these effects are expected to alter the intrinsic behavior of the unsteady separation structure as described by Van Dommelen and Shen [13]. It is therefore concluded that it is possible to make a logical extrapolation of the present results to the much higher Reynolds number cases.

2. EXPERIMENTAL FACILITY AND INSTRUMENTATION

The experiments are performed in a water towing tank facility with dimensions of 3.4 m in length and 0.6 x 0.5 m in cross section. A computer-interfaced Anorail linear motor system is used to drive the towing carriage. This system allows for fine control of the towing velocity. In the present investigation, the Reynolds number, based upon the airfoil's chord, is varied from 5,000 to 25,000. The airfoil's pitching motion is controlled by a programmable "Klinger" stepping motor control unit. Three moving platforms, one for model-mounting, one for the rotating mirror system used to create the pulsed laser illumination, and the other for image recording, are synchronized using a gear/belt system (figure 1). All motions are controlled by a desktop IBM PS/2 model 70 computer. The pulsed laser sheet is created by means of a 24-faceted rotating mirror system. This mirror sweeps a 5 Watt Argon laser beam into a laser sheet which is projected along the mid-span of the airfoil, providing multiple particle image illumination required for the PIV image recording.

The PIV technique can be regarded as a quantitative flow visualization method that is capable of providing a two-dimensional, instantaneous velocity and vorticity fields with accuracy. Please refer to Lourenco et al [11] for a detailed description. To resolve the directional ambiguity of the velocity vector, a "velocity bias technique" is used. A uniform reference motion is added to the flow, thus superposing a velocity shift to the real flow field. A properly chosen shift can insure that all image displacements occur in the same direction, thereby eliminating the ambiguity. The true flow field can be recovered later by removing this artificial shift from the raw velocity data. In this work, a rotating mirror is used to produce the image shift. Optical and digital image processing techniques are used to convert the acquired PIV photographic records into local velocity data. This process uses a focused laser beam to interrogate a small area of the multiple exposed photographic film. The diffraction pattern produced by the coherent illumination of the correlated multiple images on the film generates Young's fringes. These fringes have an orientation that is perpendicular to the direction of the local displacement and a spacing inversely proportional to the

displacement. A fully automated PIV image processing bench, controlled by the Fluid Flow Diagnostics Mark II program is used to digitize and process the fringe images.

Metallic coated particles (TSI model 10087), with an average diameter of 11 μm, are used as the flow tracers. A phase-triggered 35 mm SLR camera (Nikon F-3) is used to record the image at a controllable rate, ranging from 1 frame/sec to a maximum rate of 6 frames/sec. Synchronization between components is accomplished using a Tektronix modular electronics system. This system also provides the phase-reference between the motion of the airfoil and the PIV photographic timing sequence (figure 2).

3. EXPERIMENTAL RESULTS AND DISCUSSION

Shih et al [10] described the overall flow field of an airfoil pitching at a constant rate. However, that study is based primarily on a single set of experiments with a Reynolds number of 5,000 and α^+ of 0.131. The present study is carried out in an improved new facility and for a larger range of testing parameters: the pitching rate is varied from 0.04 to 0.131, and at two different Reynolds numbers of 5,000 and 25,000. The general description of the global flow at different pitch rates is given in the following sections. The data reported corresponds to a Reynolds number of 5,000 unless otherwise specified.

3.1 High Pitch Rate, α^+=0.131, Global Flow Description

This case has been reported in reference 4 and no significant differences are found between the two sets of measurements, in spite of the fact that both the time and spatial resolutions are improved in the present experiments. A general description of the formation and evolution of the leading and trailing edge vortical structures and a detailed analysis of interactions of these structures with local boundary layers is given in this section. Flow development will be characterized by a sequence of PIV velocity and associated iso-vorticity fields as shown in figures 3(a)-(k).

As the airfoil pitches beyond the static stall angle angle (approximately 12 deg.), two distinct regions can be identified according to their local flow development: a trailing edge region which extends from the airfoil's midchord to the trailing edge, and a leading edge region which spans approximately the first 40% of the chord length measured from the nose. It is interesting to

note that there seems to be little interaction between the dynamic development of these two regions. Near the trailing edge, a layer of reversed flow begins to propagate upstream as the result of an increasing adverse pressure gradient imposed by the pitching-up motion. This part of the flow movement resembles that of a steady state trailing edge stall. The local boundary layer separates and forms a free vortex layer near the trailing edge. Near the midchord region, accumulation of boundary layer vorticity leads to the formation of a discrete vortex (figure 3(a)). This accumulation may be attributed to the slowdown of the downstream vorticity convection as a result of the emergence of flow reversal from the trailing edge. This vortex collects all local vorticity and convects downstream toward the airfoil's trailing edge. During the progression, as can be seen from figures 3(a) - (d), it merges with the vorticity layer near the trailing edge and coalesces into one large vortical structure (figure 3(e)). This vortex eventually pairs with the counter-rotating vortex shed from the lower surface to form a trailing edge vortex pair structure. A more detailed analysis of this trailing edge vortex system will be discussed later.

At the leading edge, clockwise vorticity is continuously generated at a rapidly increasing rate because of the imposing pressure gradient created by the pitching-up motion. Concomitantly, the downstream vorticity transport is impeded by a slowdown of the flow near the midchord as shown in figures 3(a) and 3(b). A local accumulation of the vorticity near the leading edge leads to the emergence of a leading edge vortex (figures 3(a) - (d)). The exact mechanism that leads to the formation of the vortex has not be determined yet. It is proposed that the upper part of the leading edge boundary layer forms a "free" shear layer due to the local adverse pressure gradient. This shear layer rolls up into individualized vortices as it is being perturbed by the initiation of the local unsteady boundary separation. A flow model based on the Van Dommelen/Shen unsteady separation concept is proposed in later section after the leading edge separation process is closely examined.

Initially, the leading edge vortex remains close to the surface where the downstream vorticity convection slows down due to the building up of the vortex. During this process, all the vorticity produced near the leading edge accumulates locally and there is no apparent downstream vorticity convection. The combined effect of this leading edge vorticity accumulation and the downstream convection of the midchord vortex results in the emergence of a region free from vorticity in the midchord region (figures 3(b) - (d)). The existence of this region isolates the leading edge region from the rest of the airfoil. Under the accumulated leading edge vortex, a strong flow reversal is induced due to the local adverse pressure gradient. The vortex quickly interacts with the local reversed boundary-layer fluid which leads to an upstream accumulation and eruption of reversed boundary-layer vorticity (figures 3(c) and 3(d)). This interaction initiates the

apparent ejection of the vortex from the nose region and signifies the beginning of the dynamic stall process, (figures 3(d) - (j)). This vortex interaction process will be discussed in detail later.

The ejected vortex encounters a faster convection velocity and moves more rapidly downstream as shown in figure 3(e). The boundary layer vorticity with the opposite sign has been ejected into the outer flow as shown by the presence of dotted vorticity contour lines away from the airfoil (figure 3(e)). During this convection process the vortex continues to interact with the vortical structures that are shedding off continuously from the separated leading edge shear layer. The vortex merging process involves multiple structures and is identified from the iso-vorticity field, (figures 3(f) to 3(h)). It is important to note that the dynamic stall vortex at this stage is not one coherent structure, but rather, it is a collection of several discrete vortices. The diffusive nature of the vortex implies that it is not easy, if at all possible, to control the dynamic stall vortex after it breaks away from the leading edge (figures 3(i) and 3(j)). The stall event is completed when the agglomerated vortex detaches from the trailing edge.

3.2 Unsteady Separation and the Formation of the Leading Edge Vortex, $\alpha^+=0.131$:

In this section, a detailed investigation of the unsteady flow behavior at the leading edge of the airfoil is made. In order to accurately capture the fine structures near the surface of the airfoil, the PIV data is processed with a very high spatial resolution (a physical spacing of 0.5 mm, or 0.5% chord length, in both directions). The emergence of unsteady separation up to the formation and ejection of the dynamic stall vortex, is shown with great detail in figures 4(a)-(i). The pictures cover approximately the region from the leading edge to 60% chord downstream.

As the airfoil pitches beyond its static stall angle, a strong leading edge suction pressure peak is induced by the rapidly accelerating fluid stream flowing over the nose. Downstream of the nose region up until the airfoil's trailing edge, flow reversal develops near the surface where an increasingly adverse pressure gradient dominates. However, unlike steady flow, the external flow stream continues to follow the airfoil's contour and there is no apparent "breakaway" of the boundary layer flow from its surface (figure 4(a)).

It is necessary to point out that, although there is a reversing flow layer extending from the trailing edge over the entire airfoil, the flow reversal near the leading edge and the eventual initiation of unsteady separation are essentially local flow phenomena. In other words, all

reversing fluid particles in the leading edge separation region originate locally near the leading edge region. (note: leading edge region is loosely defined as the region extending from the airfoil's nose to about 30% chord) This is in contradiction with the suggestion made by some earlier observations that the dynamic stall process is triggered by the arrival of reversing flow which originates at the trailing edge. This controversy can be resolved using a simple time/space development calculation as follows: First, assume the flow reversal starts at the instant when the airfoil approaches its static stall angle, α=10 deg., or at t^+=1.33 for this set of data. For a fluid particle that moves at an averaged reversing speed of approximately 20% of the free-stream velocity, it would have travelled for merely 27% of the chord until the time t^+=2.69 when the separation process is already initiated (figure 4(c)). Therefore, there is simply not enough time for the trailing edge flow to reach the nose region. Consequently, the trailing edge flow does not have a direct impact on the separation process. This has an important implication because it suggests that the influence from the trailing edge is an indirect one, and only through the increase of global circulation of the airfoil by shedding counter-rotating vorticity into the wake. Therefore, a local flow control such as blowing or suction in the leading edge region will be sufficient to manipulate the behavior of the flow at this stage. Any modification near the trailing edge should have no significant influence on the early development of the leading edge flow separation.

Due to the reversing flow, the upper part of the boundary layer near the trailing edge area is moved away from the surface, forming a local "free" shear layer. This shear layer is subjected to inflectional point instabilities and immediately rolls up into several large scale vortices; one of such structures can be seen near the midchord region in figure 4(b). This structure quickly convects downstream and detaches itself from the midchord region (figure 4(c)). The consequence of this departure is that it forces the leading edge shear layer to reattach and, at the same time, slows down the downstream vorticity convection from the leading edge (figures 4(b) and (c)). Basically, the leading edge region has been temporarily isolated from the direct influence of the rest of the flow field and the subsequent evolution is predominantly controlled by the emergence of local boundary layer separation and the resulting vorticity dynamics.

3.3 Initiation of the Unsteady Separation

The leading edge boundary layer is propelled away from the airfoil's surface by the reversing fluid layer near the surface which is driven by the adverse pressure gradient. Unlike steady separation, the outer flow remains unaffected by the flow reversal and continues to follow the airfoil's contour. Consequently, a local "free" shear layer emerges between the displaced leading edge boundary layer and the reversing fluid layer. This shear layer can then be subjected to

inflectional instability and leads to the generation and growth of individualized vortical structures (figures 4(a) and (b)). Before the onset of unsteady separation, these structures are small with a scale comparable to the local shear layer thickness. However, under the influence of the increasing adverse pressure gradient, the local reversing flow begins to accelerate rapidly inside the leading edge region. This leads to the emergence of a VDS interaction such that the fastest reversing particles quickly approaches and, eventually, collides with the slower-moving particles ahead of them. This collision takes place along the zero vorticity line as indicated by the interface between solid(clockwise) and dotted(counterclockwise) iso-vorticity lines. This collision results in a local movement of the particles away from the wall and as a consequence the local zero vorticity interface is displaced away from the wall. This vorticity line distortion initiates the separation process (figures 4(b) - (e)), and appears to agree well with van Dommelen and Shen's model.

Unlike the traditional shear layer instability mechanism which selectively amplifies random perturbations in the initial region to develop into organized vortical structures, the deformation triggered by the VDS interaction provides a **deterministic perturbation** to the local vorticity distribution (see figure 5 for a conceptual description of this process). The upward displacement of counter-clockwise vorticity into the outer shear layer, where clockwise vorticity dominates, makes the local vorticity arrangement highly unstable. Under their mutual induction, the interfaces between regions of concentrated vorticity of opposite sign quickly undergo further self-induced deformation. The downstream interface stretches into a peak while the upstream interface develops into a valley as shown in figure 5. Eventually, this spontaneous deformation evolves into a spike-like eruption which propels more counter-rotating vorticity into the external flow stream. This narrow-band eruption is consistent with the terminal boundary layer structure as predicted by the VDS interaction [15]. It is noted that, although the onset of VDS interaction is fairly deterministic, but a simple definition for its timing, location and physical scale is not possible. They are usually determined by many parameters, such as the Reynolds number, dimensionless pitch rate, airfoil's nose shape, Mach number, etc. However, for a given set of flow conditions, this distortion is well defined and predictable. For a detailed discussion of the unsteady separation process please refer to Van Dommelen [15]. Since the emergence of this perturbation is deterministic, therefore, it is possible to control the separation process by proper management of this local interaction.

Immediately after the distortion of the zero vorticity line, discrete vortical structures evolve very quickly. During the short period of time spanning from the appearance of the first individualized structure in the shear layer(figure 4(a)) to the emergence of the dynamic stall vortex (figure 4(h)), the size of the shear layer vortex increases dramatically. For an example, as shown in figure 4(b), four of the leading edge shear vortices appear to undergo a collective merging

process and coalesce into a much large structure as shown in figure 4(c). This extraordinarily rapid growth can not be explained by the typical Kelvin-Helmoholtz type instability mechanism. Two possible models are suggested: (1) The zero vorticity line distortion triggered by the VDS interaction provides a strong perturbation with a wavelength much longer than the local shear layer thickness. This distortion displaces the shear layer into an unstable arrangement so that many shear layer vortices can undergo merging through mutual induction and eventually form a large vortical structure. Similar nonlinear instability mechanism has been referred to as "collective interaction" by Ho & Nosseir [16] in their study of an impinging jet in self-sustained oscillation. They found that the collective interaction always leads to higher spreading rate of the shear layer and the formation of a large coherent structure. (2) During separation, the instantaneous, reversing boundary layer flow (U_r) can be as high as 50% of the outer shear layer velocity (U_s). The local shear layer velocity ratio, defined as $(U_s-U_r)/(U_s+U_r)$, can be more than 3. This value well exceeds the critical ratio of 1.315 for the theoretical transition of shear layer instability from convective to absolute mode (Huerre and Monkewitz [17]). Therefore, the local shear layer can become self-excited at a discrete frequency with higher amplification. In the present case, the VDS interaction provides the initial perturbation and the shear layer undergoes self-excited oscillations. Consequently, the shear layer vorticity quickly coalesces into large structure and leads to the formation of the dynamic stall vortex.

Both models appear to be able to explain the relatively high growth rate of the separated leading edge shear layer and the formation of the dynamic stall vortex. It is also possible that these two mechanisms are complementary to each other. More detailed study is necessary to confirm the validity of these suggestions.

3.4 Secondary Separation and Vortex Interaction

During separation process, clockwise vorticity is continuously being generated at the airfoil's nose and being fed into the separating shear layer, resulting in further accumulation of vorticity and the strengthening of the primary vortex. This agglomeration process slows down the vorticity convection and induces flow attachment downstream of the leading edge region, (figures 4(b) - (d)). Near the airfoil's midchord, a vortex convects towards the trailing edge region which will eventually couple with a trailing edge vortex shed from the lower surface to form the trailing edge vortex pair. This interaction will be described in a later section.

At the next instant, figure 4(d), under the influence of the primary vortex, the reversing flow also separates from the surface and develops into another "free" shear layer, carrying vorticity

of counterclockwise sense. This shear layer quickly rolls into a secondary vortical structure, (figures 4(d) - (g)). In the meantime, the primary vortex continues to grow in size and strength, and a counter-rotating vortex pair is formed (figure 4(g)). The secondary vortex is smaller with a circulation that is 35% of the primary vortex at this instant. However, the secondary vortex is much more compact in size and actually, has a relatively higher vorticity concentration. Therefore, the secondary vortex is able to move the primary vortex upward away from the surface where it encounters a faster convection velocity and moves rapidly downstream, initiating the dynamic stall process. On the other hand, the primary vortex also imposes strong interaction on the secondary structure which eventually leads to the eruption of the reversed boundary layer into a spike-like structure. This eruption of counterclockwise vorticity cuts off the supply of vorticity from the leading edge shear layer into the primary vortex (figures 4(g) - (i)). Consequently, the dynamic stall vortex is formed and begins to move away from the leading edge area. This type of strong inviscid/viscous interaction is a generic characteristic of unsteady separated flow as suggested by Shih et. al.[10], Ho and Didden [18], and Smith and Walker [19].

3.5 Vortex Dynamics

In order to examine the dynamics of the leading edge separated vortex, the identity of each individual vortical structure has to be clearly defined. This is not easy since the vortical structure is not completely separated from the leading edge shear layer until very late during the vortex formation stage (figure 4). Therefore, a subjective identification is inevitable. From the vorticity contour plots, it is always possible to visually identify a vortex as the region where highly-concentrated vorticity is enclosed by closed iso-vorticity contour lines. Use figure 4(f) as an example, where the vortex can be identified as the region enclosed by the box. If one accepts the concentrated vorticity region as a vortex, then the strength of this vortex is determined by its circulation, $\Gamma = \int \omega dA$, where the integration is taken inside the enclosed area and ω is the vorticity. This is a measure of the instantaneous strength of the vortex. A low threshold vorticity integration limit of 5% of the local maximum vorticity level is chosen to eliminate the influence from the background and the reversed vorticity region. The convecting motion of the vortex can be characterized by examining its velocity of convection. The convection velocity of the vortex is defined as the averaged velocity of the integrated vorticity carried by the vortex, that is,

$$u_c = \frac{1}{\Gamma} \int u\omega dA, \text{ and } v_c = \frac{1}{\Gamma} \int v\omega dA,$$

where u_c and v_c are calculated in a reference frame moving with the airfoil. u_c measures the downstream convection velocity of the vortex, v_c measures the normal velocity of the vortex relative to the airfoil's surface. The evolution and interaction of the leading edge vortex system can be studied by following the development of the strength and convection speed of the primary vortical structure by integrating the vorticity data from figures 4(b) to (i).

Figure 6(a) shows the variation of the circulation of the leading edge vortex. While there is no distinguishable primary vortical structure in figure 4(b) when $t^+ = 2.52$, the integration of the circulation of the four small structures inside the shear layer is included for comparison. The collective circulation of these four vortices is calculated to be approximately equal to the circulation of the primary vortex at the next instant, $t^+ = 2.69$, when it first emerges. This confirms our previous observation that the formation of the vortex results from the collective merging of the vortices inside the shear layer. From the development of the circulation data, the growth of the primary vortex can be separated into two stages. During the first stage, the strength of the primary vortex increases immediately after the initiation of the unsteady separation structure (figures 4(b)-(e), $t^+ = 2.52 - 3.03$). It is believed that the strong nonlinear instability development of the separated shear layer is responsible for the growth of the primary vortex during this stage. As a consequence of the intrusion of the reversed boundary layer vorticity into the outer shear layer, another large scale vortex develops upstream of the separation structure. During this period, the separated shear layer continues to feed vorticity into these two structures. However, there is no significant interaction between these vortices during this stage. The second stage starts when these two structures begin to interact. Under their mutual induction, these two vortices roll around each other and eventual merge into one single vortex (figures 4(e)-(h), $t^+ = 3.03 - 3.54$). It can be seen that, at the same time, this strong interaction forces the eruption of the reversed boundary layer into a strong counter-rotating secondary structure (figure 4(g)). This secondary structure has a circulation that is 35% of the primary vortex at this time. However, due to its compactness, the local vorticity concentration is actually higher than that of the primary vortex. Consequently, under its induction, the primary vortex is displaced away from the surface and starts to convect downstream. During the second stage, the circulation of the primary vortex increases with a high rate as a result of this large scale merging process.

This two-stage evolution can also be identified from the measurement of the vortex convection velocity as presented in figures 6(b) and (c). During the first stage, the primary vortex convects downstream at an almost constant velocity, u_c, of 36% of the free-stream velocity. During the same period, the vortex seems to move gradually toward the surface as indicated by the negative value of the normal convection velocity, v_c. The second stage starts with a sudden

decrease of the downstream convection velocity. As discussed before, two large scale vortices are undergoing a merging process. As they roll around with respect to each other, their collective convection velocity decreases significantly. As a matter of fact, the merging vortex system becomes virtually standing still at one instant, t^+=3.36. The merging of these two structures increases considerably the strength of the primary vortex and, correspondingly, prompts the accumulation of the secondary vortex. Moments later, t^+=3.53, the newly-formed vortex is ejected away from the airfoil surface because of the induction from the secondary vortex. This upward movement can be characterized by the sudden increase of the normal convection velocity of the primary vortex (figure 6(c)). As a result of this outward motion, the vortex is moved further into the free-stream where it experiences the faster downstream convection. The instantaneous convection velocity of the vortex is suddenly increased to as high as 50% of the free-stream velocity. At the same time, the ejection of the secondary vortex into a spike-like structure cuts off the primary vortex from the leading edge shear layer and completes the formation of the dynamic stall vortex.

3.6 Implication of Flow Control

It is certainly more difficult to devise an effective scheme to manipulate this energetic structure after it moves away from the leading edge than at its early stage of development. Therefore it is reasonable to assume that the stage most accessible to manipulation would be the vortex formation process as described in the previous section. Among all, the existence of a deterministic VDS interaction suggests the possibility of controlling the separation process in a well-defined fashion. It is suggested that if one can delay or remove the particle collision process at the onset of the separation, then the formation of the large scale separated structures and their subsequent evolution can be delayed or, eliminated. On the other hand, the strong interaction between the primary vortex and the secondary separated vortex seems to be another promising candidate from the viewpoint of effective flow control. The numerical simulation, based upon the point vortex method, has been developed to examine the possibility of controlling the leading edge separated flow [20]. The preliminary results show that the ejection of the leading edge vortex can be delayed significantly by applying flow suction at the leading edge region. It is believed that, through suction, the reversing flow under the vortex is kept close to the surface, which either delays or eliminates the eruption of the VDS type separation. Without this perturbation, the nonlinear instability mechanism that leads to the formation of the primary vortex can not be initiated. At the same time, this modification also prevents the emergence of the secondary separation and the highly unstable counter-rotating vortex pair arrangement. Consequently, the stall process can be delayed.

3.7 Trailing Edge Flow, $\alpha^+=0.131$

The role that the trailing edge plays during the initial vortex formation has been shown in the previous section to be not important, especially for cases corresponding to high pitch rates. However, through continuously shedding of counter-rotating vorticity into the wake, the trailing edge has an indirect but considerable influence on the the global flow dynamics, that is, it can increase the overall circulation around the airfoil. This circulation increase results in more vorticity accumulation near the leading edge which eventually leads to the formation of stronger vortices. On the other hand, at later stages of the dynamic stall, the influence of the trailing edge flow may be significant on the dynamics of the primary vortex.

The onset of the trailing edge separation can be seen as the upper boundary layer flow separates and accumulates into discrete vortices (figures 7(a) and (b)). Two of these structures can be observed to undergo a merging process into one single vortex (figures 7(c) and (d)). This local accumulation increases the shedding of counter-clockwise trailing edge vorticity from the lower surface, which gradually coalesces into a vortex rotating in opposite sense. The upper surface shear layer vortex interacts with the reversed trailing edge vortex to form a counter-rotating vortex pair as shown in figure 7(d). These two counter-rotating vortices have comparable strength (their difference is less than 10 %). Consequently, the mutual downward induction from these two vortices can stabilize the vortex pair and slow down its breakaway from the trailing edge (figures 7(c)-(e)). On the other hand, because of their individual strength (approximately 30% of the primary vortex) it is possible that the trailing edge vortex system can play an important role in influencing the dynamic stall process.

At later stage during the stall process, as the primary vortex is approaching the trailing edge of the airfoil, strong flow reversal prevails along the upper surface (figures 8(a) and (b)). When the dynamic stall reaches the trailing edge, it induces a local suction pressure which drives the lower surface separating layer across the wake into the upper surface. This lower surface shear layer vorticity quickly rolls into an intense counterclockwise vortex (figures 8(c) and (d)). This emergence of this vortex signifies the completion of the dynamic stall process and the subsequent sudden loss of vortex lift as the dynamic stall vortex is departing from the trailing edge. From the integrated flow control point of view, the shedding of a strong vortex can be detected through surface probe at the trailing edge and be utilized as a warning signature for the flow management system.

3.8 Lower Pitch Rate, α^+=0.08, Global flow description

At a lower pitch rate, α^+=0.08, the global flow behaves significantly different from the higher pitch rate case. The first leading edge vortex appears at a much lower angle of attack, (figure 9(a)) at 14.8 deg. For identification purposes, this vortex is labeled as leading edge vortex number one, LE1. At the same time, two discrete vortices, one at the midchord and the other located at the trailing edge region, emerge and will be denoted as TE1 and TE2, respectively. These two structures form as a result of accumulation of local boundary layer vorticity via the Kelvin-Helmoholtz instability. They will eventually convect downstream and detach from the trailing edge. At this time, the outer flow appears to follow closely the airfoil's contour with no apparent breakaway.

Unlike the higher pitch rate case, the LE1 vortex immediately breaks away from the leading edge which triggers the reattachment of the leading edge separated shear layer and the formation of another leading edge vortex, LE2, (figure 9(b)). The second leading edge vortex convects quickly away from the leading edge as shown from figures 9(b), (c) & (d). This breakaway/reattachment process continues for several cycles, (figures 9(c) to 9(g)), releasing three additional vortices, denoted as LE3, LE4 and LE5, from the leading edge region. As a result, there is an array of vortices traveling along the airfoil's surface. During this progression, strong interaction between vortices can be seen; for example, two vortices, LE1 and LE2, merge into one structure as shown from figures 9(e) to 9(g). These structures remain close to the surface, and have relatively little influence on the outer flow behavior until α = 20.5 deg. Each time the breakaway vortex appears to be stronger than the previously forward vortex. For α > 20.5 deg., vortex LE3 breaks away from the leading edge and merge with vortices LE4 and LE5 (figures 9(h) and 9(i)). This integrated structure appears to behave like the dynamic-stall vortex as discussed in the higher pitch rate case. This vortex eventually convects downstream and complete the stall process. The continuous release of vortices from the leading edge region tends to weaken the dynamic-stall vortex and reduce its later influence on the global flow dynamics.

3.9 Quasi-Periodic Leading Edge Separation/Reattachment, α^+=0.08:

In this section, the quasi-periodic leading edge separation/reattachment process for the low pitch rate case will be examined more closely. As the boundary layer first separates from the nose region, as shown in figure 10(a), several large scale structures evolve as a consequence of shear

layer instability as discussed in the previous section. The reversed boundary layer vorticity starts to accumulate under the influence of the vortices. Similar to the higher pitch rate case, the reversed boundary layer separates from the surface, forming a secondary separating shear layer which quickly rolls into a counter-rotating vortex, (figure 10(b)). Due to mutual induction of the two vortices of opposite sense, the reversed vorticity layer erupts out of the surface, forcing the release of a vortex from the upper shear layer. However, unlike the higher pitch rate case, the shear layer does not detach completely from the surface. Instead, it reattaches to the surface as shown in figure 10(c). At the next instant, the first detached vortex begins to move away from the region and another vortex emerges at the end of the reattached shear layer as shown in figure 10(d). As the second vortex grows in strength, a similar vortex/reversed boundary layer interaction develops and the cycle repeats itself, (figure 10(e)). This separation/reattachment process is important since it releases excessive vorticity from the leading edge region without triggering a complete breakdown of the flow field. As a result, the dynamic stall vortex is weaker with a less devastating effect on the flow dynamics as it convects along the airfoil's surface.

3.10 Higher Reynolds Number, R_e=25,000, Global Flow Description

To examine the effect of Reynolds number, a set of experiments with a higher Reynolds number of 25,000, while keeping all other parameters unchanged, was performed. In general, the features observed appear to be quite similar. For comparison, a typical case with a dimensionless pitch rate of 0.131 is presented. As the angle of attack increased well beyond static stall angle, a leading edge dynamic stall vortex first emerges near the airfoil nose region. Due to the higher Reynolds number, this structure stays much closer to the surface as compared to the previous case. As expected, it undergoes a similar viscous/inviscid interaction process as discussed in the earlier section. Also, the location where the vortex first emerges is much closer to the airfoil's nose as compared to its low Reynolds number counterpart. This vortex moves away and convects out of the leading edge area as shown in figure 11(a). This vortex continues to grow in size through viscous diffusion and vortex merging mechanism, see the sequence from figures 11(b) to 11(d). No significant differences can be found concerning the formation, convection of the leading edge dynamic stall vortex. This observation is consistent with the common presumption that the vortex dynamics of an unsteady airfoil is insensitive to the variation of the Reynolds number. However, the trailing edge flow is different since the counter-rotating vortex pair in the trailing edge region does not exist for the higher Reynolds number case.

4. SUMMARY:

The flow past an airfoil pitching at a constant rate is studied in a water towing tank facility. Instantaneous velocity and associated out-of-plane vorticity fields were measured using the whole-field PIV technique. Special emphasis has been placed on the study of flow structure near the airfoil's leading and trailing edge regions. At a dimensionless pitch rate of 0.131, leading edge vortex develops as the airfoil pitches well beyond the static stall angle. Strong inviscid/viscous interaction between the vortex and the reversed boundary layer leads to a secondary separation and the formation of a reversed vortex. The mutual induction of the counter-rotating vortex pair triggers the breakaway of the vortex from the leading edge, at the same time, initiating the dynamic stall process. The evolution of the vortex dominate the later flow behavior. For a lower pitch rate of 0.08, the leading edge separating shear layer undergoes a quasi-steady separation/reattachment process, which generates an array of discrete vortices along the airfoil's surface. Finally, no significant difference of the formation, convection of the leading edge vortex can be found when comparing two cases with Reynolds numbers of 5,000 and 25,000, respectively.

5. Acknowledgements

The authors wish to thank Mr. S. Shankar and Mr. Z. Ding for their contribution to the PIV data collection and analysis. This work is supported by the Air Force Office of Scientific Research under contract AFOSR F49620-89-C0014.

6. REFERENCES:

1. McCroskey, W.J., "Unsteady Airfoils," Ann. Rev. Fluid Mech., Vol. 11, 1982, pp 285-311.

2. Carr, L.W., "Progress in Analysis and Prediction of Dynamic Stall," Journal of Aircraft, Vol. 25, No. 1, pp. 6-17, January 1988.

3. Ericsson, L.E. and Reding, J.P., "Fluid Dynamics of Unsteady Separated Flow, Part II, Lifting Surfaces," Prog. Aero. Sci., 24, pp. 249-356, 1987.

4. Herbst, W.B., "Supermaneuverability," Proceedings of Workshop on Unsteady Separated Flow, Colorado Spring, pp. 1-9, Aug. 10-11, 1983, eds. Francis & Luttges, 1984.

5. Visbal, M., "Dynamic Stall of a Constant-Rate Pitching Airfoil," J. of Aircraft, Vol. 27, NO. 5, pp. 400-407, May 1990.

6. Acharya, M. and Metwally, M.H., "Unsteady Pressure Field and Velocity Production over a Pitching Airfoil," AIAA Journal, Vol. 30, No. 2, pp. 403-411, Feb. 1992.

7. Lorber, P.F., and Carta, F.O., "Airfoil Dynamics Stall at Constant Pitch Rate and High Reynolds Number," Vo. 25, No. ?, pp. 548-556, June 1988.

8. Lee, G., Buell, D.A., Licurisi, J.P., and Craig, J.E., "Laser Holographic Interferometry for an Unsteady Airfoil Undergoing Dynamic Stall," AIAA Journal, Vol. 22, No. 4, pp. 504-511, April 1984.

9. Chandrasekhara, M.S., and Carr, L.W., "Flow Visualization Studies of the Mach Number Effects on Dynamic Stall of an Oscillating Airfoil," Journal of Aircraft, Vol. 27, pp. 316-522, June 1990.

10. Shih, C., Lourenco, L., Van Dommelen, L., and Krothapalli A., "Unsteady Flow Past an Airfoil Pitching at a Constant Rate," AIAA Journal, Vol. 20, No. 5, May 1992, pp. 1153-1161.

11. Lourenco, L. and Krothapalli, A. and Smith, C.A., "Particle Image Velocimetry," Lecture Notes in Engineering: Advances in Fluid Mechanics Measurements, ed. Gad-el-Hak, M., 1989, pp. 128-199.

12. Adrian, R.J., "Particle-Imaging Techniques for Experimental Fluid Mechanics," Annu. Rev. Fluid Mech. 23, pp. 261-304, 1991.

13. Van Dommelen, L. and Shen, S.F., "The Spontaneous Generation of the Singularity in a Separating Laminar Boundary Layer," Journal of Computational Physics, Vol. 38, pp.125-140, 1980

14. Peridier. V.J., Smith, F.T., and Walker, J.D.A., "Vortex-Induced Boundary-Layer Separation. Part 2. Unsteady Interacting Boundary-Layer Theory," J. Fluid Mechanics, 232, pp. 133-165, 1991.

15. Van Dommelen, L.L., "Lagrangian Description of Unsteady Separation," Lectures in Applied Mathematics, Vol. 28, pp. 701-718, 1991.

16. Ho, C.-M., and Nosseir, N.S., "Dynamics of an Impinging Jet. Part 1. The Feedback Phenomenon," J. Fluid Mechanics, 105, pp. 119-142, 1981.

17. Huerre, P. and Monkewitz, P.A., "Local and Global Instabilities in Spatially Developing Flows," Annu. Rev. Fluid Mech. Vol. 22, pp. 473-537, 1990.

18. Didden, N. and Ho, C.M., "Unsteady Separation in a Boundary Layer Produced by an Impinging Jet," J. Fluid Mechanics, 160, pp. 235-256, 1985.

19. Smith, C.R. and Walker, J.D.A., "Some Aspects of Unsteady Separation," Proceedings of the NASA/AFOSR/ARO Workshop on the Physics of Forced Unsteady Separation, NASA Ames Research Center, Moffett, CA, 1990.

20. Van Dommelen, L., private communication 1993.

Appendix I: Figures

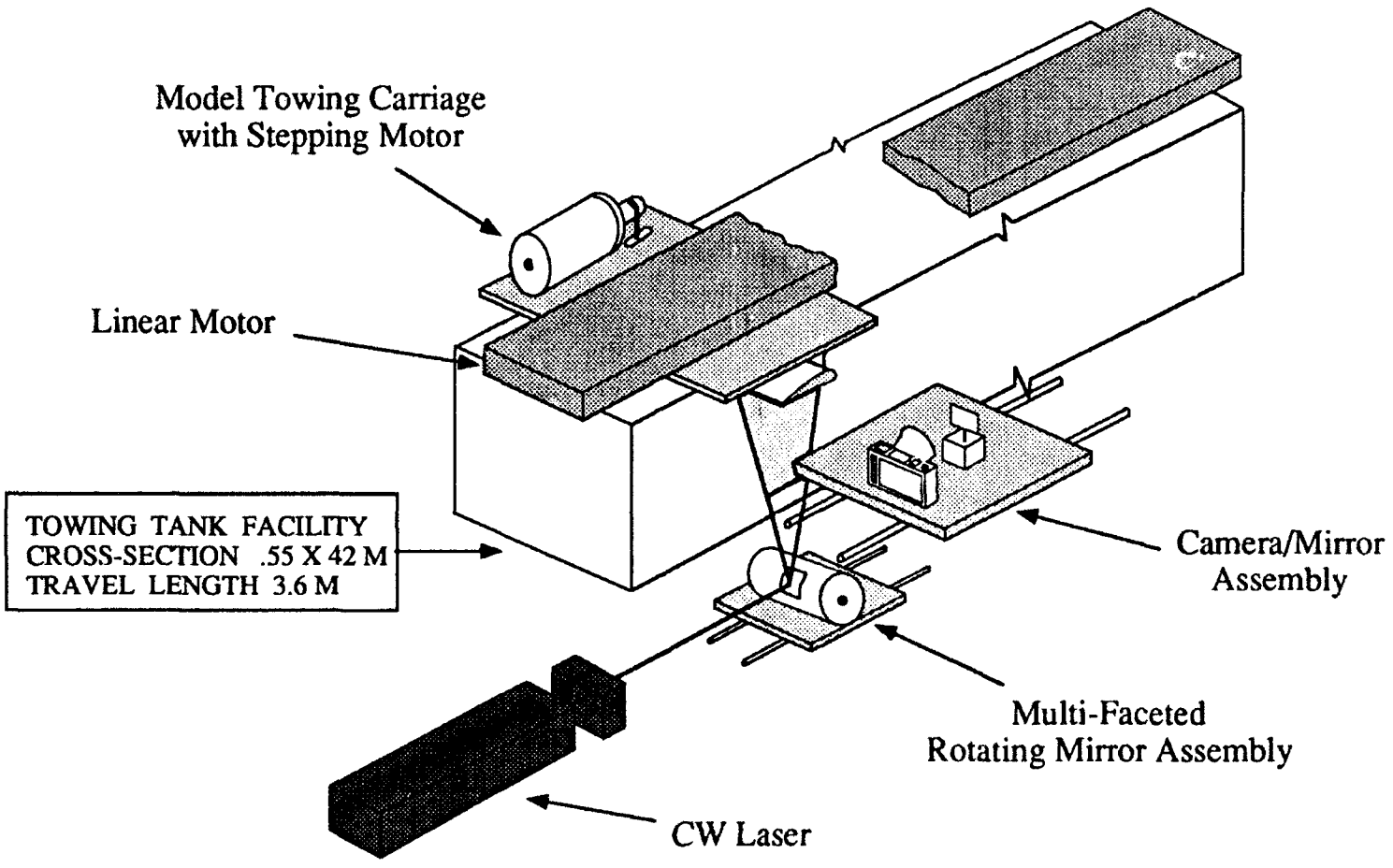

Figure 1 Schematic sketch of the towing tnk and the PIV facility

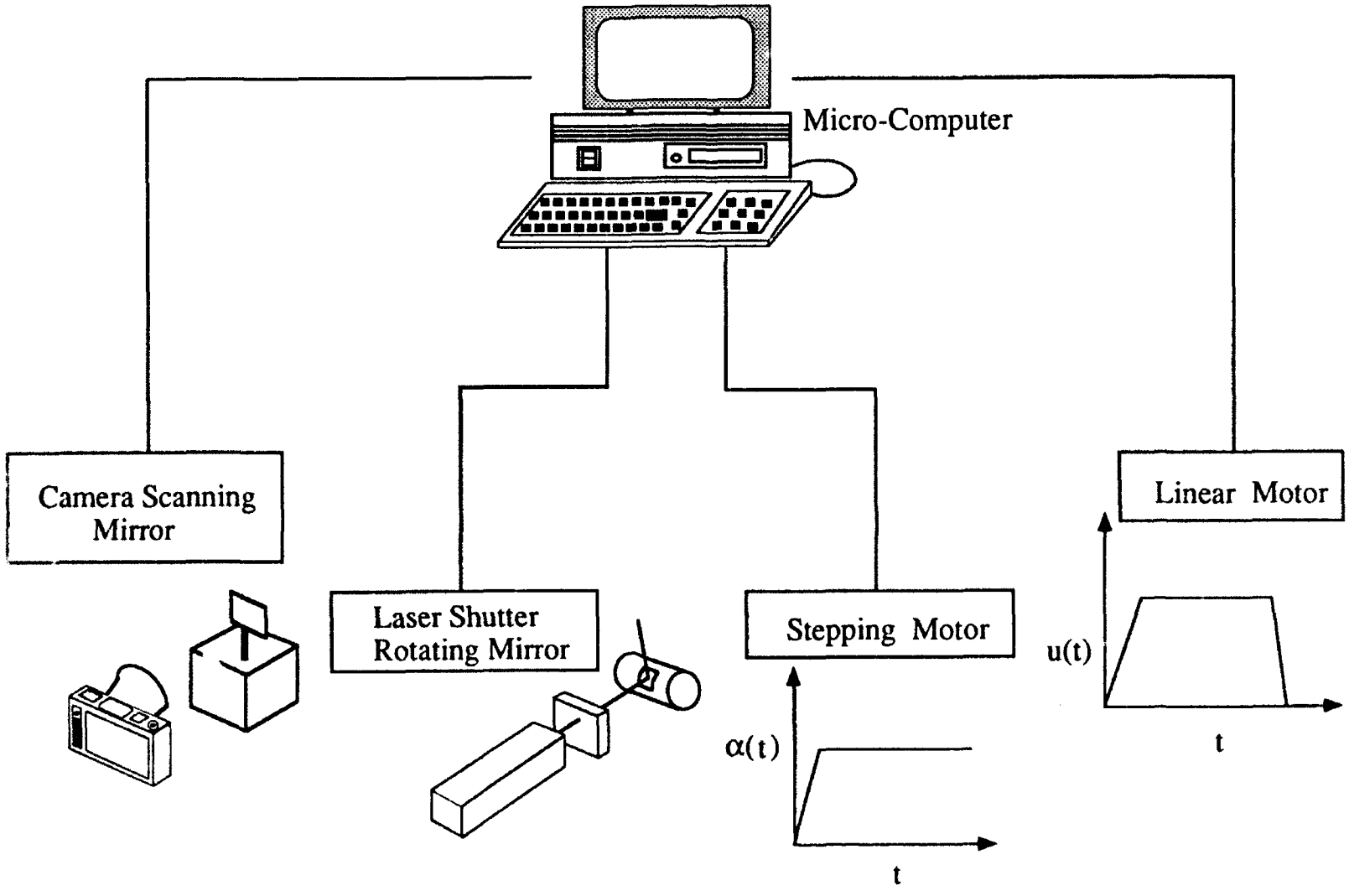

Figure 2 Control system of the towing tank and PIV image acquisition

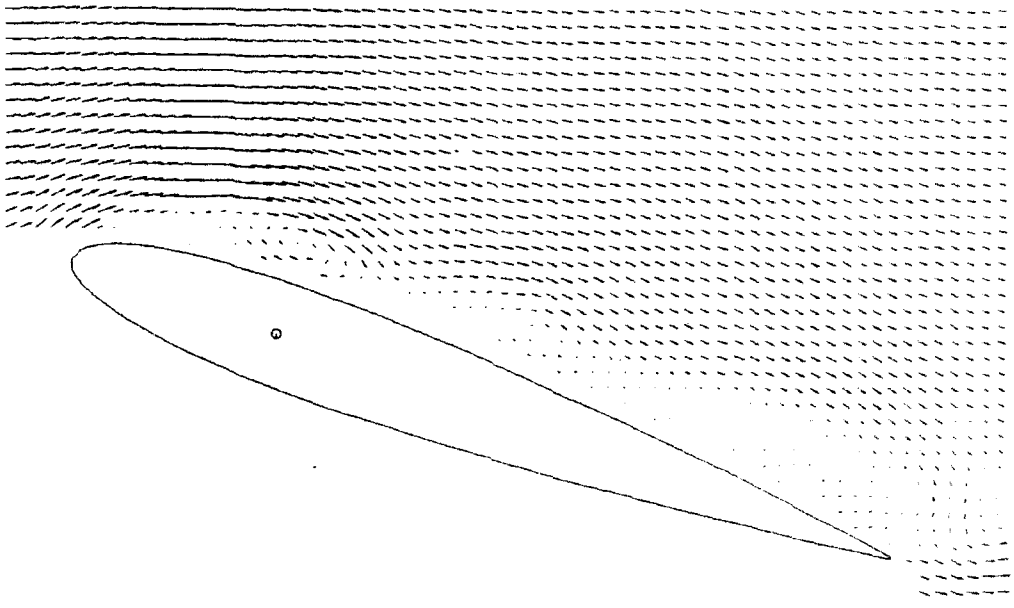

Instantaneous Velocity

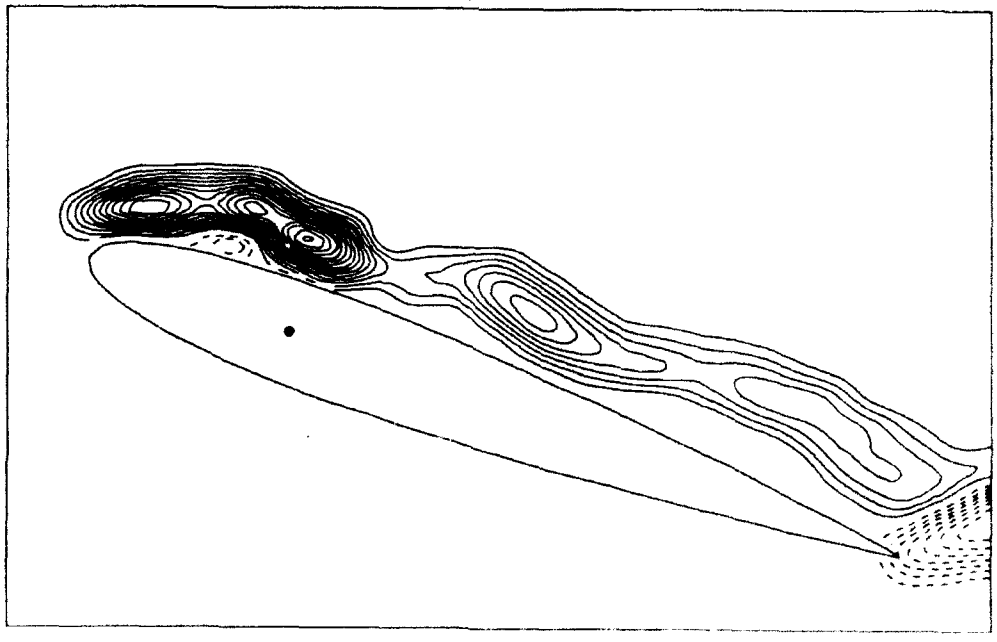

Instantaneous Vorticity

(a) $t^+=2.85$, $\alpha=21.3^\circ$

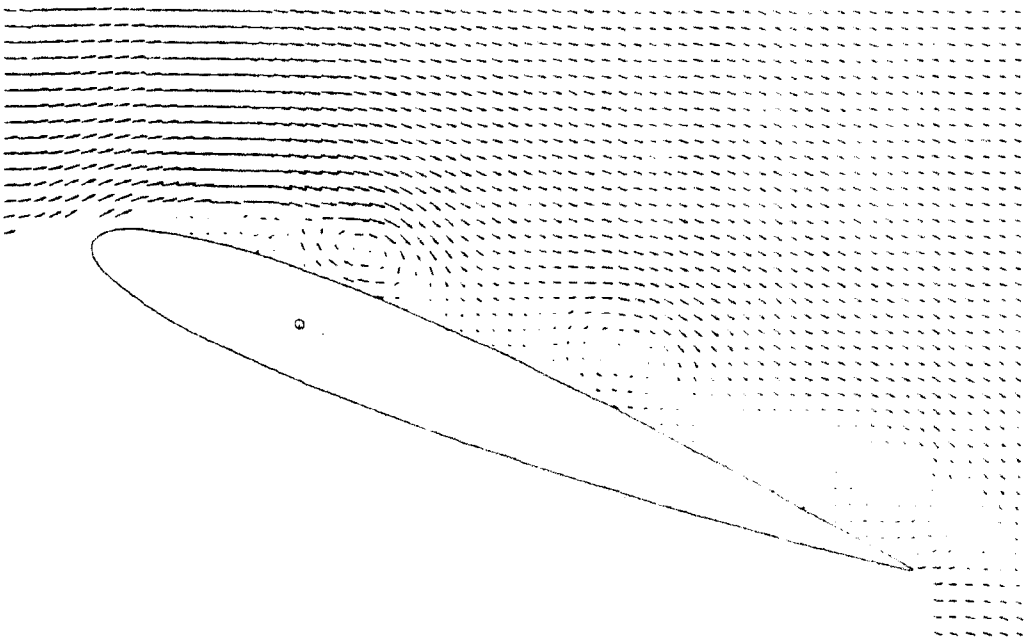

Instantaneous Velocity

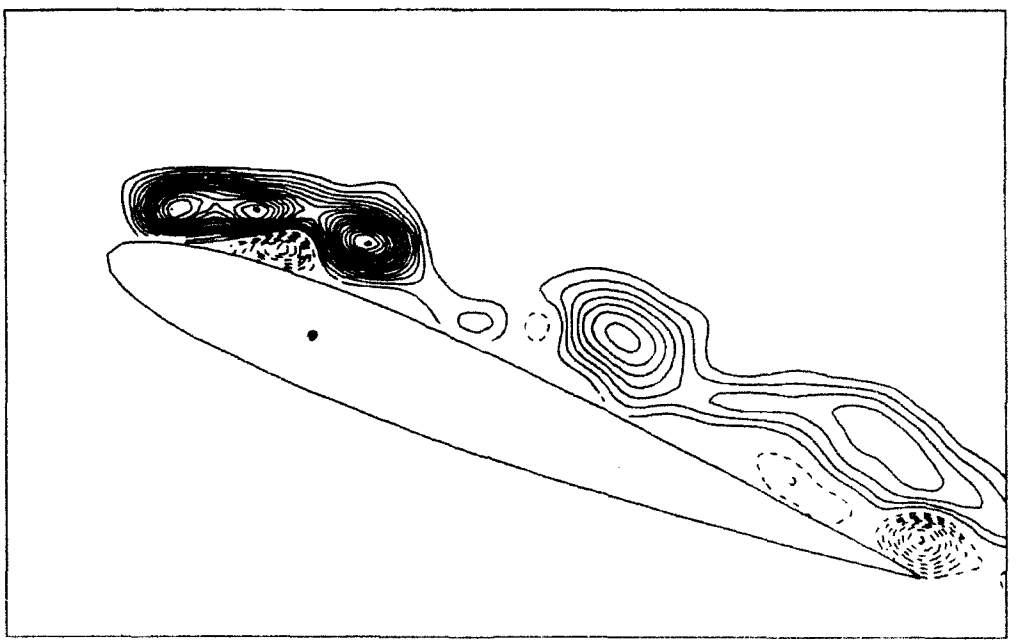

Instantaneous Vorticity

(b) $t^+=3.02$, $\alpha=22.6^\circ$

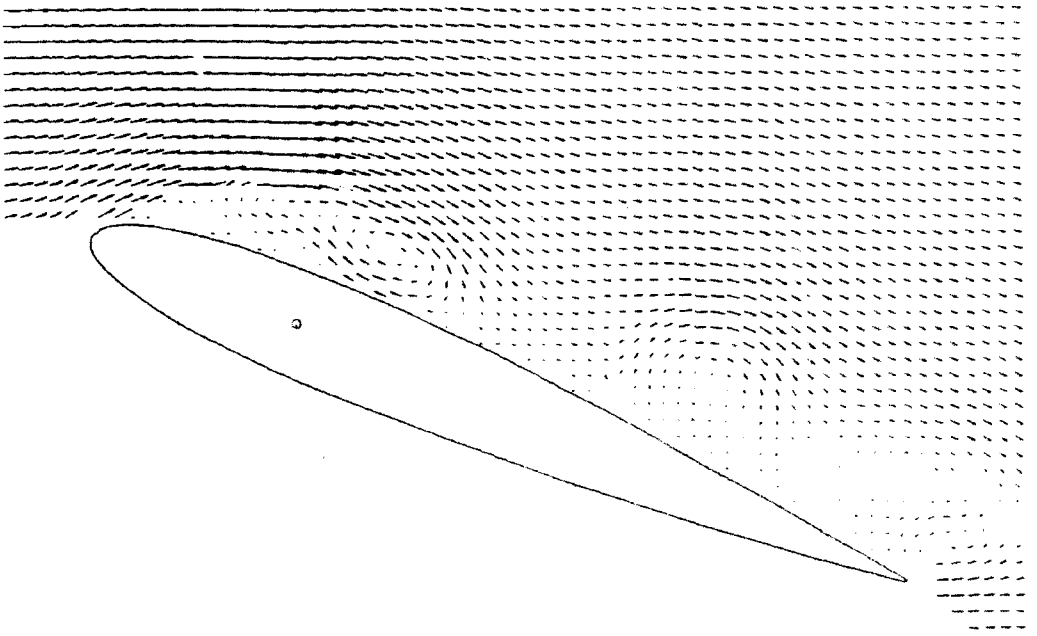

Instantaneous Velocity

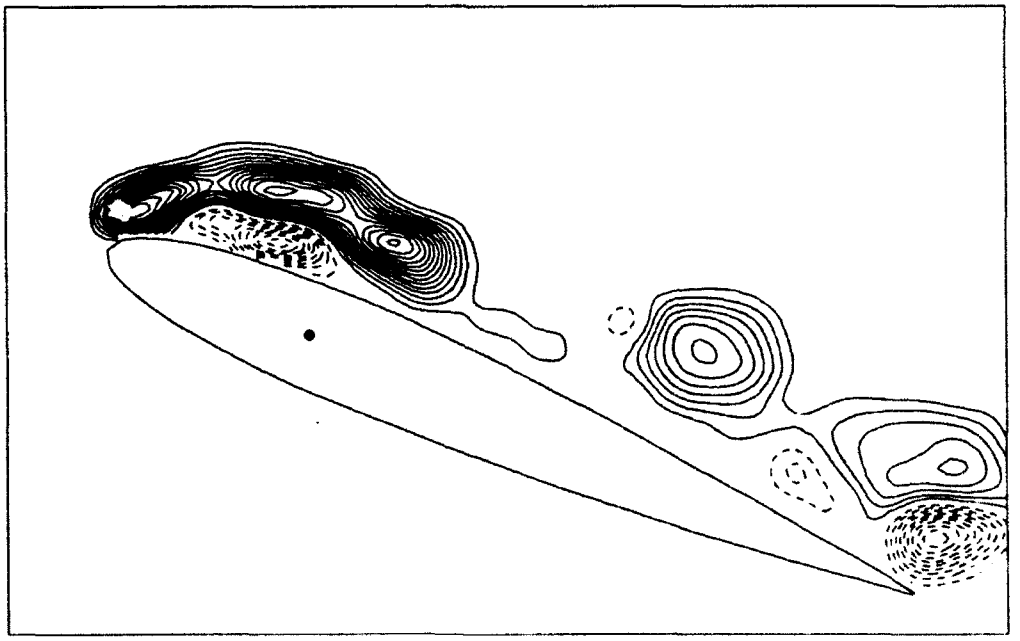

Instantaneous Vorticity

(c) $t^+=3.19$, $\alpha=23.9^\circ$

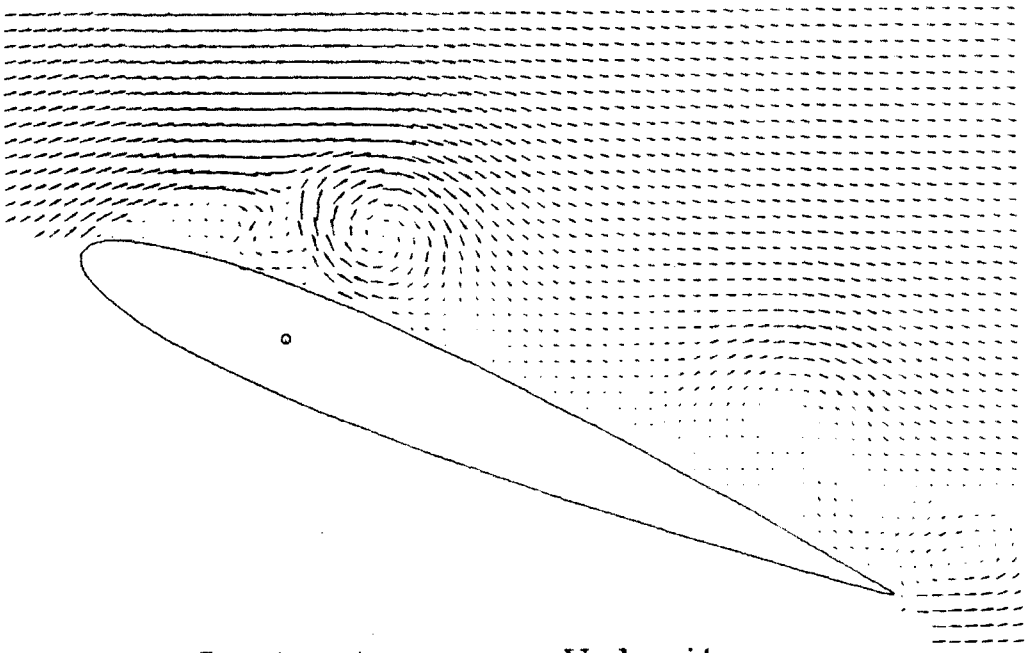

Instantaneous Velocity

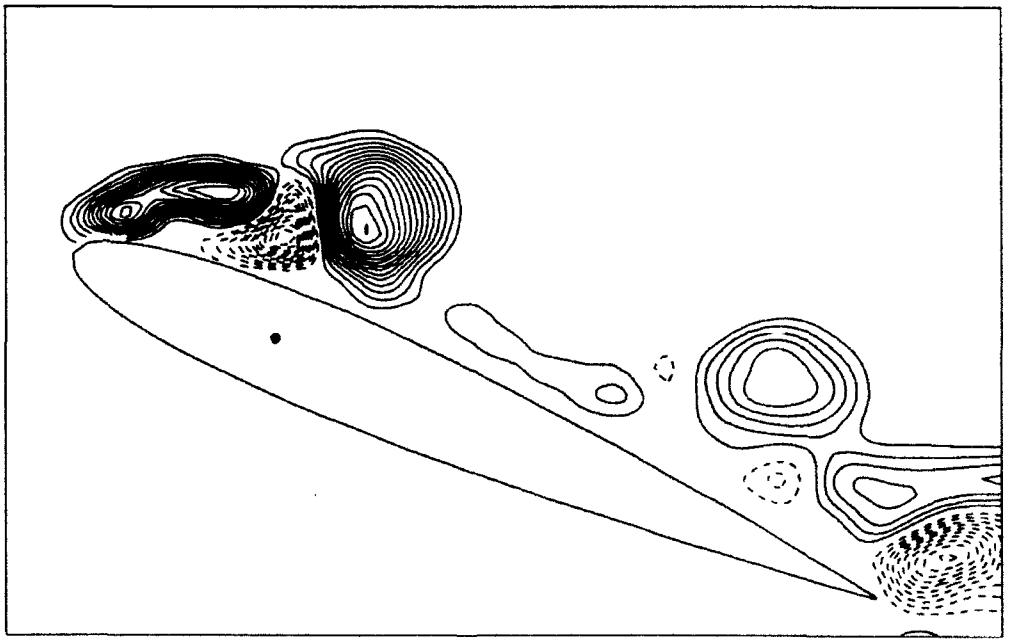

Instantaneous Vorticity

(d) $t^+=3.36$, $\alpha=25.2^o$

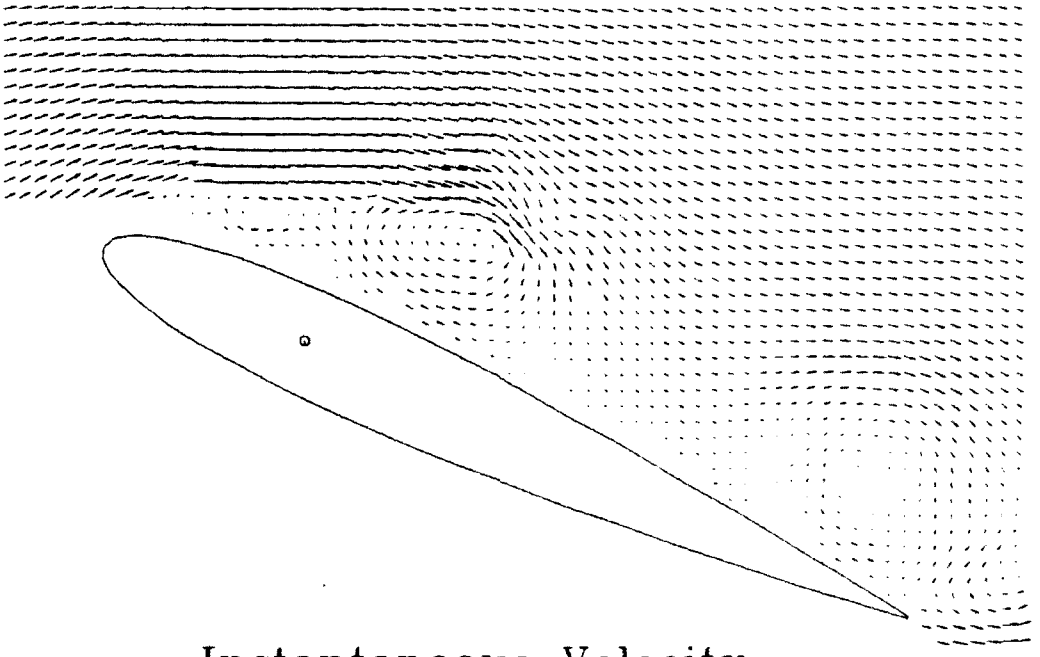

Instantaneous Velocity

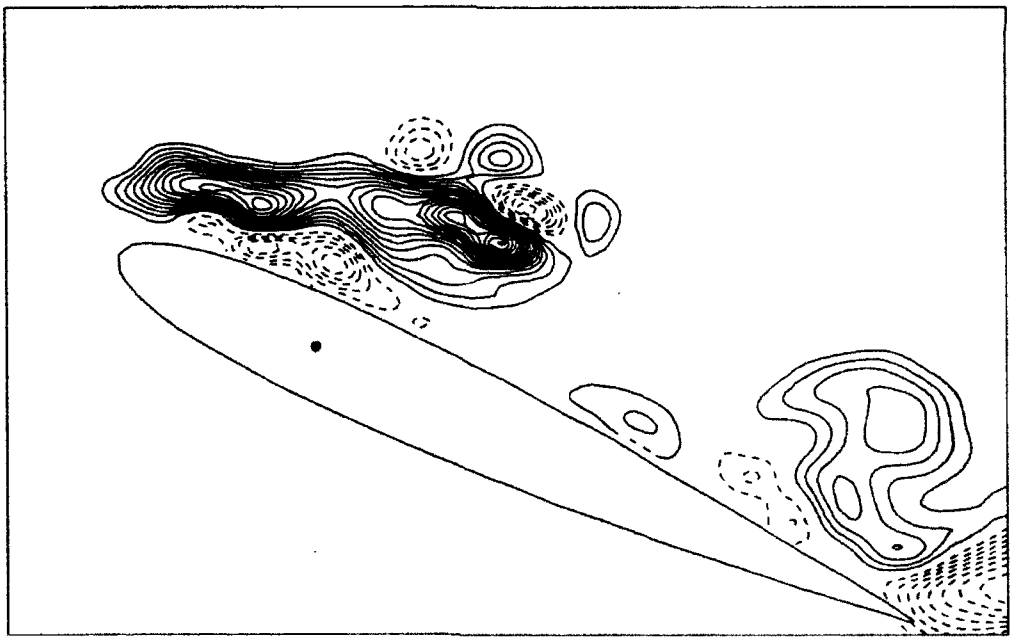

Instantaneous Vorticity

(e) $t^+=3.53$, $\alpha=26.5^\circ$

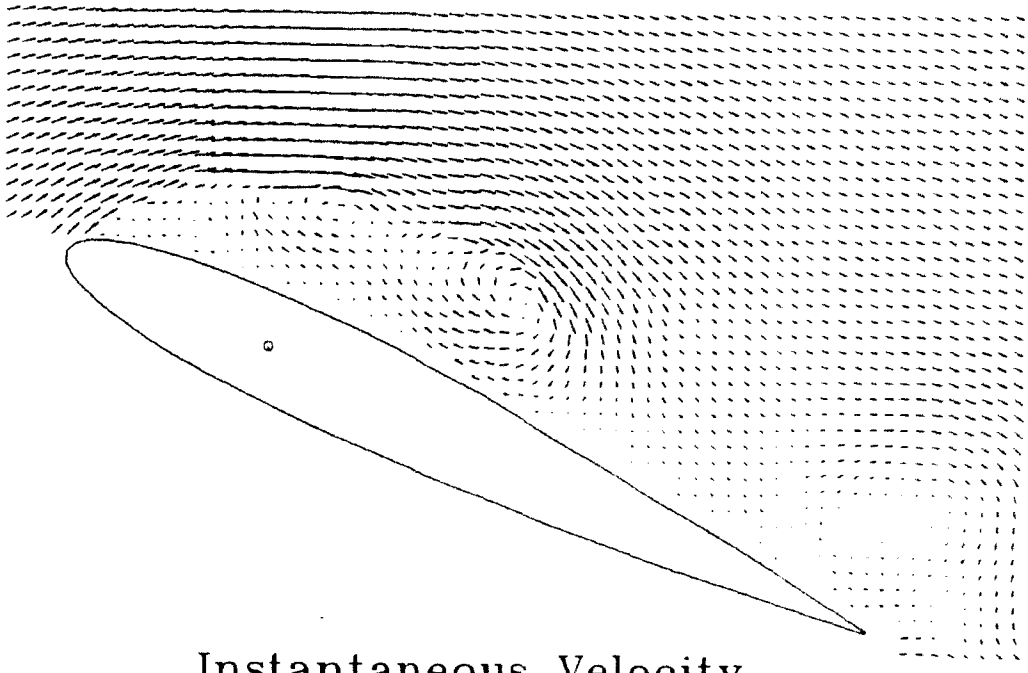

Instantaneous Velocity

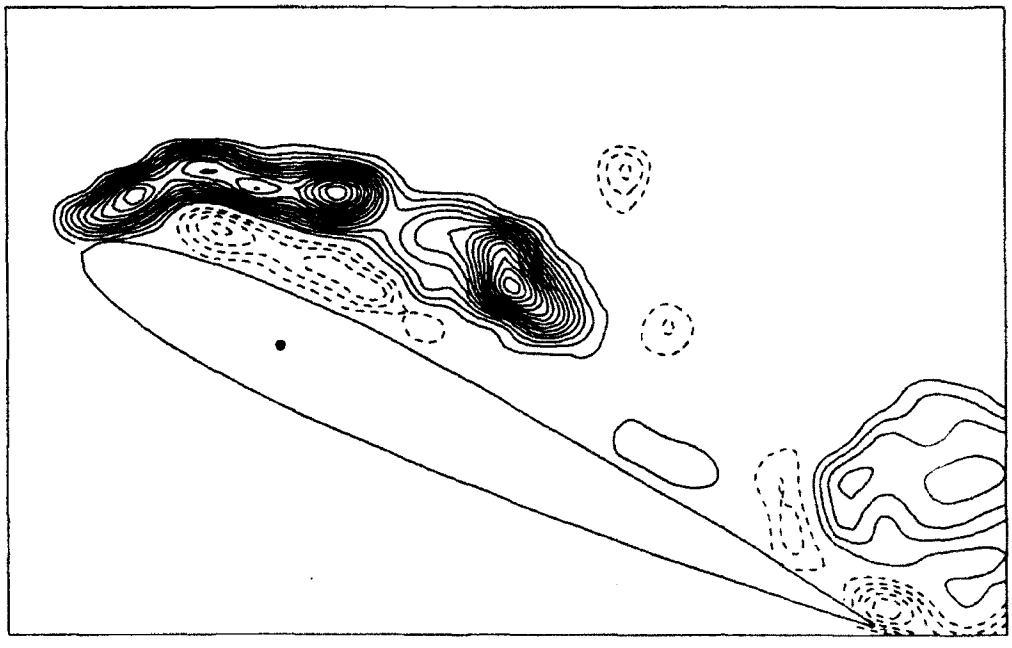

Instantaneous Vorticity

(f) $t^+=3.70$, $\alpha=27.8^\circ$

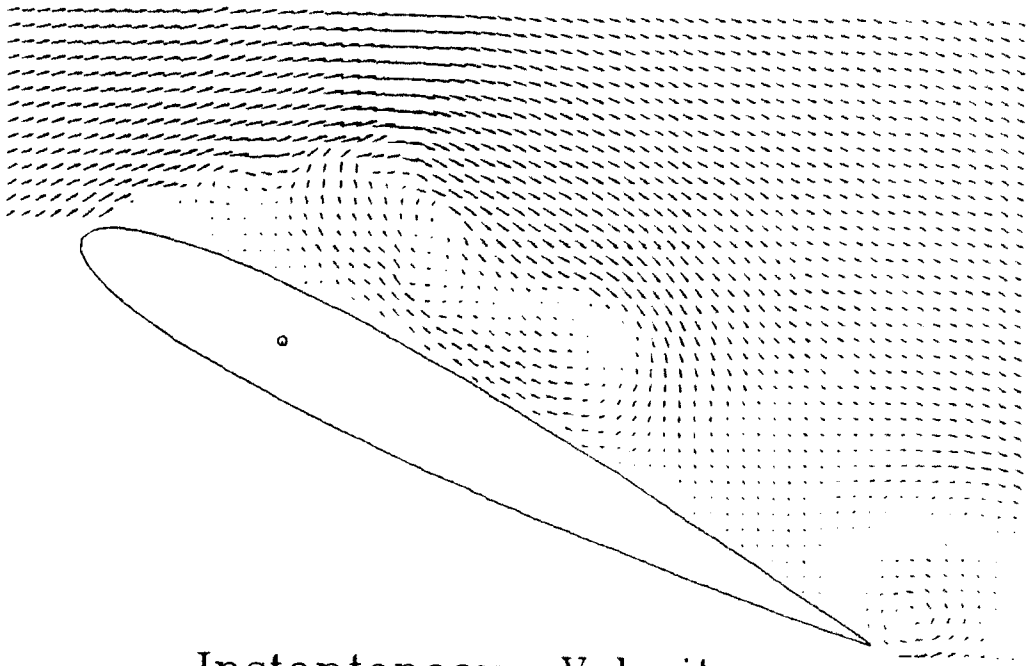

Instantaneous Velocity

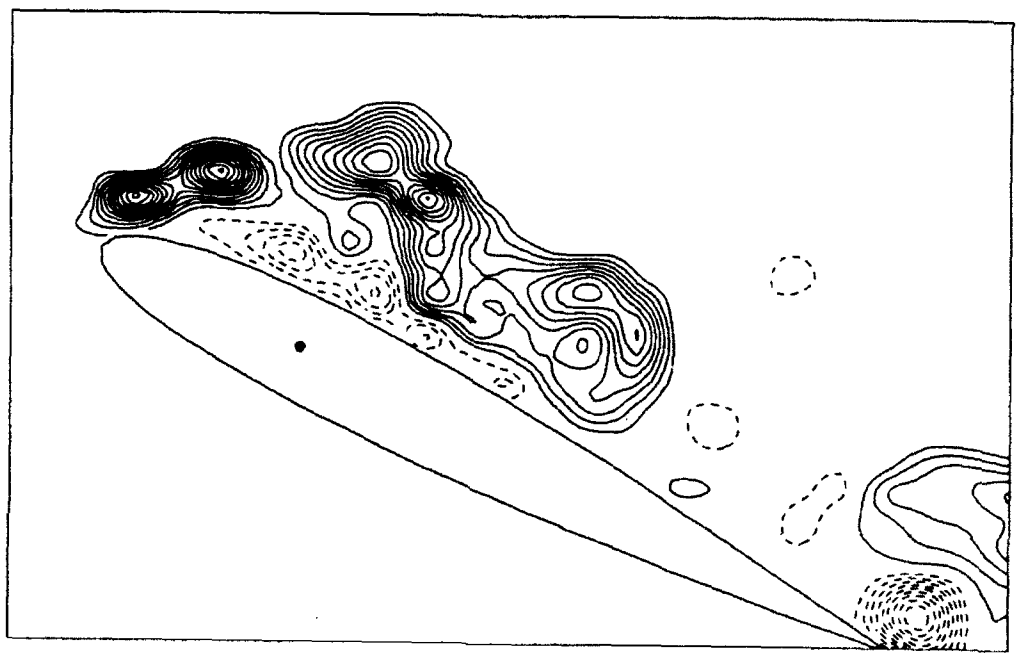

Instantaneous Vorticity

(g) $t^+=3.87$, $\alpha=29.1°$

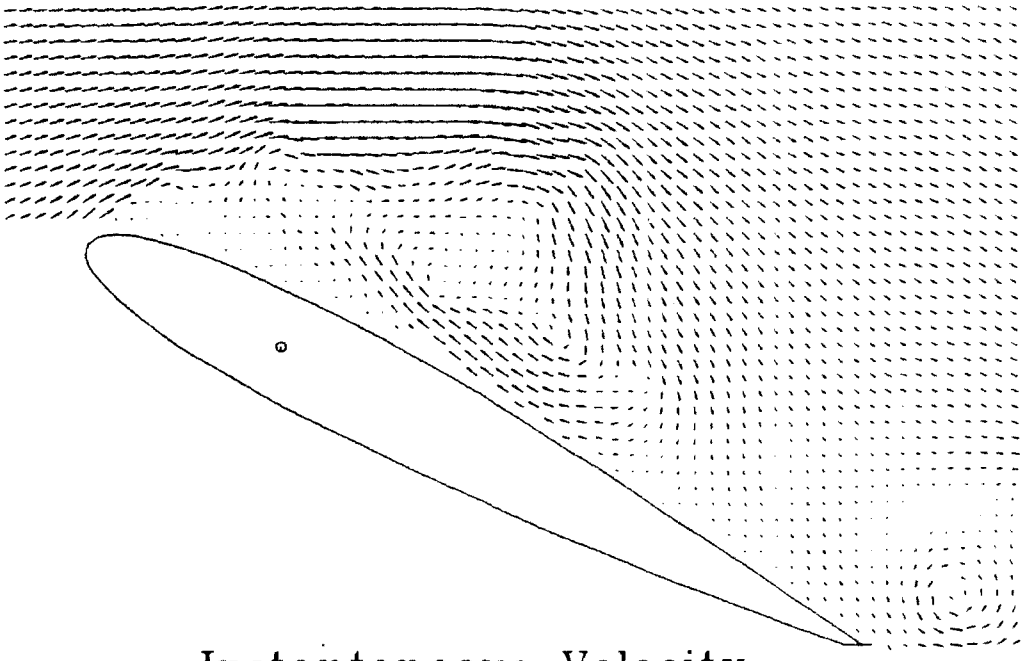

Instantaneous Velocity

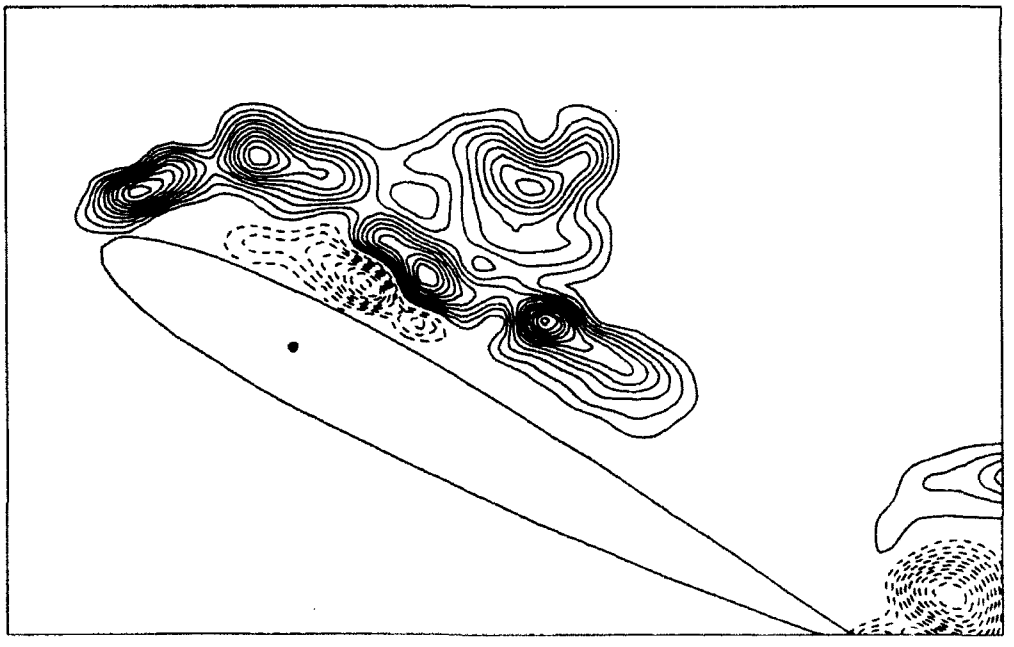

Instantaneous Vorticity

(h) $t^+=4.04$, $\alpha=30.0^\circ$

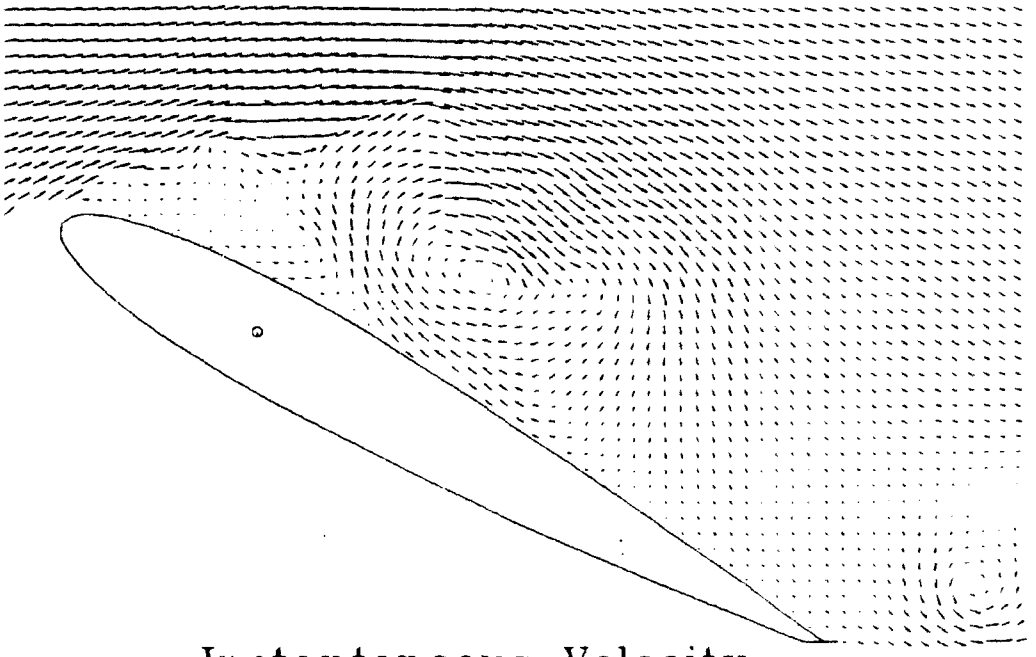

Instantaneous Velocity

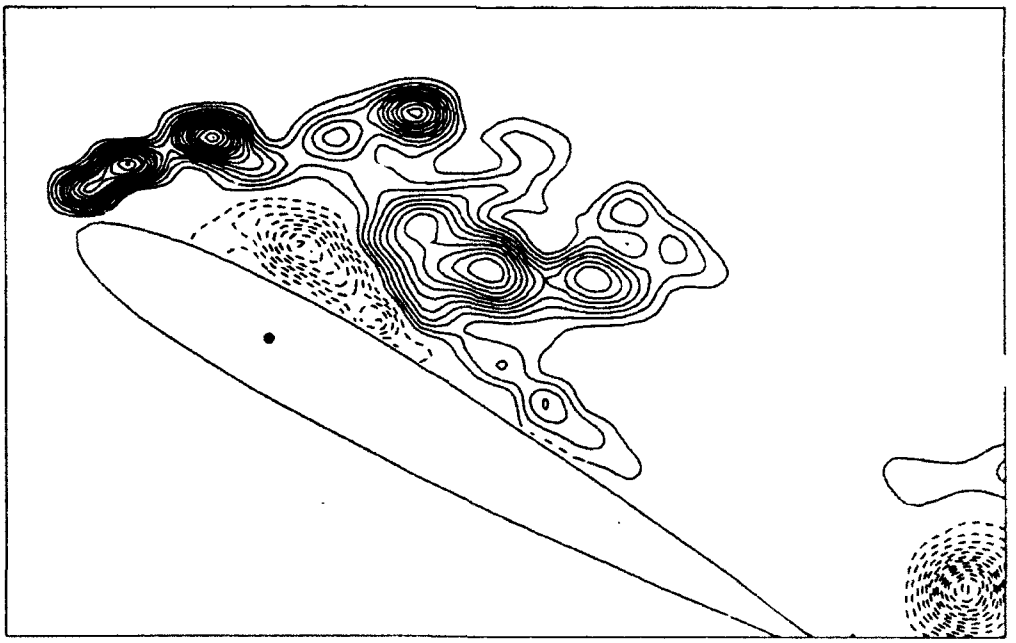

Instantaneous Vorticity

(i) $t^+=4.21$, $\alpha=30.0^\circ$

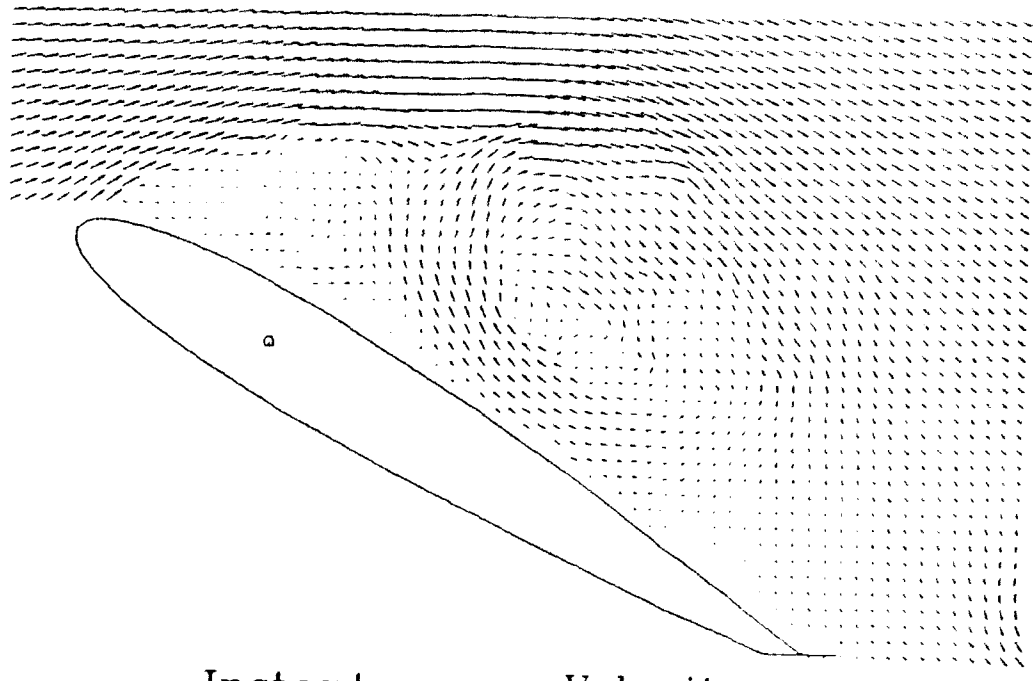

Instantaneous Velocity

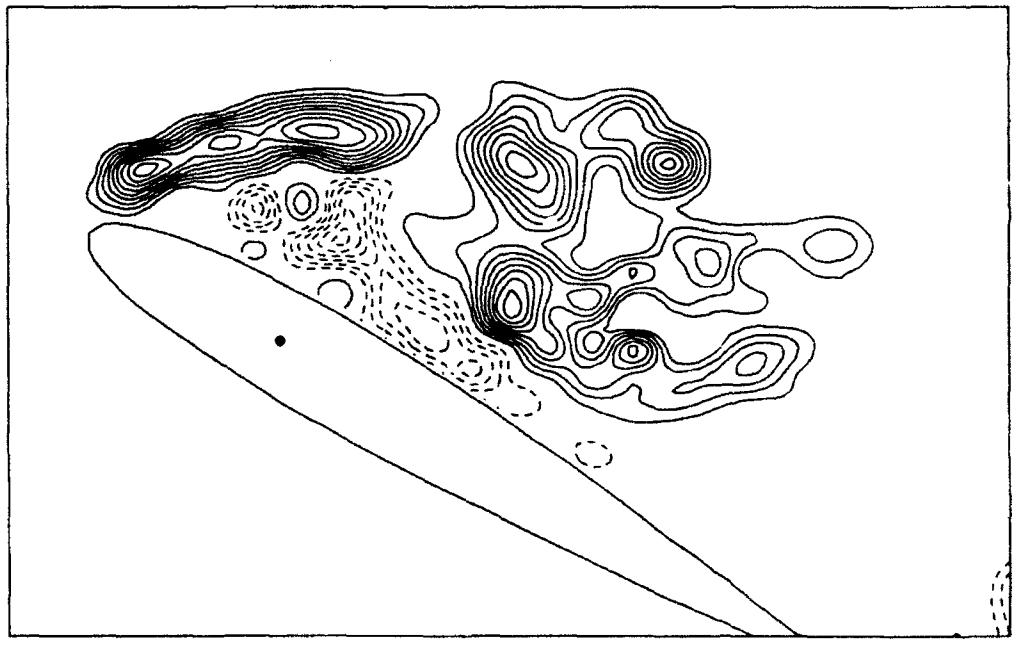

Instantaneous Vorticity

(j) $t^+=4.38$, $\alpha=30.0^\circ$

Figure 3 Time sequence of the instantaneous velocity and vorticity fields. Global flow field, Re=5,000, $\alpha^+=0.131$

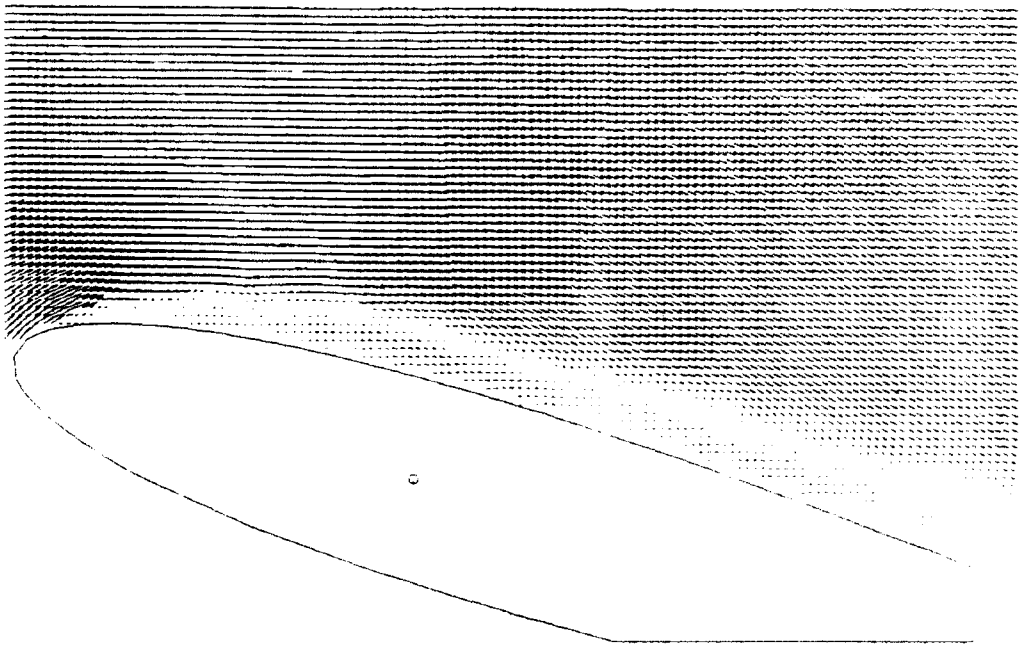

Instantaneous Velocity

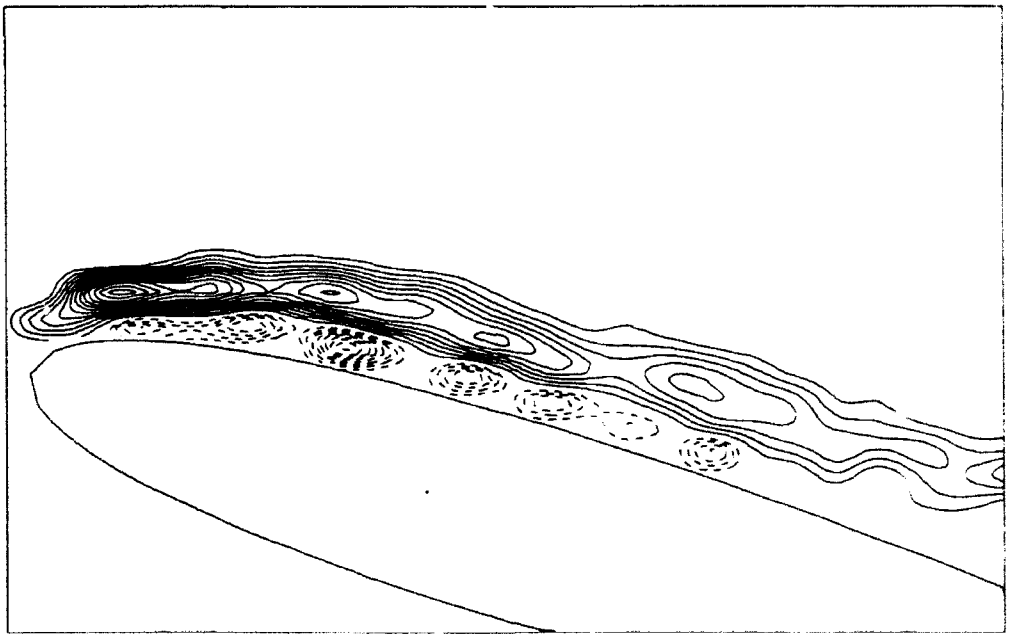

Instantaneous Vorticity

(a) $t^+=2.35$, $\alpha=17.6^\circ$

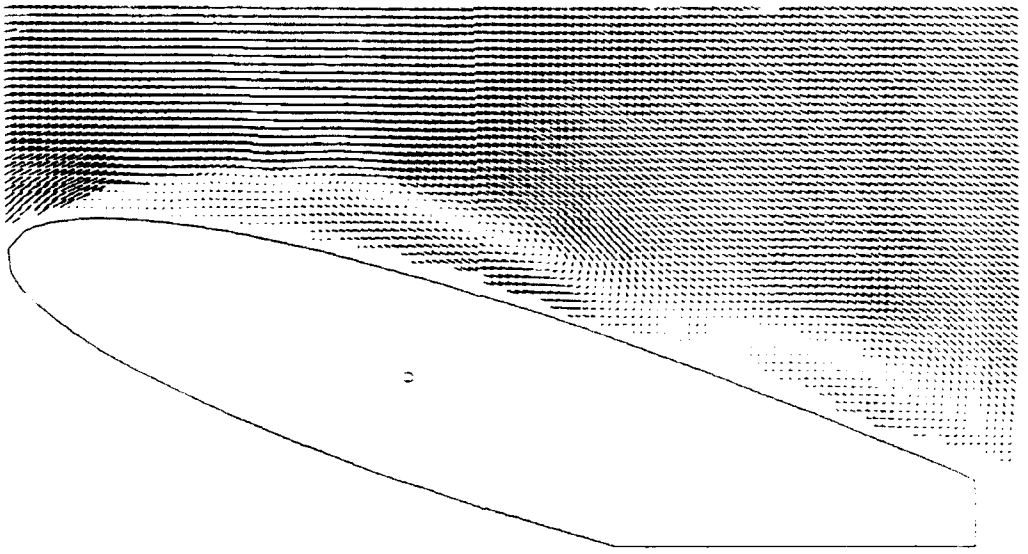

Instantaneous Velocity

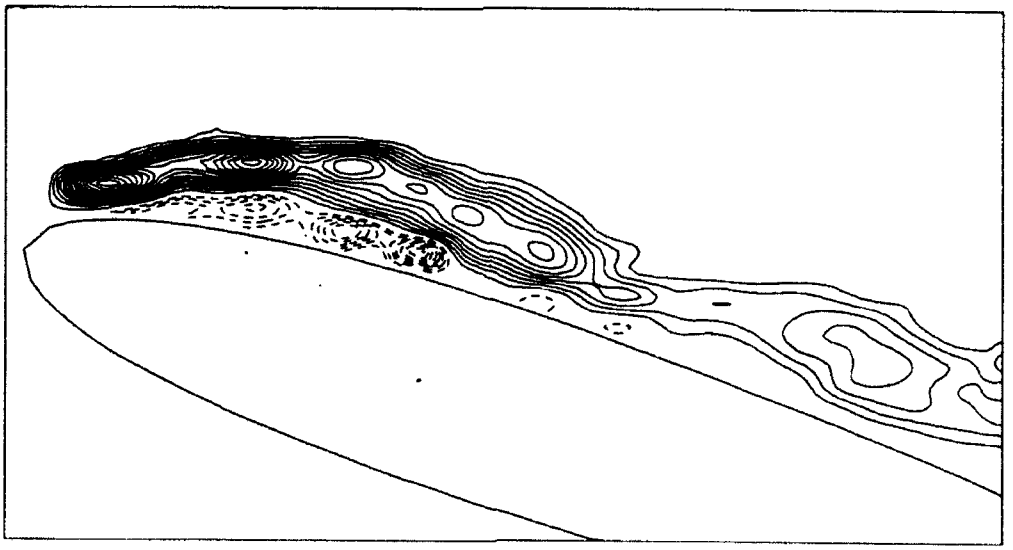

Instantaneous Vorticity

(b) $t^+=2.52$, $\alpha=18.9^\circ$

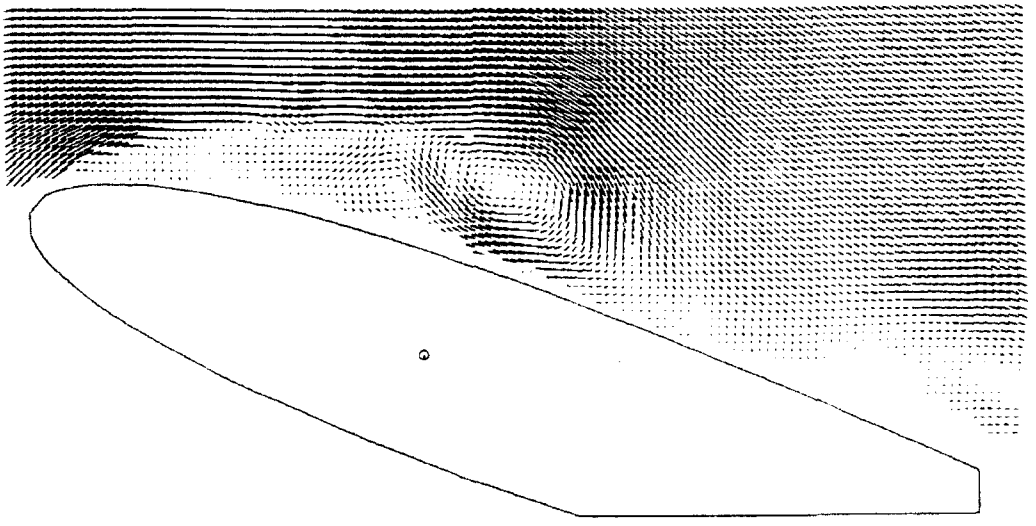

Instantaneous Velocity

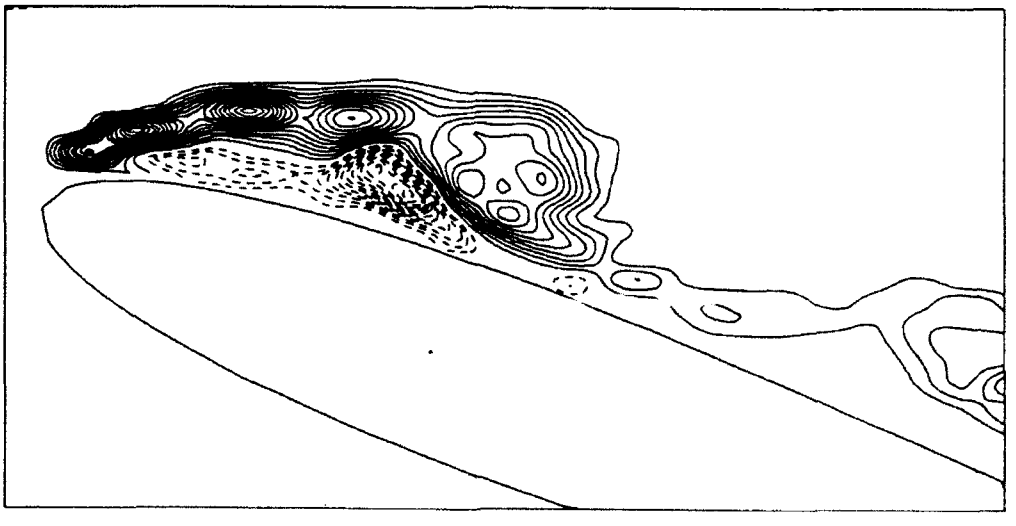

Instantaneous Vorticity

(c) $t^+=2.69$, $\alpha=20.2^\circ$

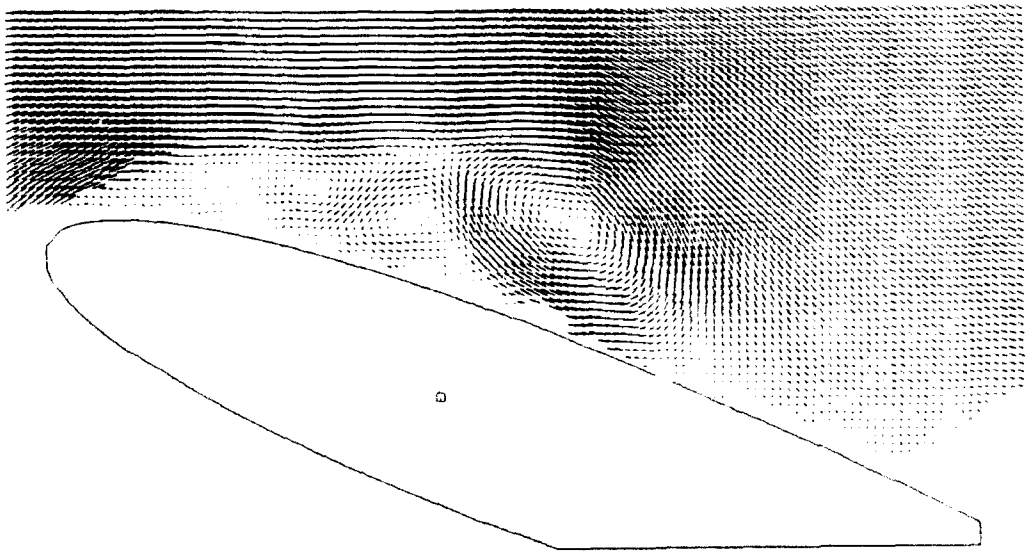

Instantaneous Velocity

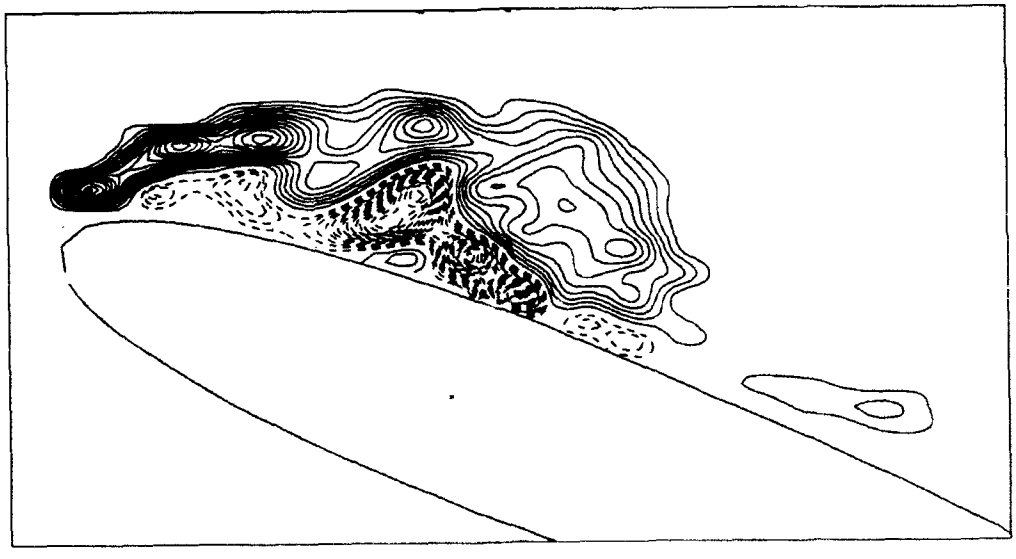

Instantaneous Vorticity

(d) $t^{+}=2.86, \quad \alpha=21.5^{\circ}$

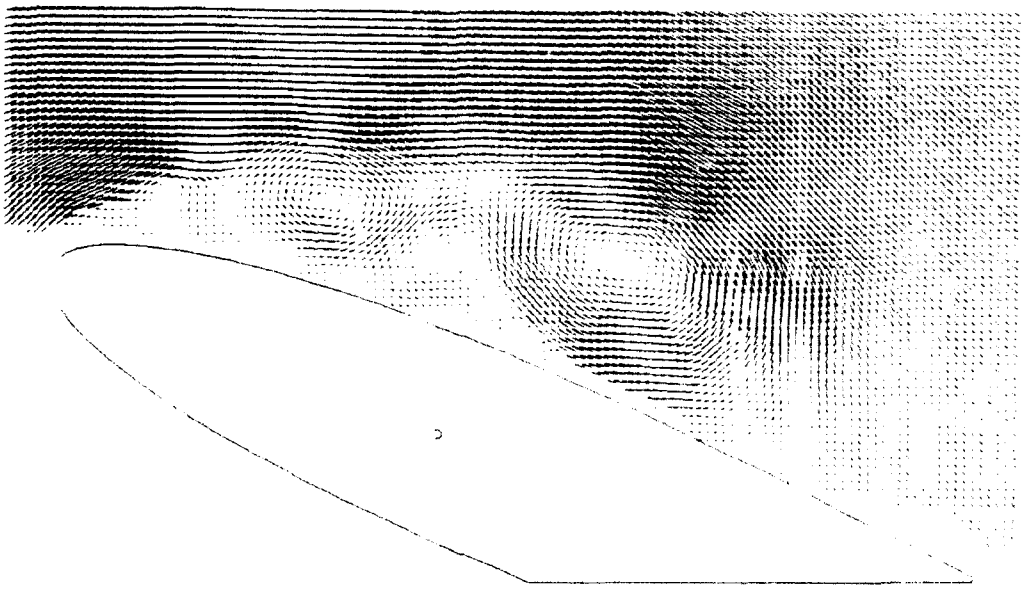

Instantaneous Velocity

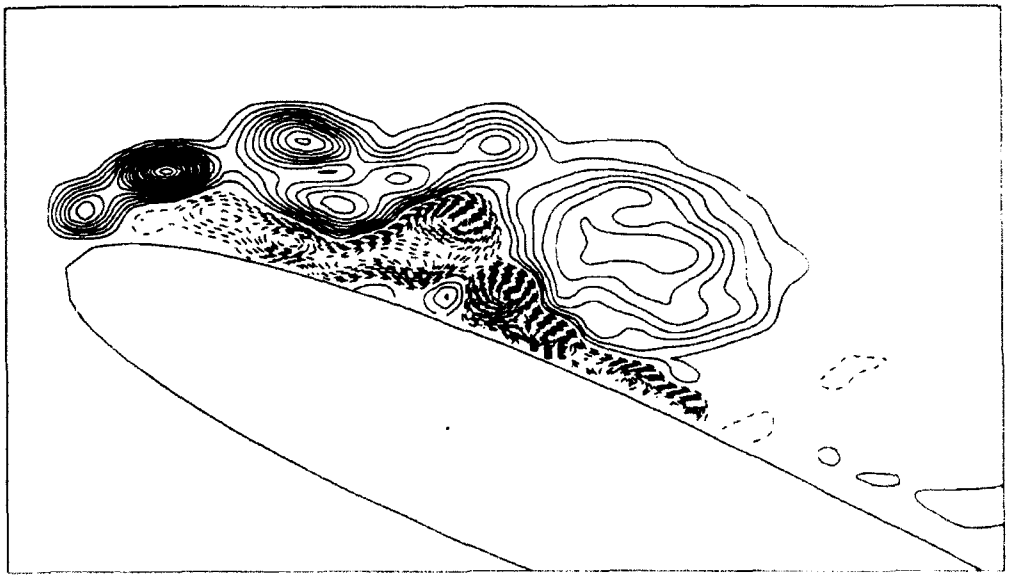

Instantaneous Vorticity

(e) $t^+=3.03$, $\alpha=22.7^\circ$

Instantaneous Velocity

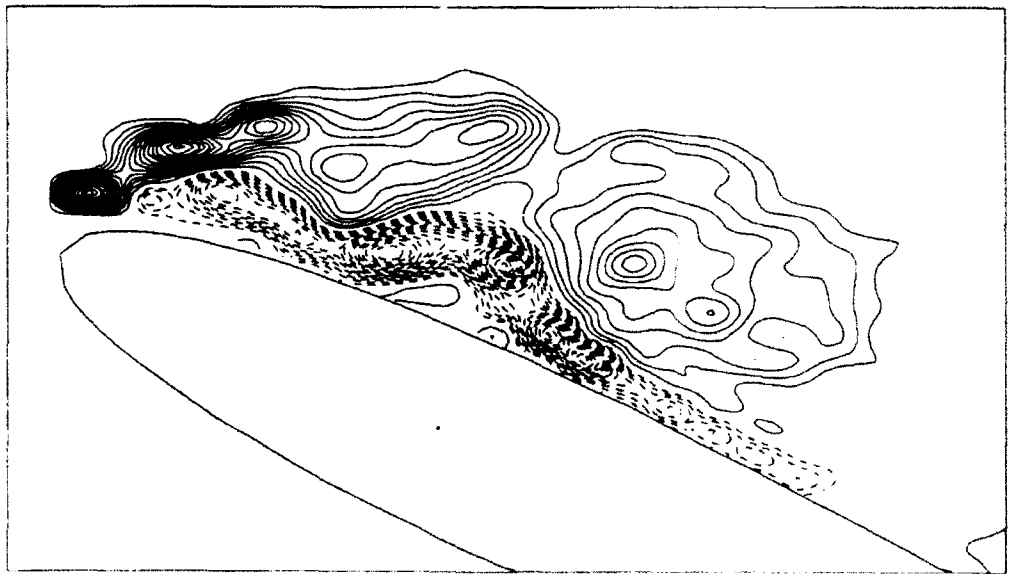

Instantaneous Vorticity

(f) $t^+=3.20$, $\alpha=24.0^o$

Instantaneous Velocity

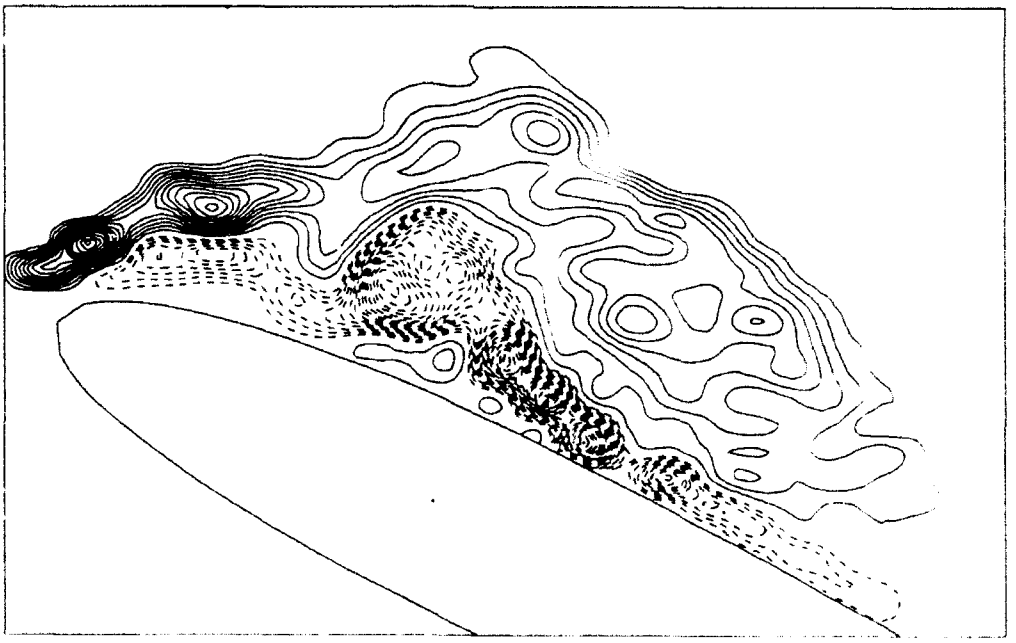

Instantaneous Vorticity

(g) $t^+=3.37$, $\alpha=25.3^\circ$

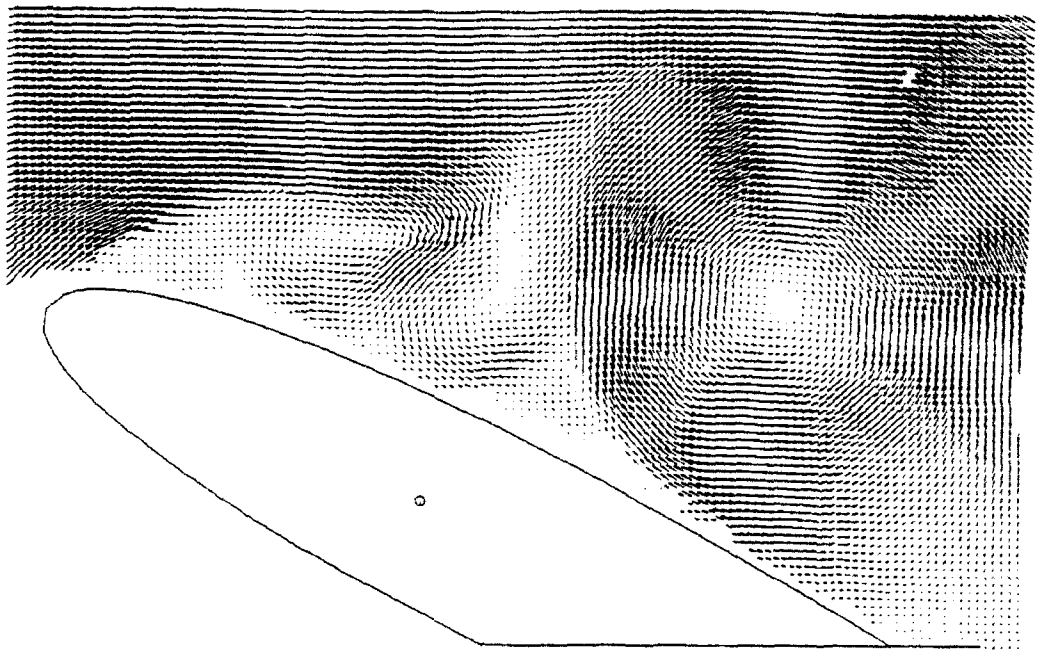

Instantaneous Velocity

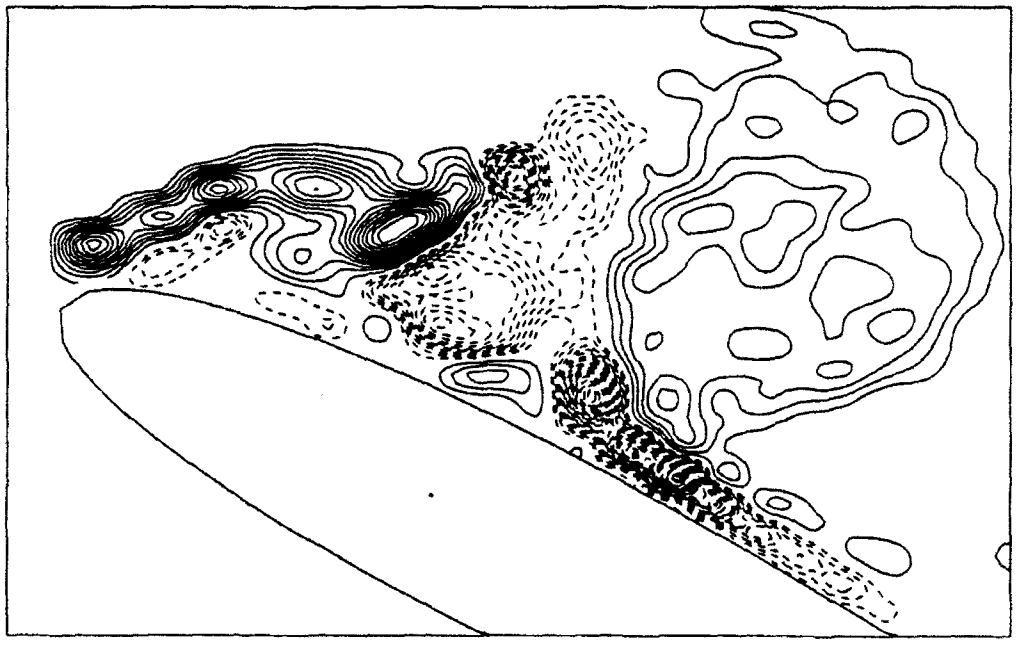

Instantaneous Vorticity

(h) $t^+=3.54$, $\alpha=26.6^\circ$

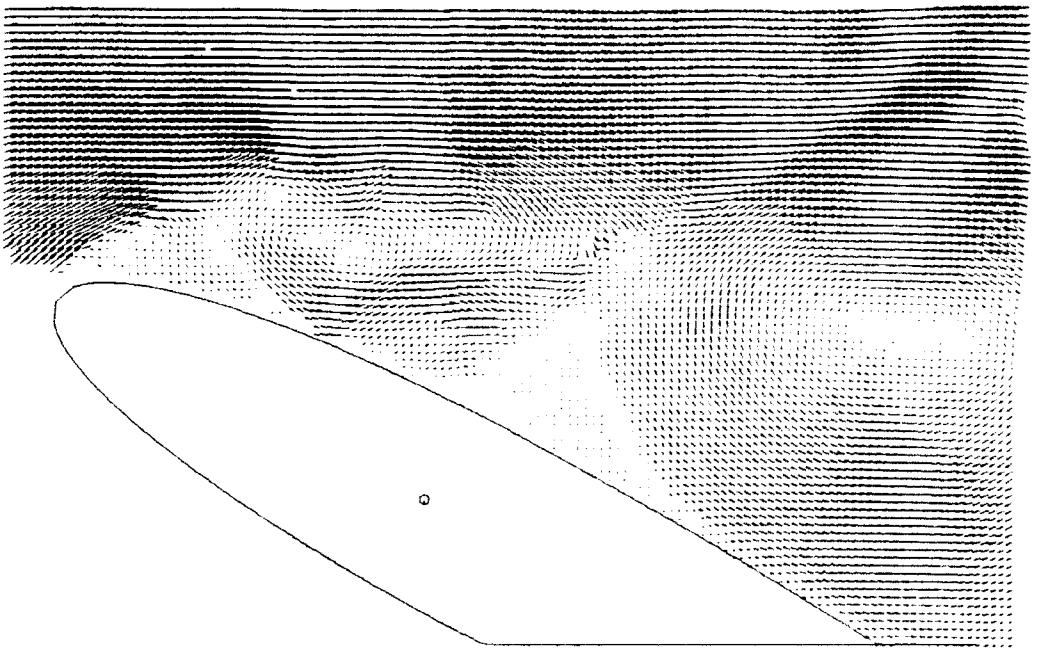

Instantaneous Velocity

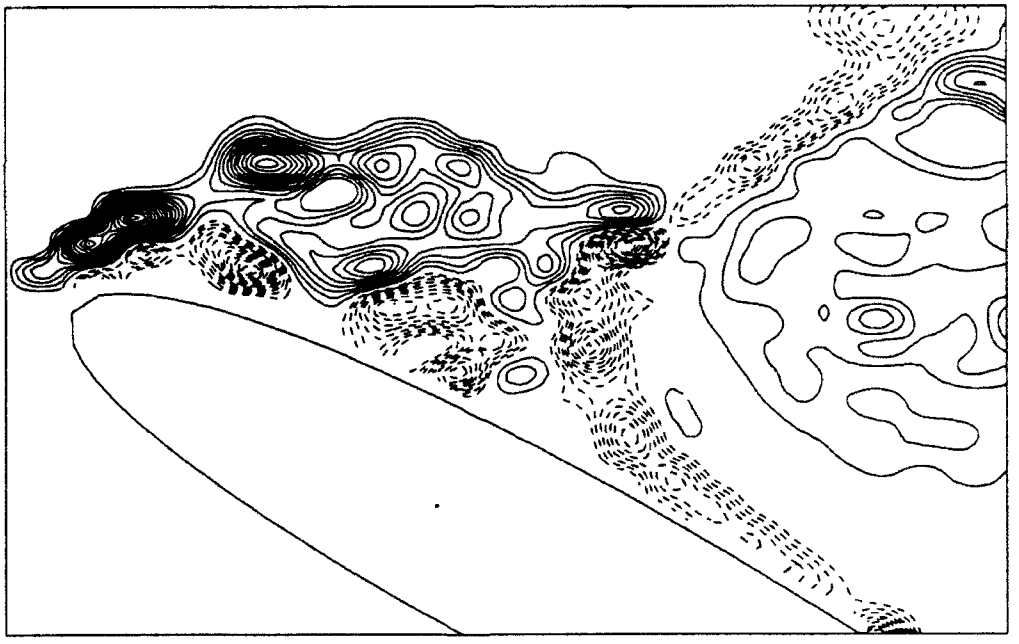

Instantaneous Vorticity

(i) $t^+=3.71$, $\alpha=27.9^\circ$

Figure 4 Time sequence of the instantaneous velocity and vorticity fields,leading edge region, Re=5,000, $\alpha=0.13$

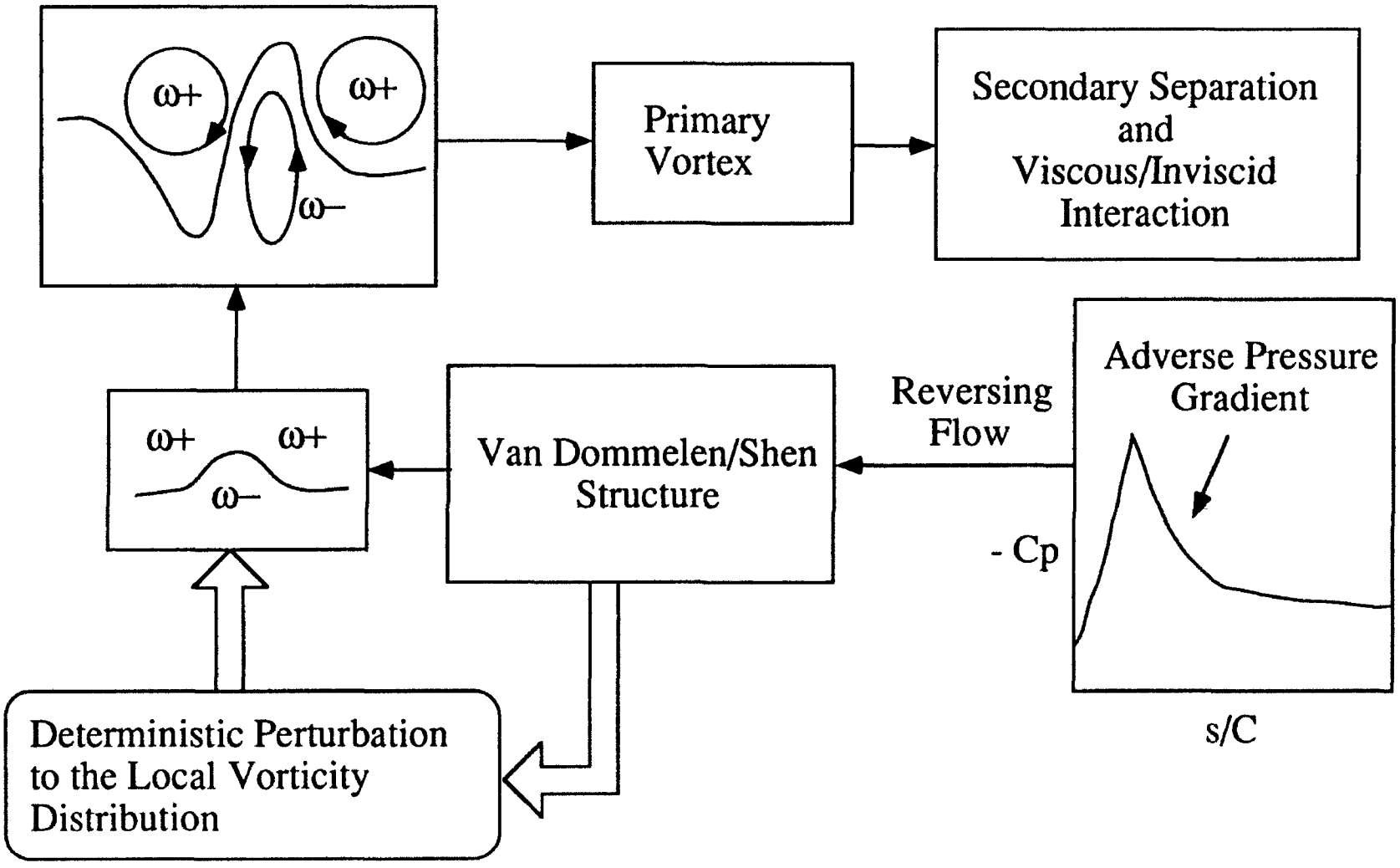

Figure 5 Proposed time development of the unsteady separation process

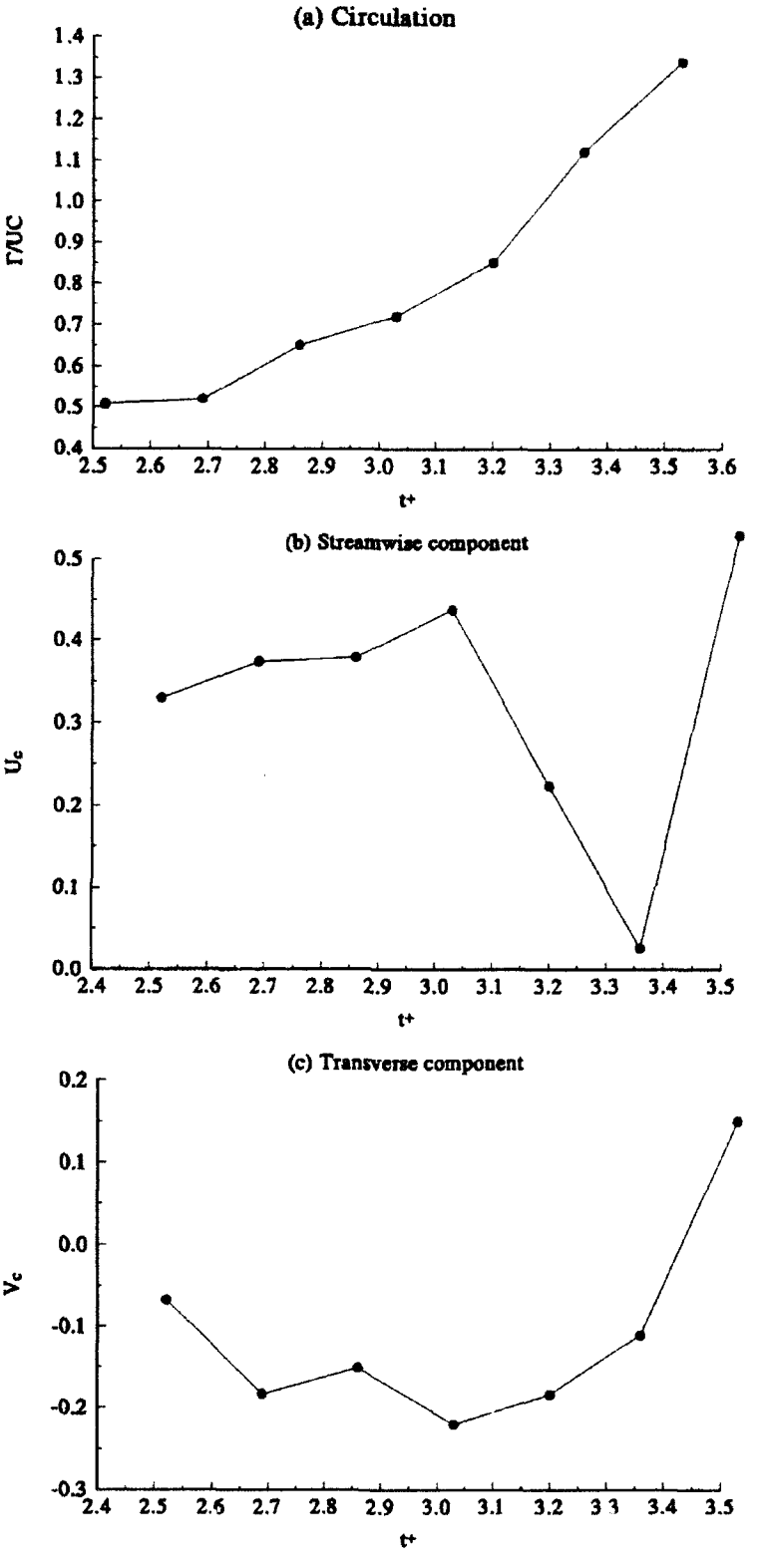

Figure 6 Time evolution of the circulation and the convection velocity of the primary vortex

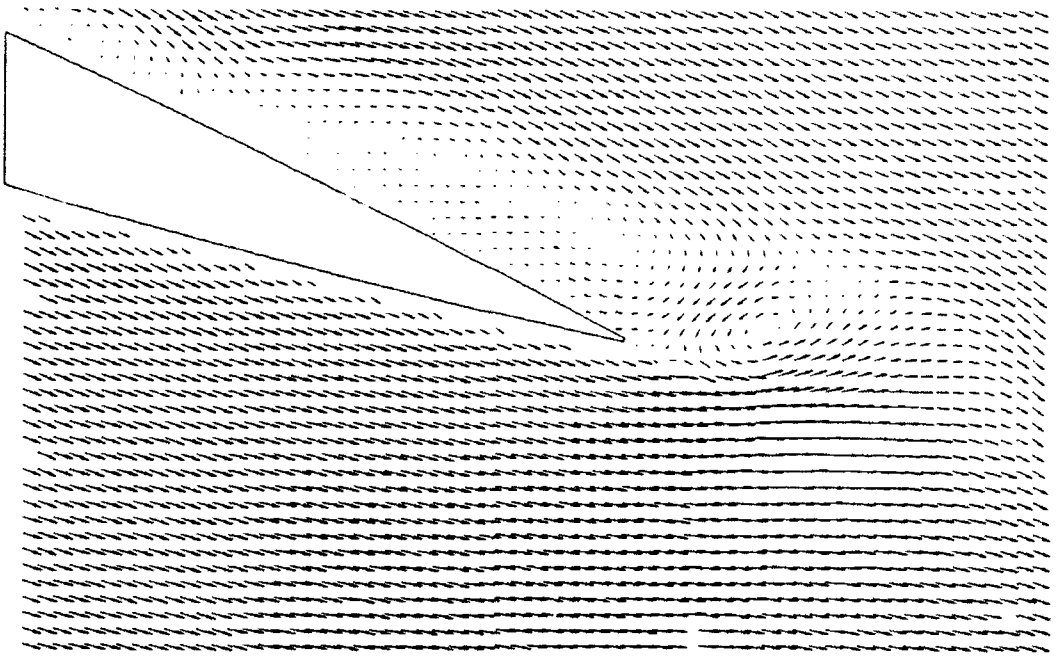

Instantaneous Velocity

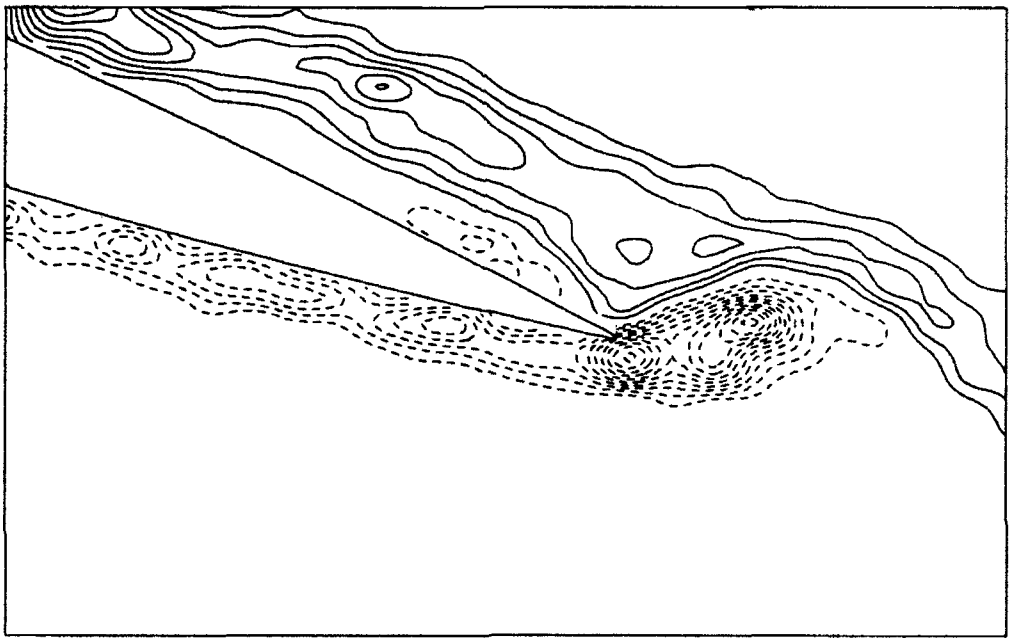

Instantaneous Vorticity

(a) $t^+=2.54$, $\alpha=19.1^\circ$

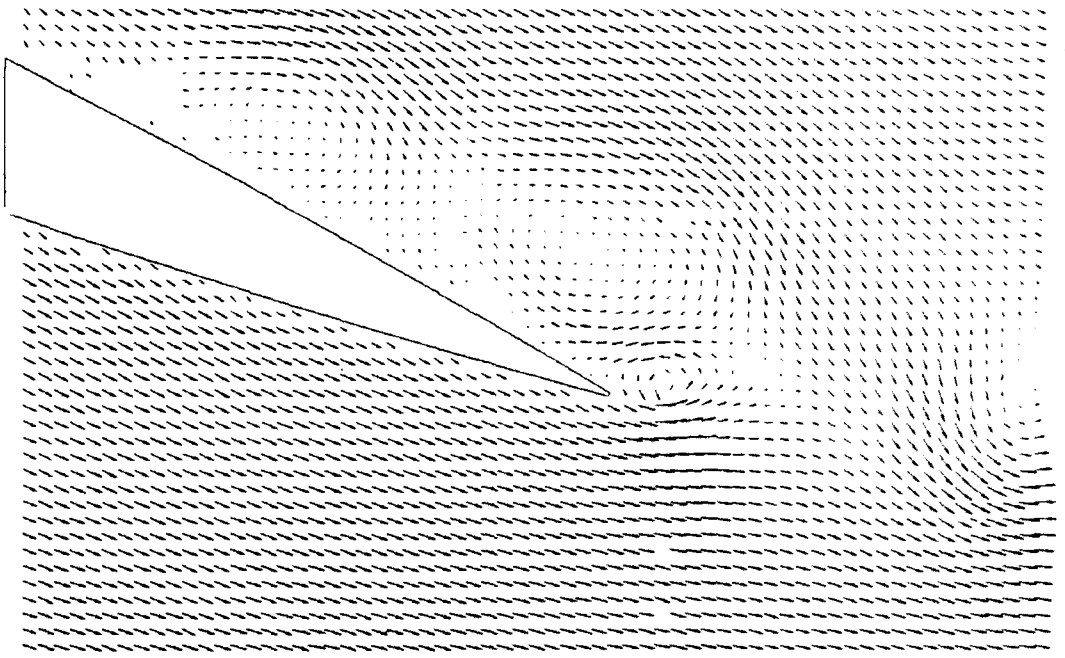

Instantaneous Velocity

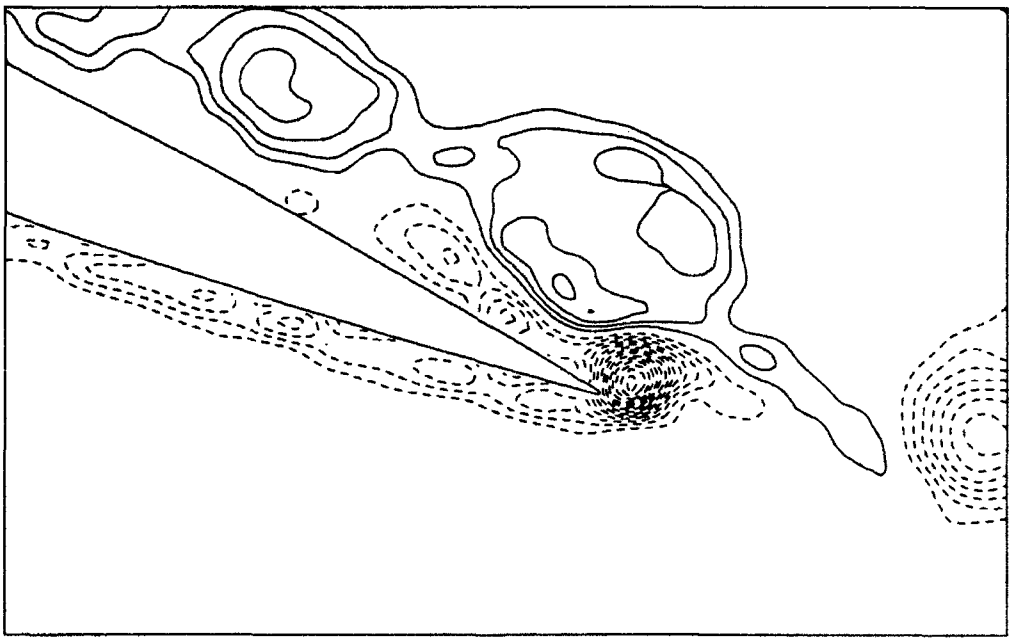

Instantaneous Vorticity

(b) $t^+=2.87$, $\alpha=21.7^\circ$

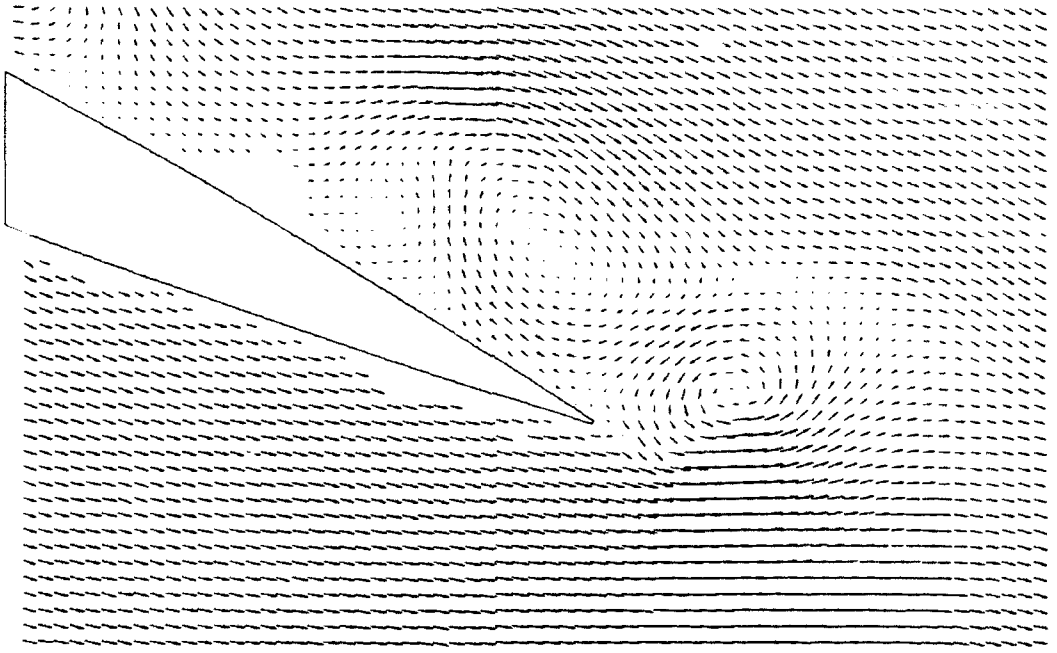

Instantaneous Velocity

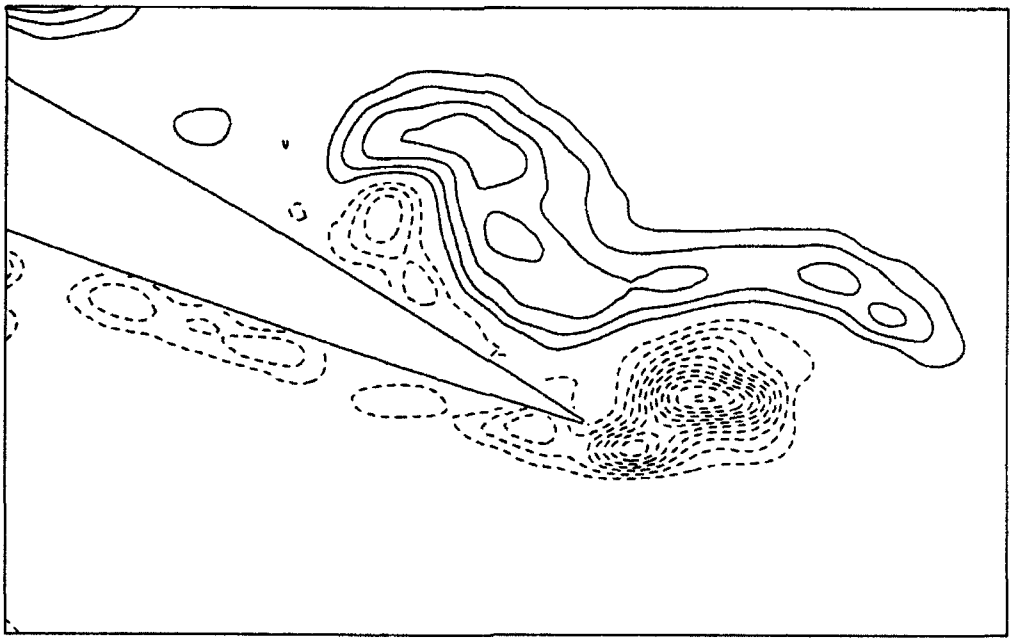

Instantaneous Vorticity

(c) $t^+=3.21$, $\alpha=24.3^\circ$

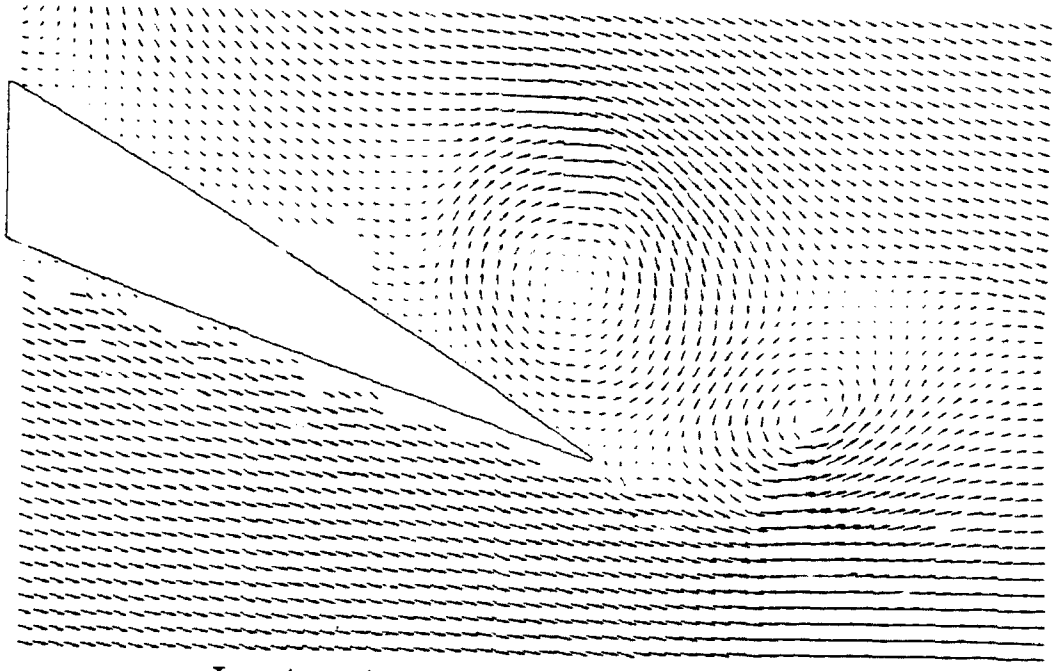

Instantaneous Velocity

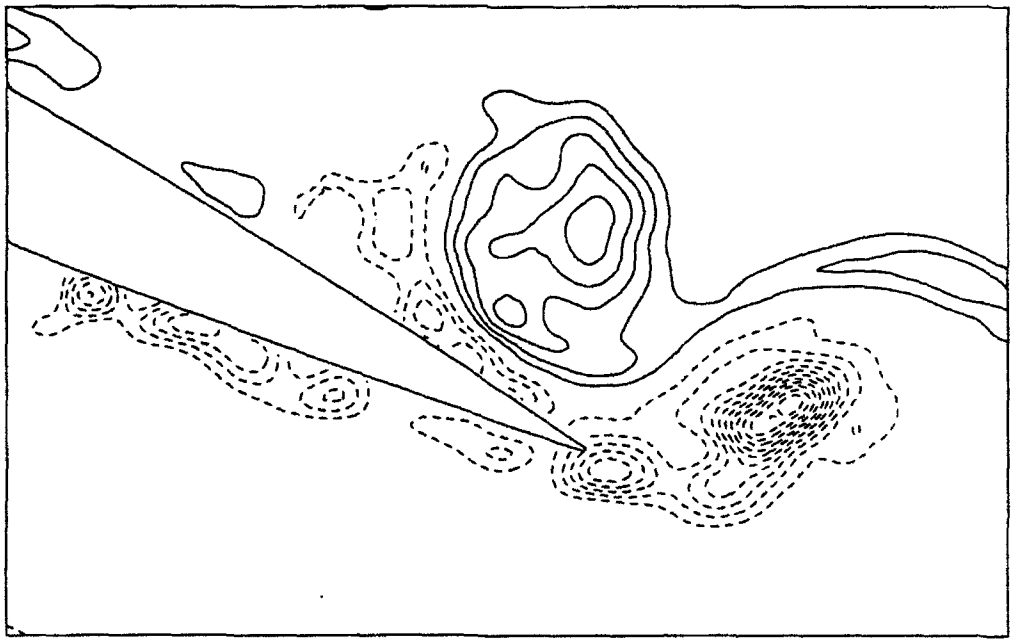

Instantaneous Vorticity

(d) $t^+=3.38$, $\alpha=25.6^\circ$

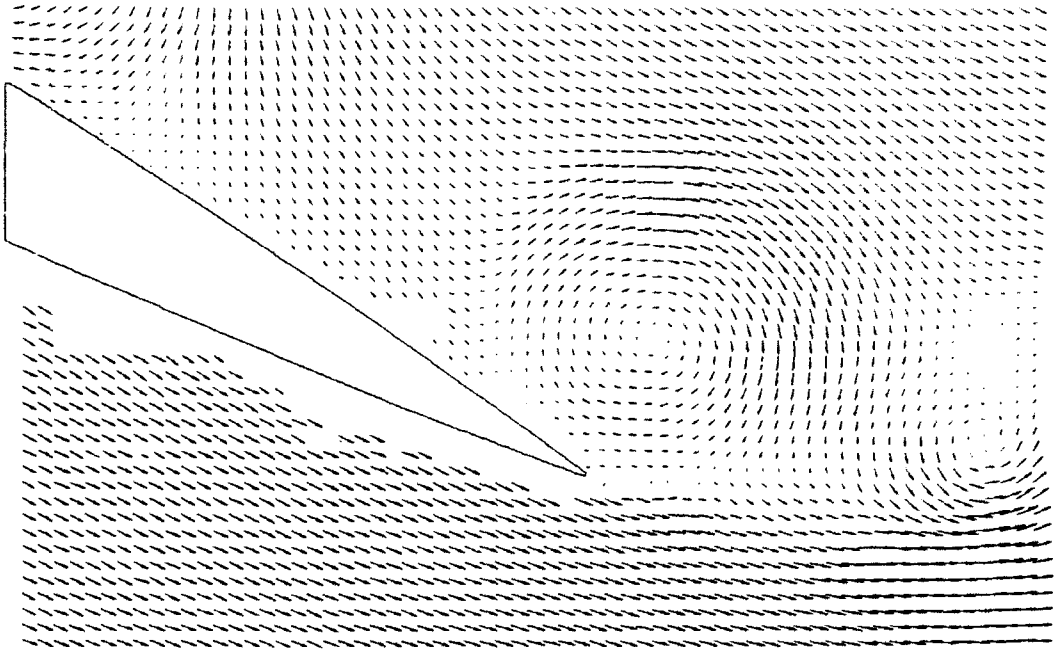

Instantaneous Velocity

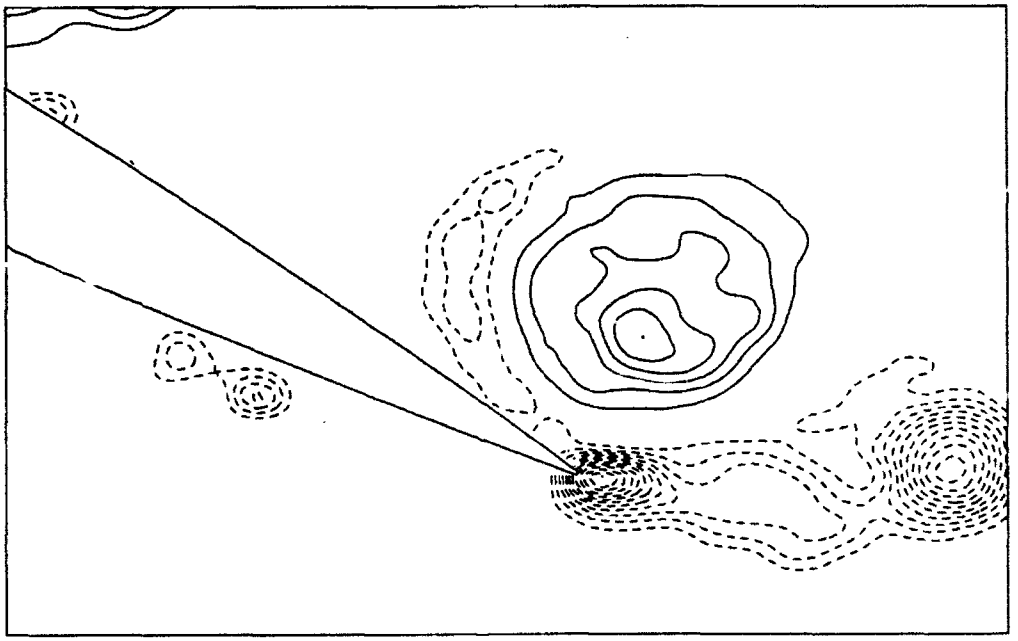

Instantaneous Vorticity

(e) $t^+=3.55$, $\alpha=26.9^\circ$

Figure 7 Time sequence of the instantaneous velocity and vorticity fields,trailing edge region Re=5,000, $\alpha^+=0.131$

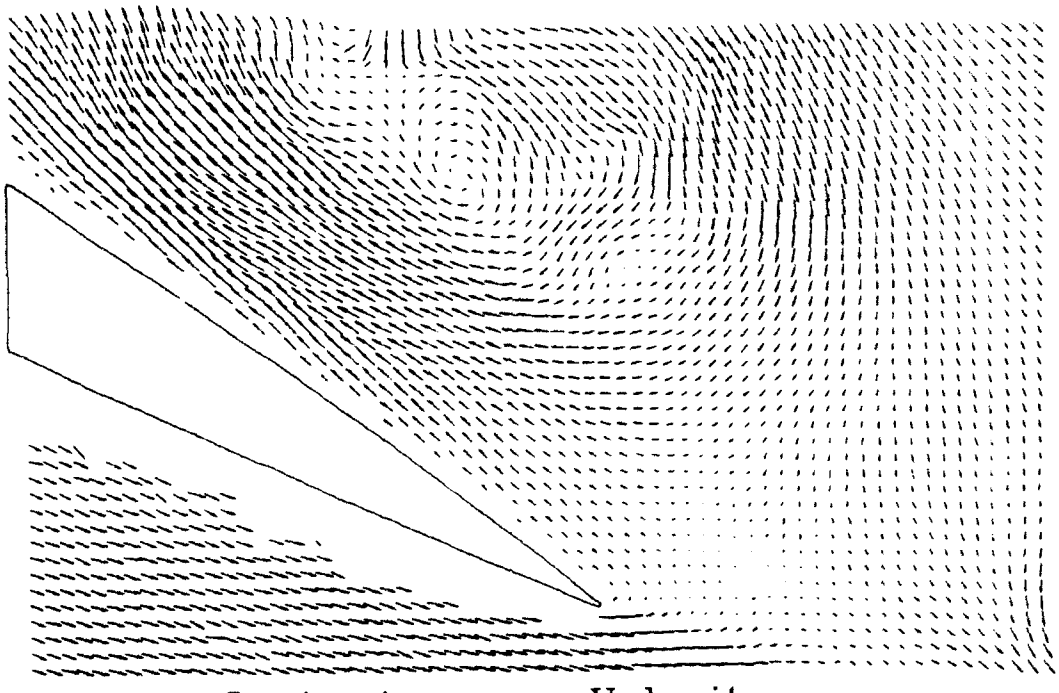

Instantaneous Velocity

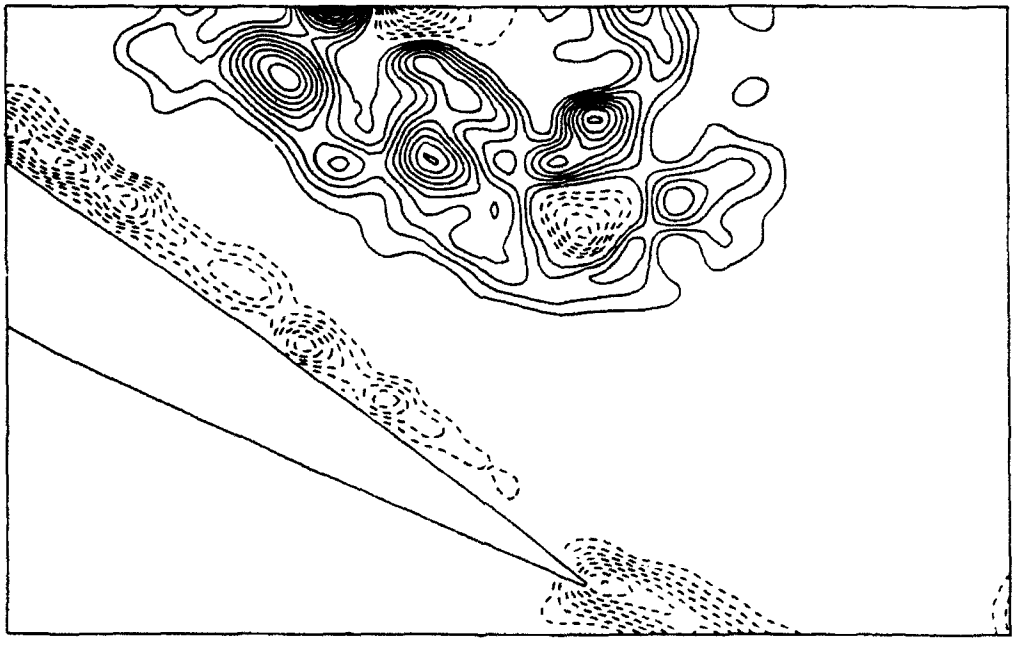

Instantaneous Vorticity

(a) $t^+=4.57$, $\alpha=30.0°$

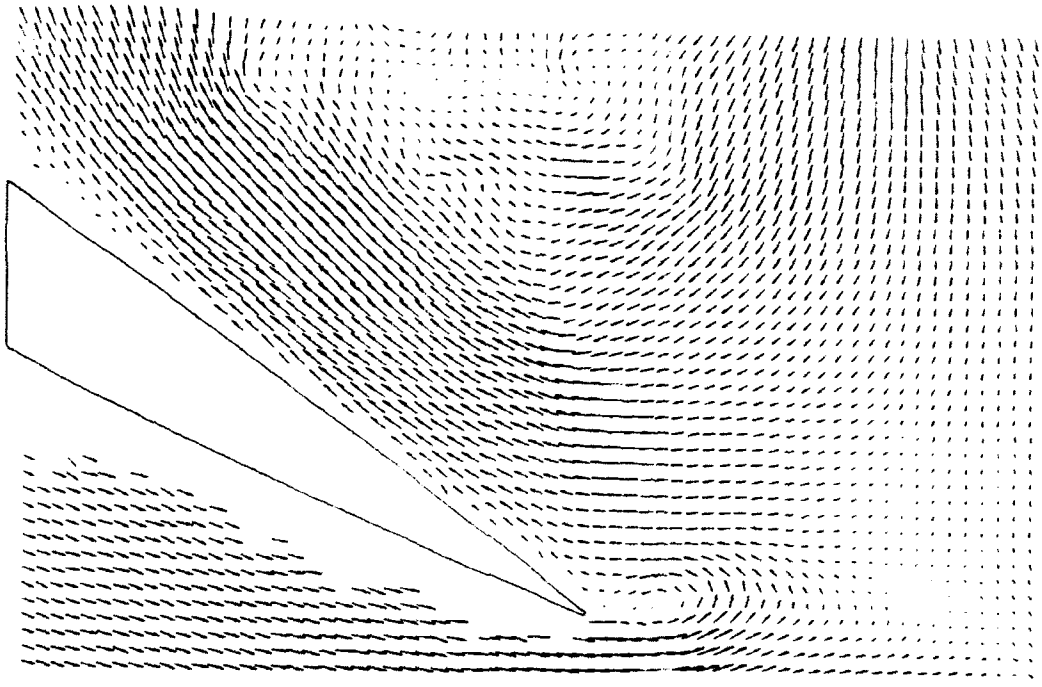

Instantaneous Velocity

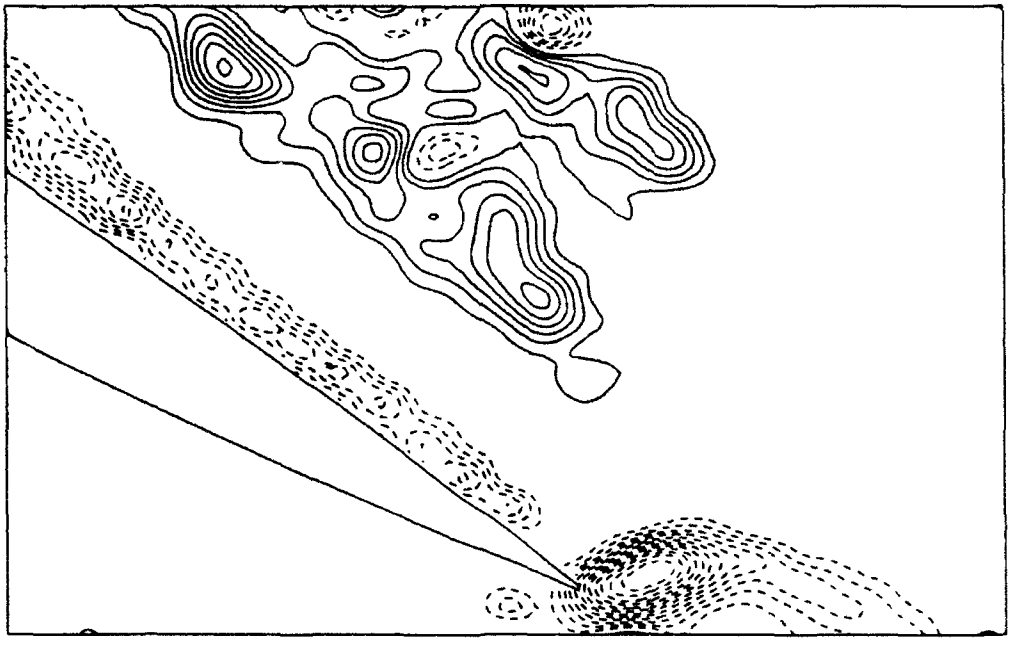

Instantaneous Vorticity

(b) $t^+=4.91$, $\alpha=30.0°$

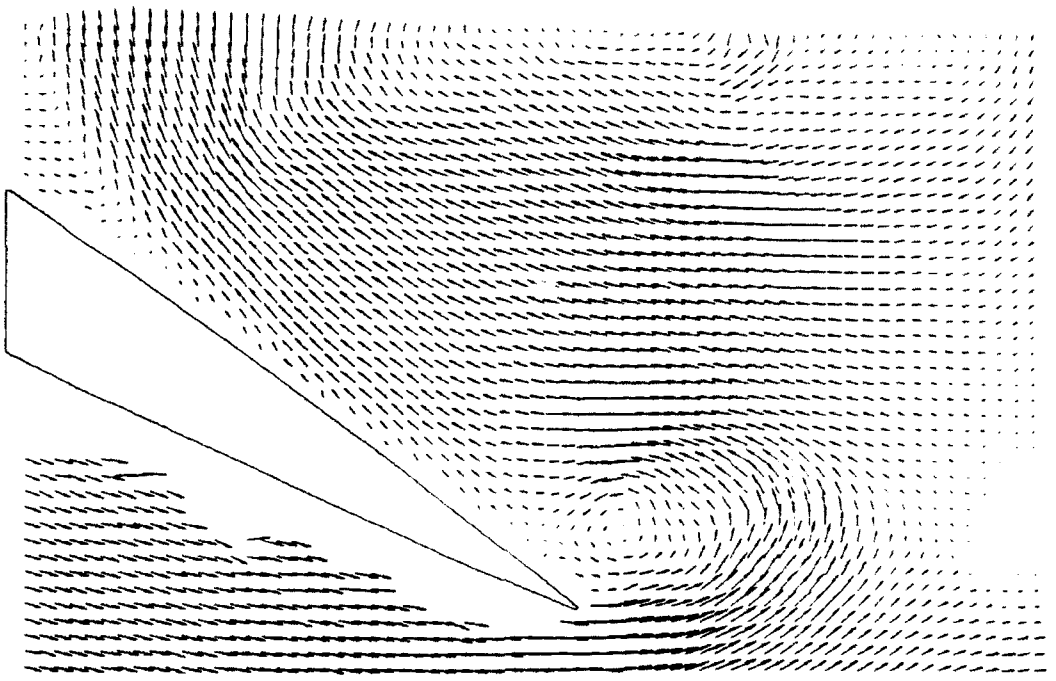

Instantaneous Velocity

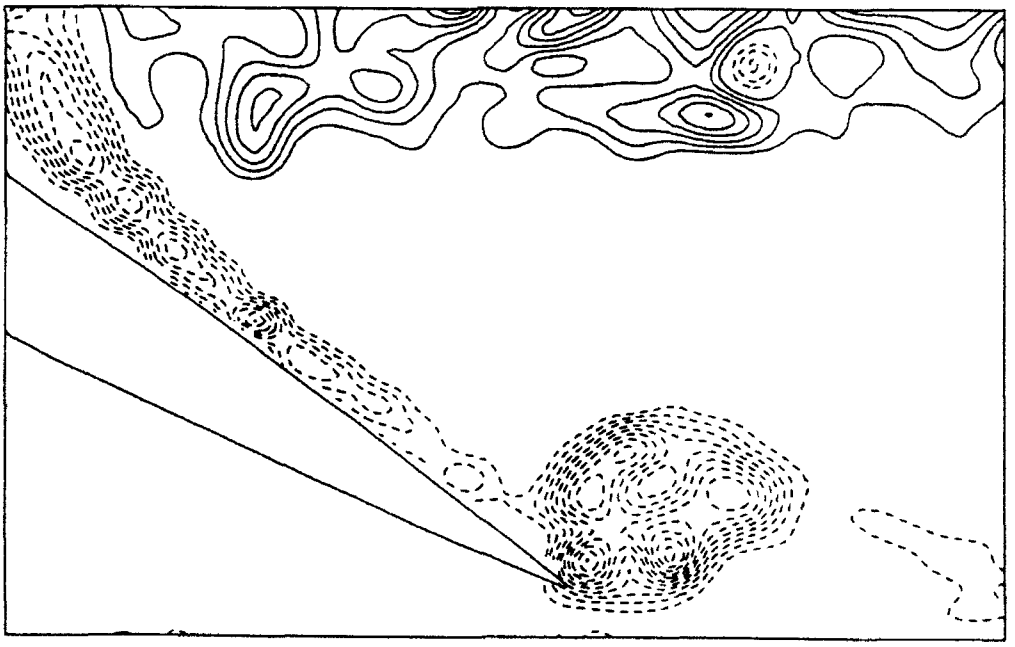

Instantaneous Vorticity

(c) $t^+=5.25$, $\alpha=30.0°$

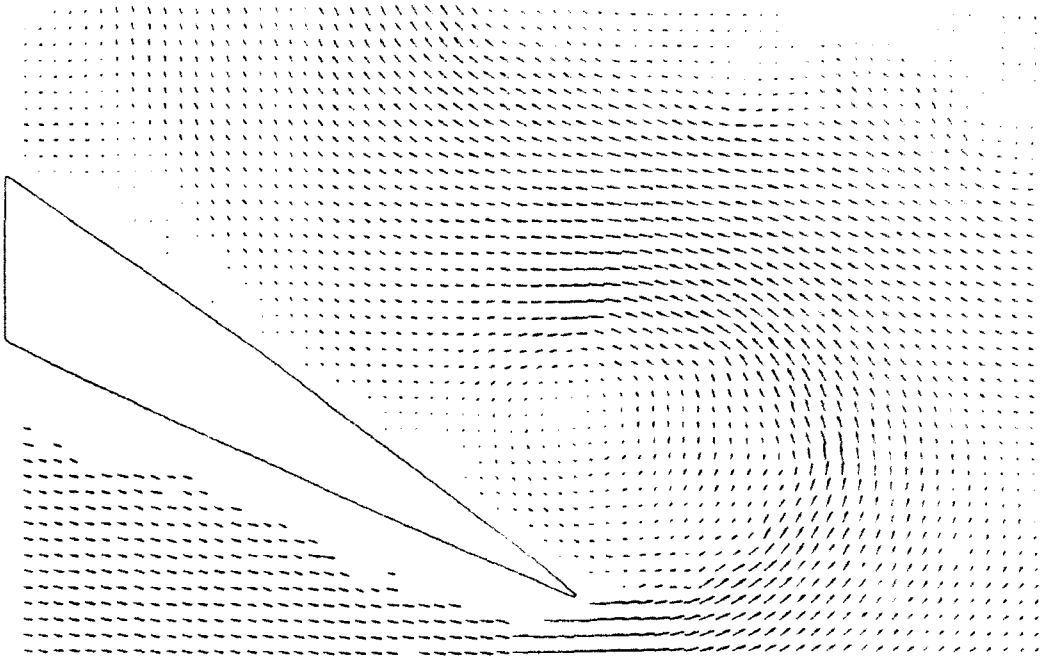

Instantaneous Velocity

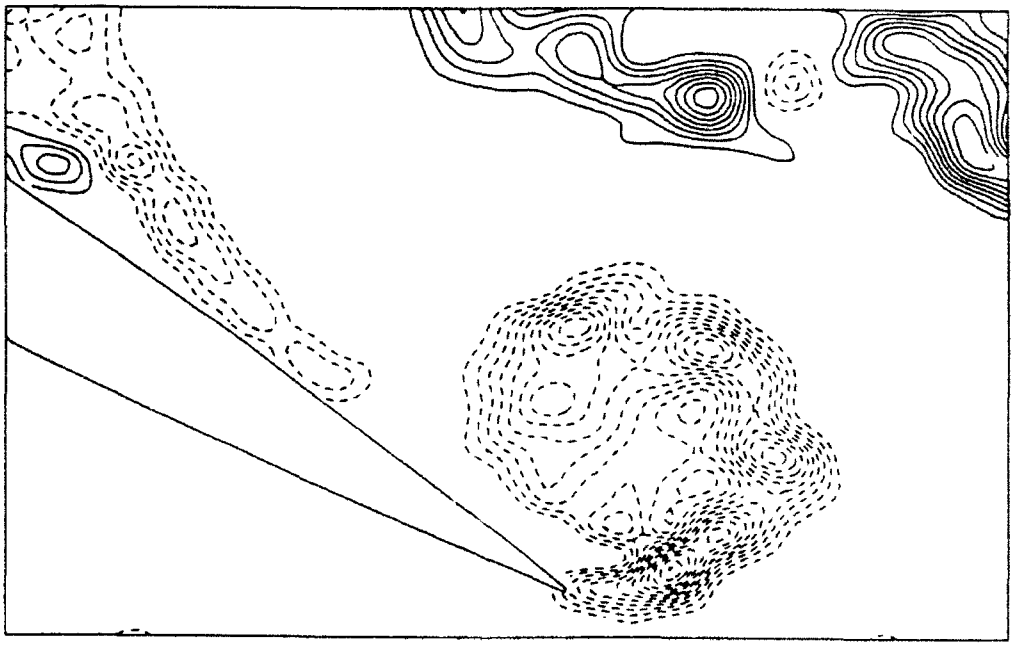

Instantaneous Vorticity

(d) $t^+=5.59$, $\alpha=30.0^\circ$

Figure 8 Time sequence of the instantaneous velocity and vorticity fields,trailing edge region Re=5,000, $\alpha^+=0.131$

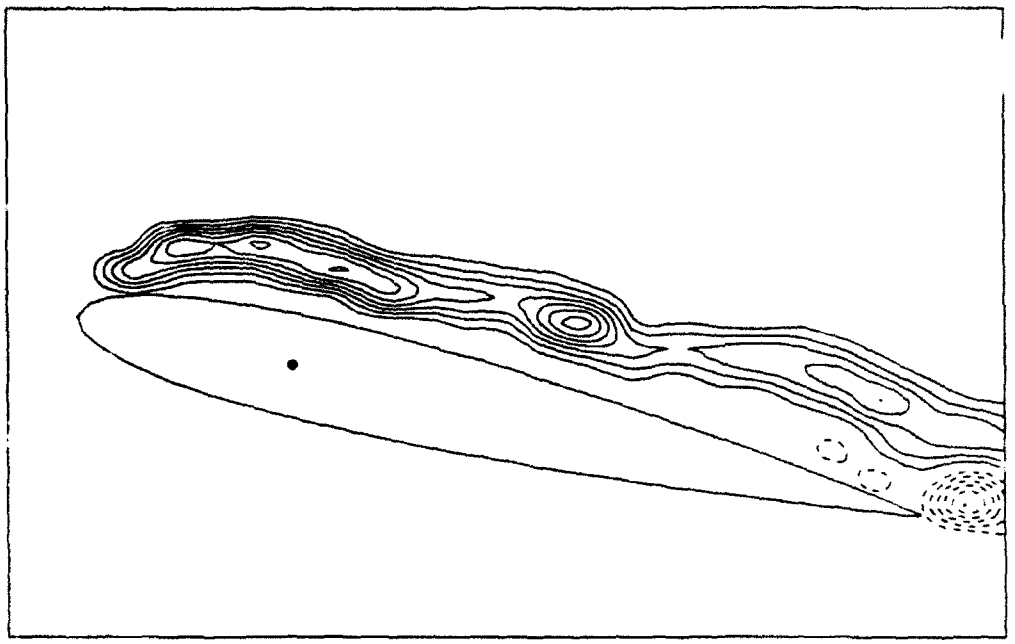

(a) $t^+=3.02$, $\alpha=13.6^\circ$

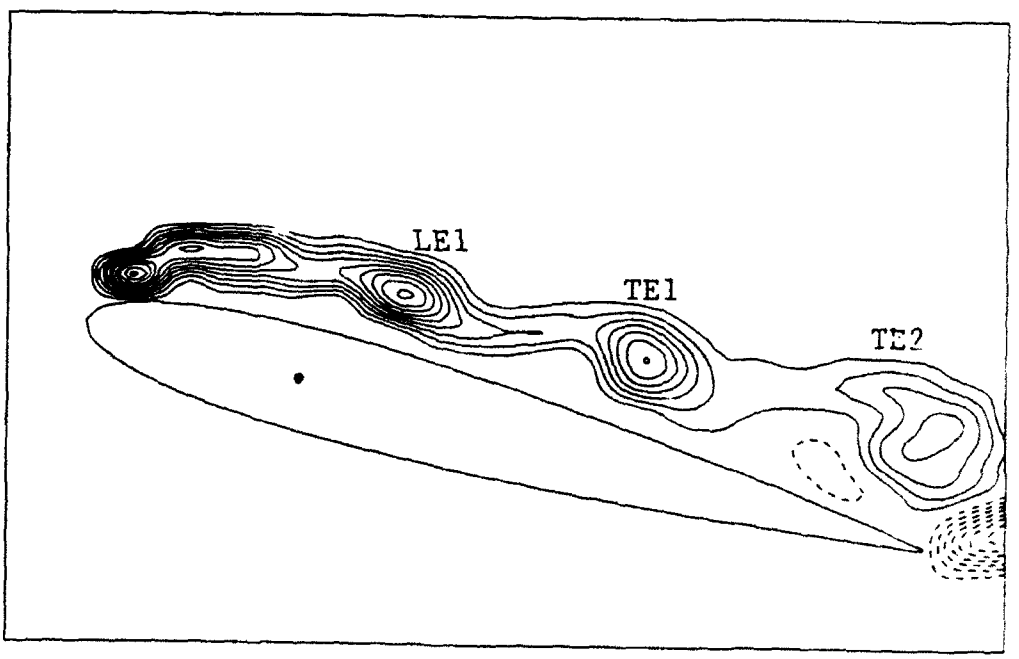

(b) $t^+=3.27$, $\alpha=14.8^\circ$

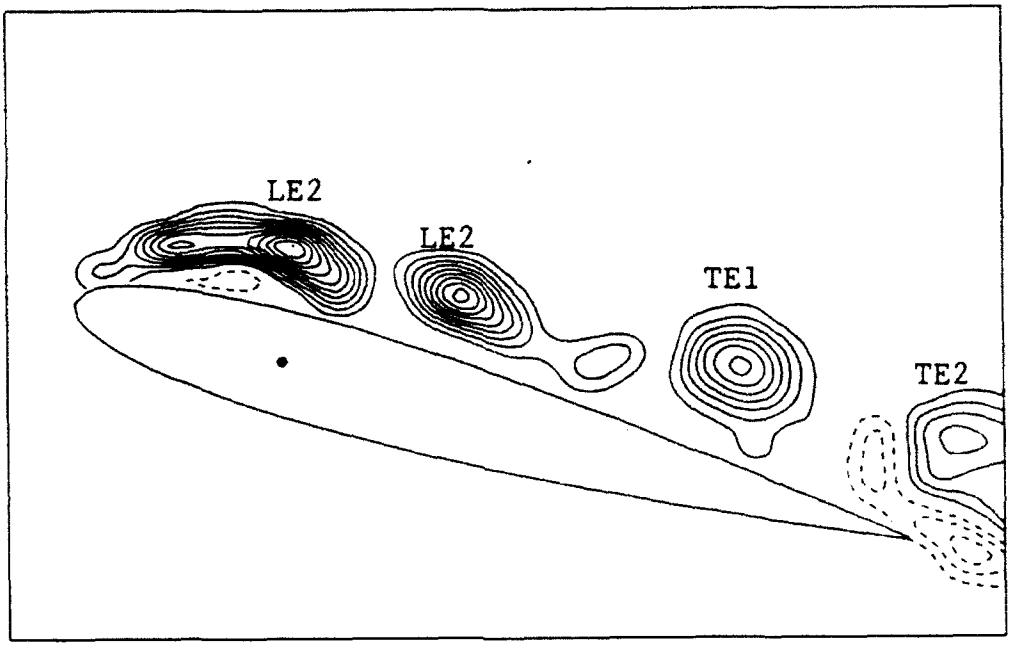

(c) $t^+=3.52, \quad \alpha=16.0^\circ$

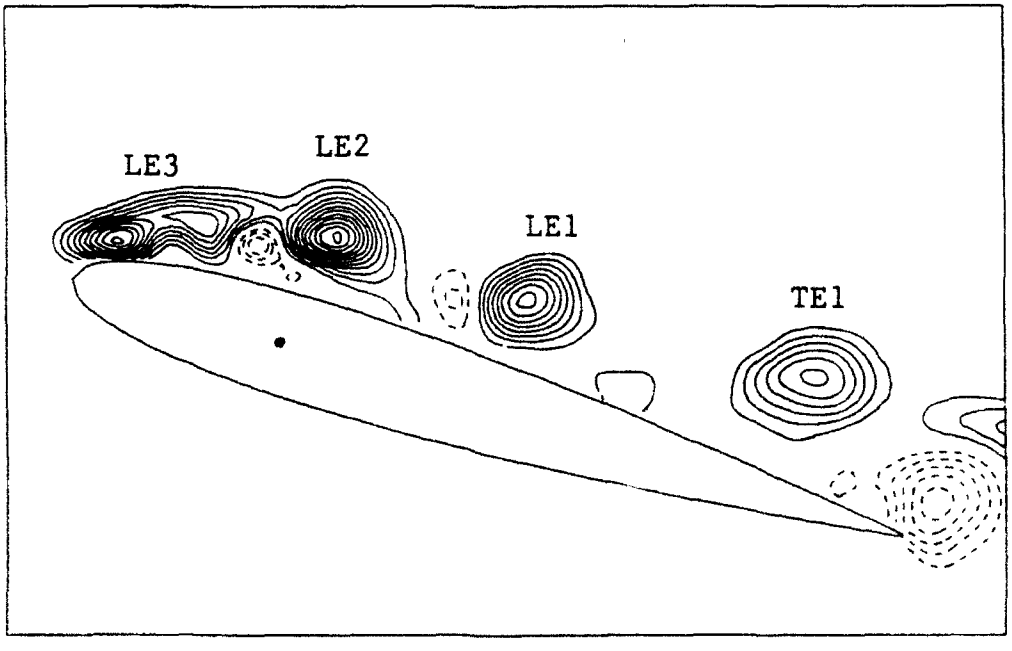

(d) $t^+=3.77, \quad \alpha=17.1^\circ$

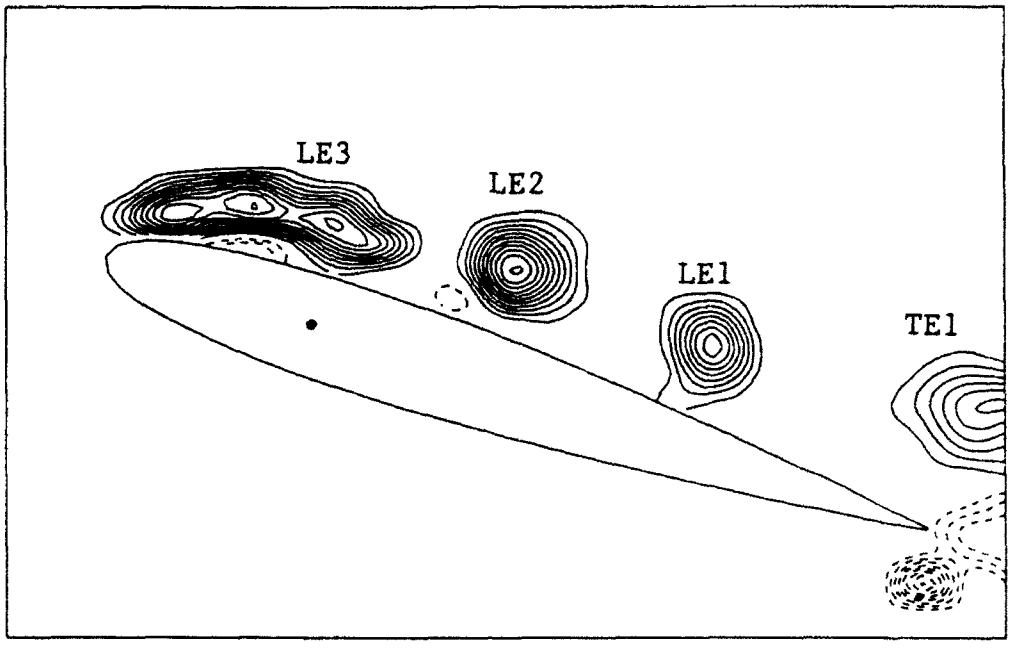

(e) $t^+=4.02$, $\alpha=18.3^\circ$

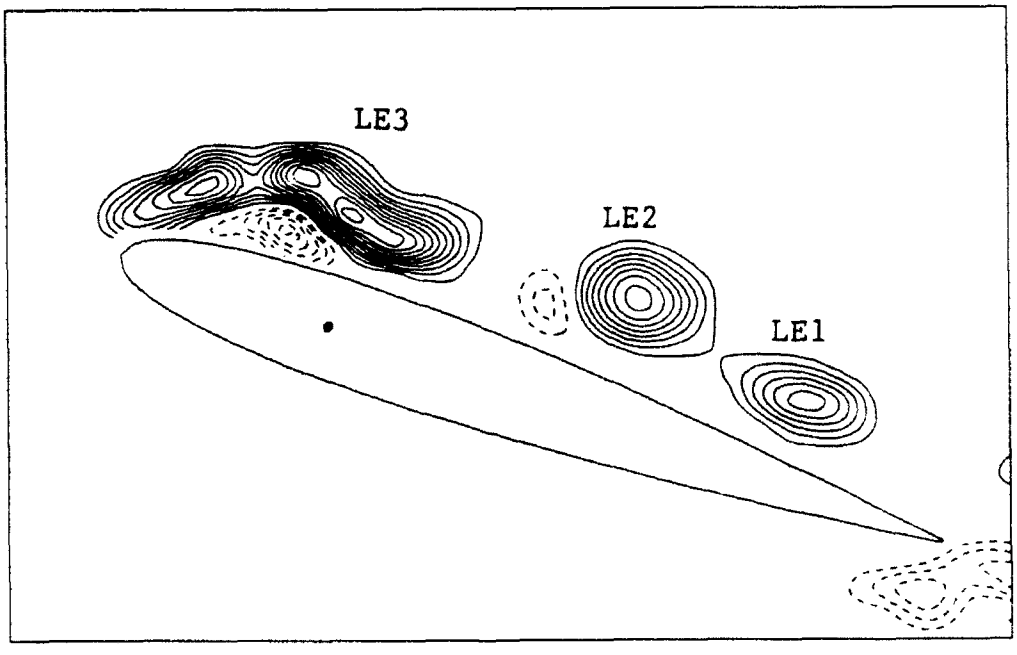

(f) $t^+=4.28$, $\alpha=19.4^\circ$

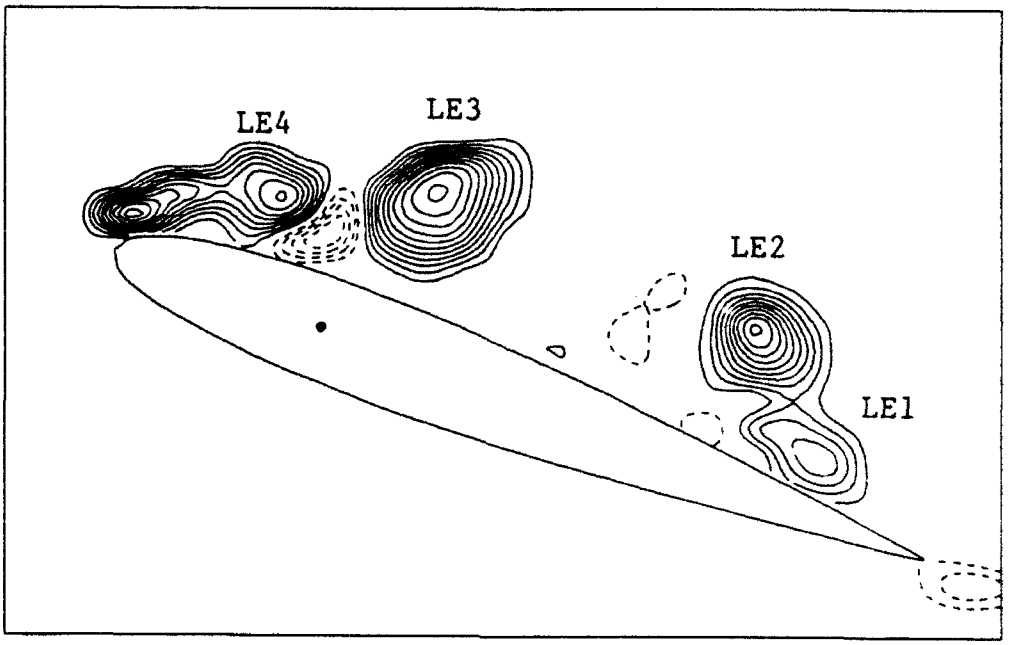

(g) $t^+=4.53$, $\alpha=20.5^\circ$

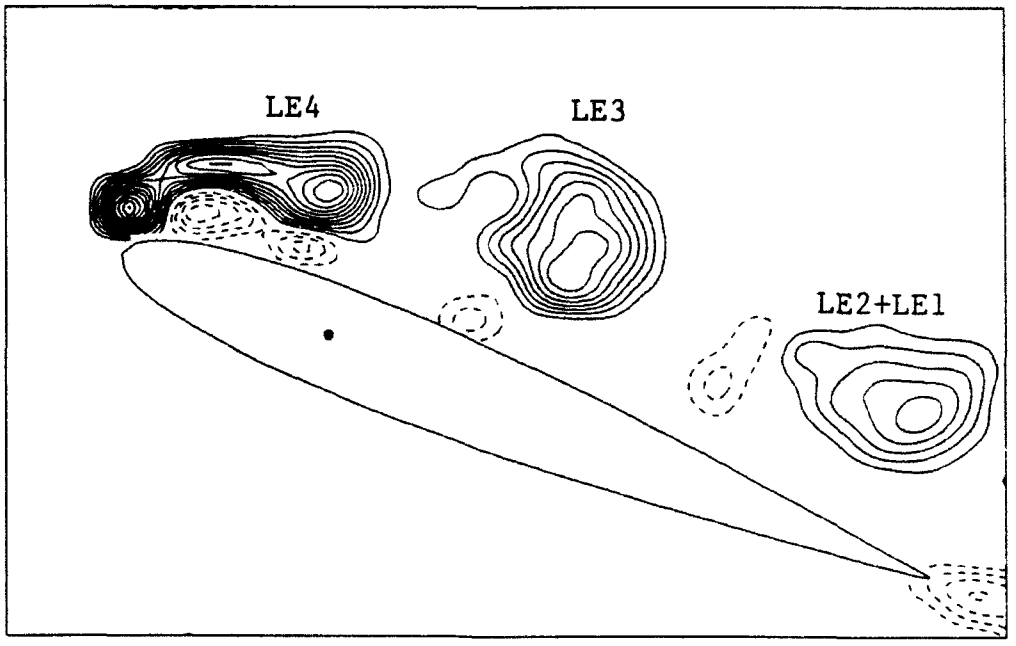

(h) $t^+=4.78$, $\alpha=21.7^\circ$

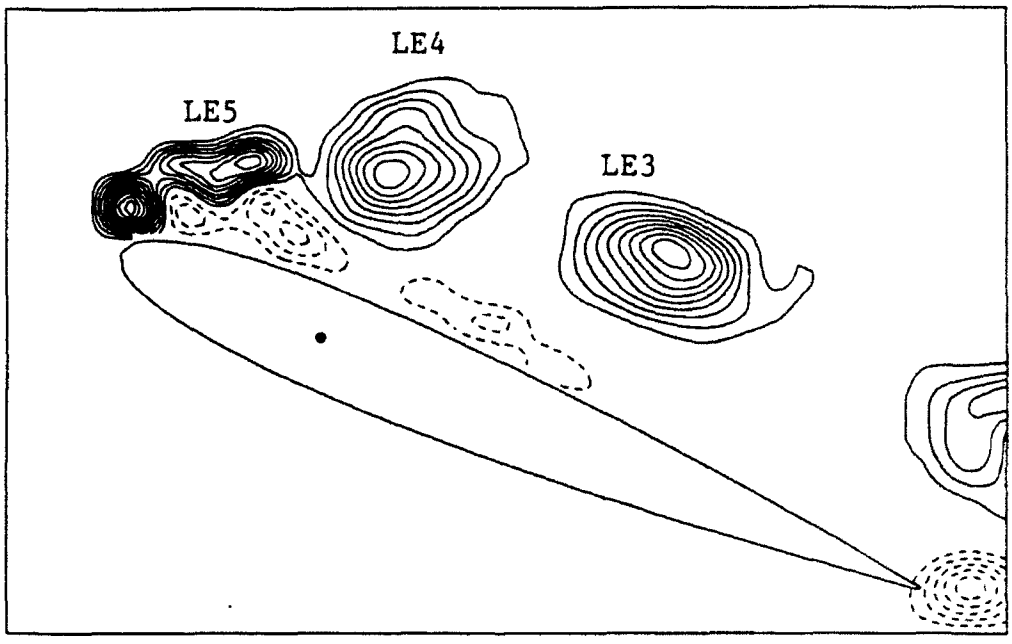

(i) $t^+=5.04$, $\alpha=22.8°$

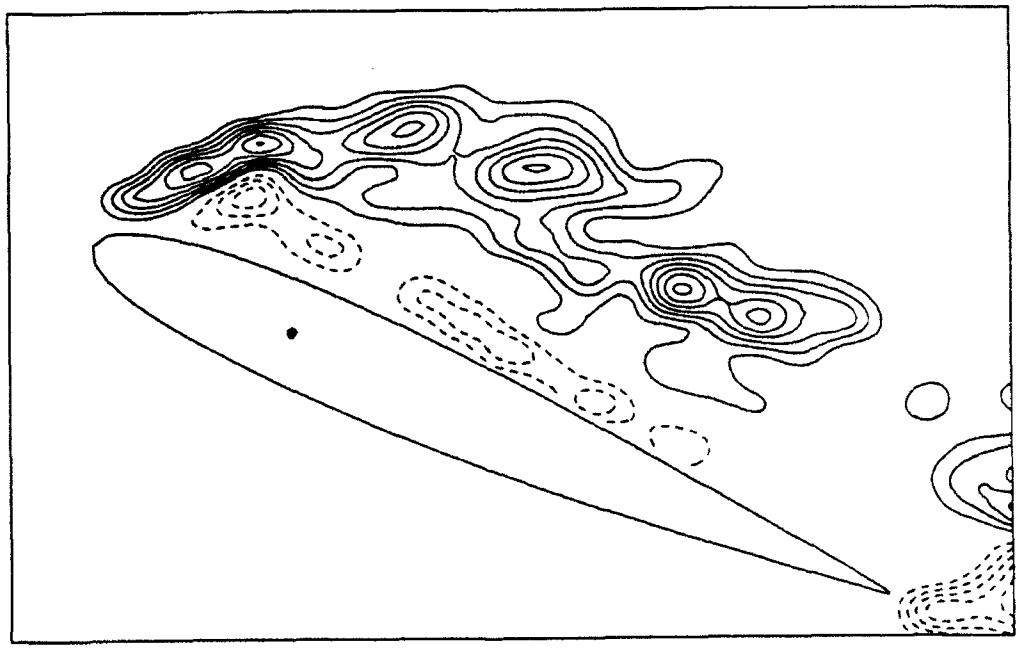

(j) $t^+=5.29$, $\alpha=24.0°$

Figure 9 Time sequence of the instantaneous vorticity field. Global flow field,

Re=5,000, $\alpha^+=0.08$

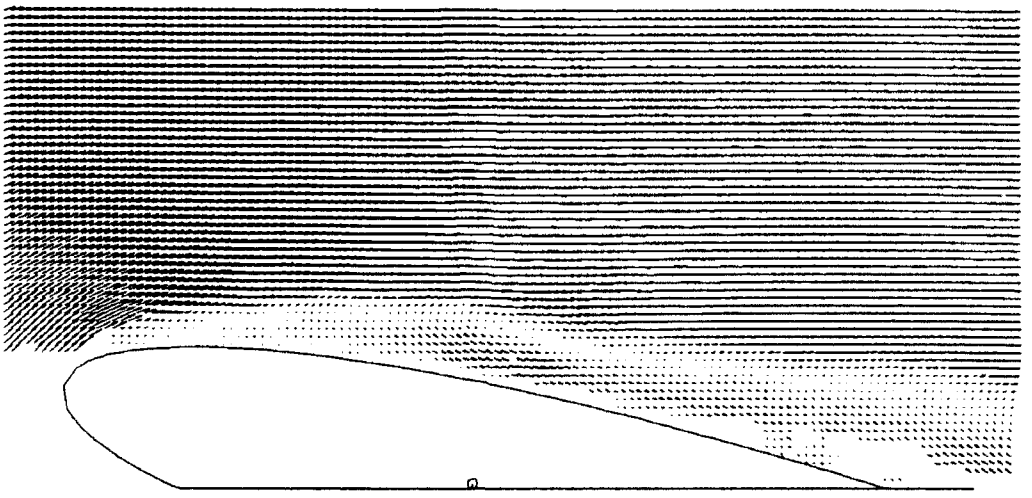

Instantaneous Velocity

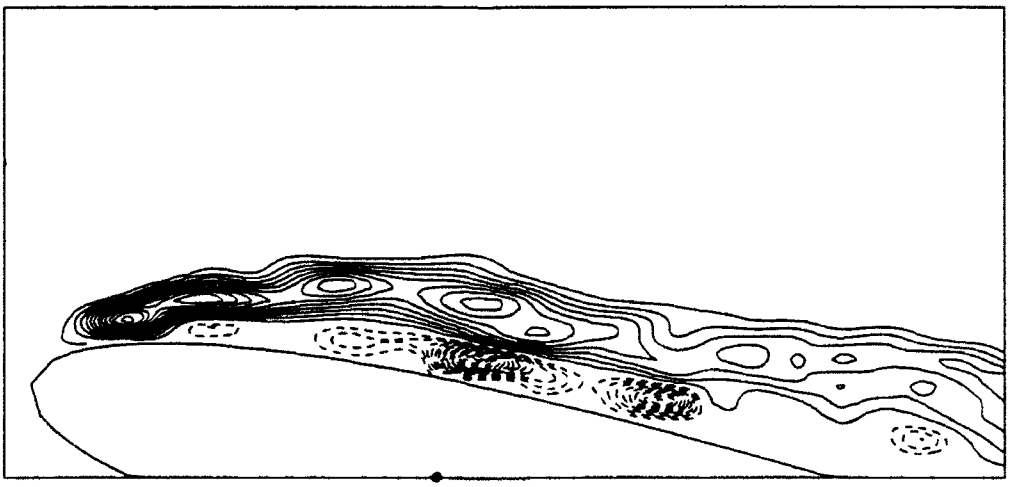

Instantaneous Vorticity

(a) $t^+=2.87$, $\alpha=13.0^\circ$

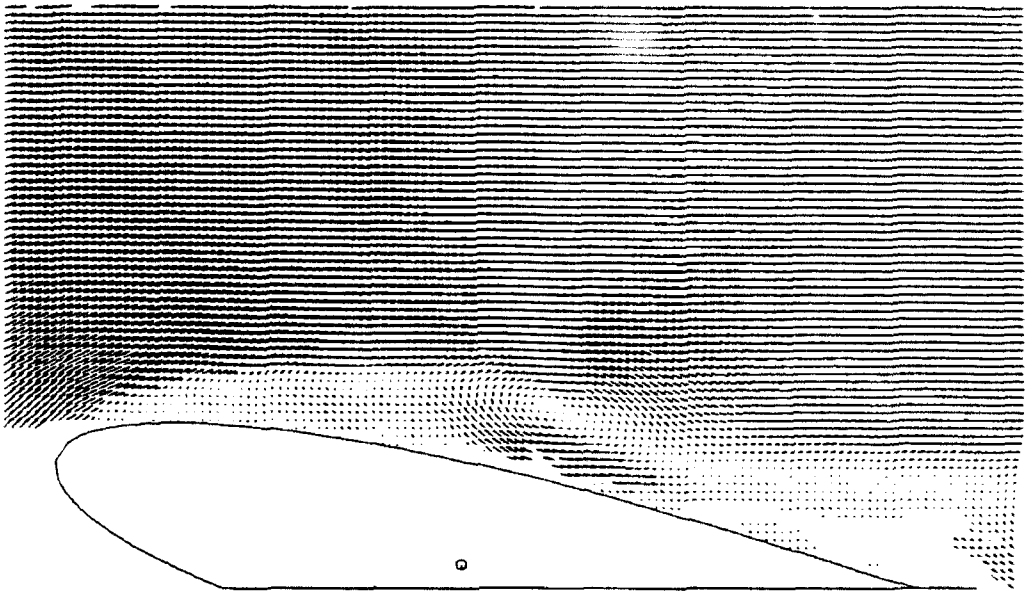

Instantaneous Velocity

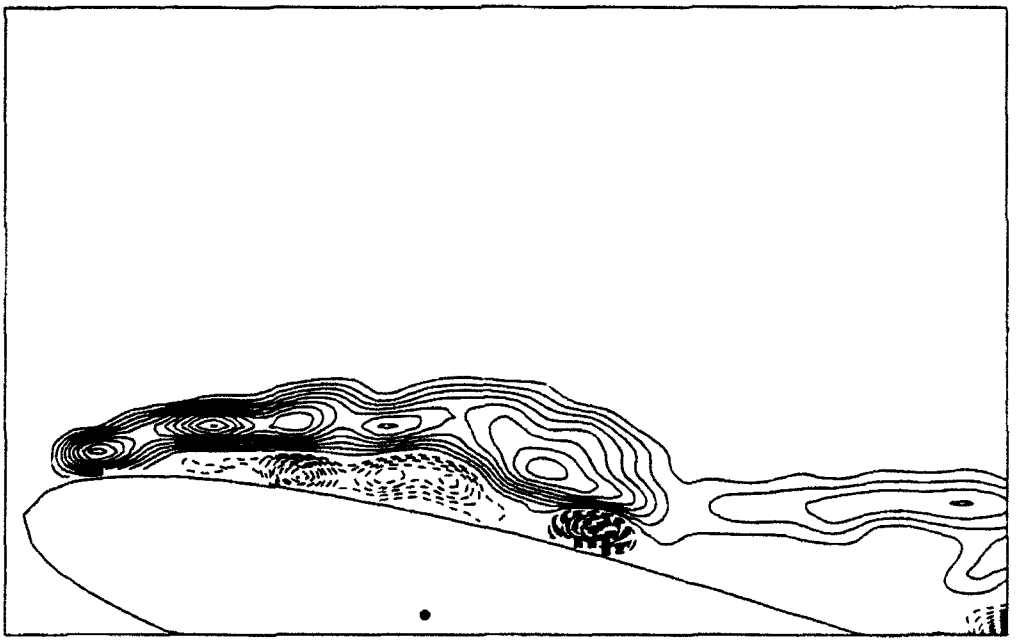

Instantaneous Vorticity

(b) $t^+=3.04$, $\alpha=13.8^o$

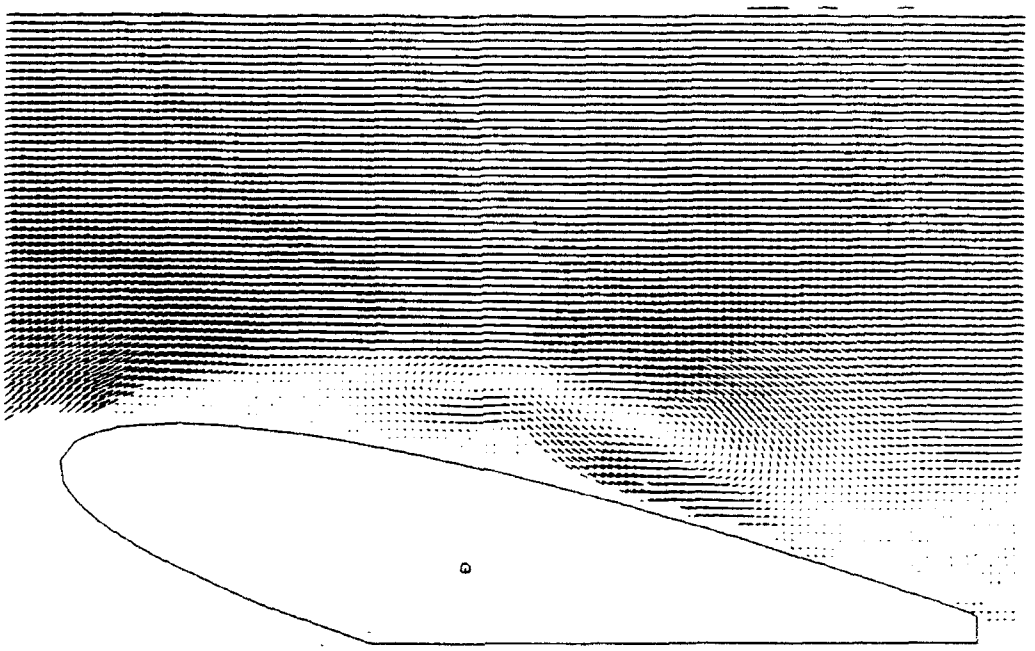

Instantaneous Velocity

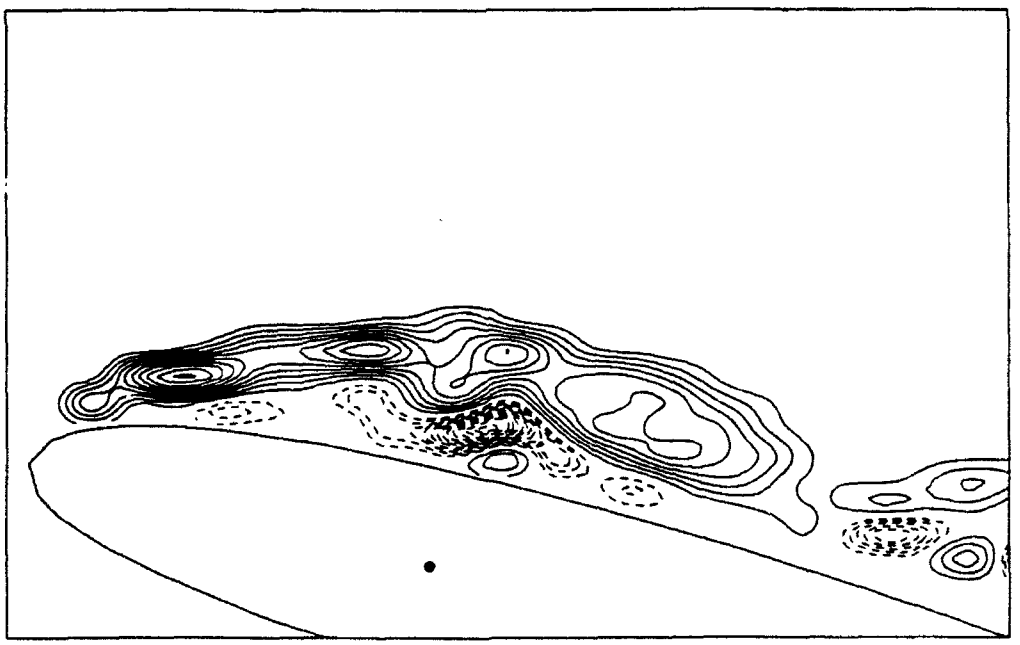

Instantaneous Vorticity

(c) $t^+=3.21$, $\alpha=14.6^\circ$

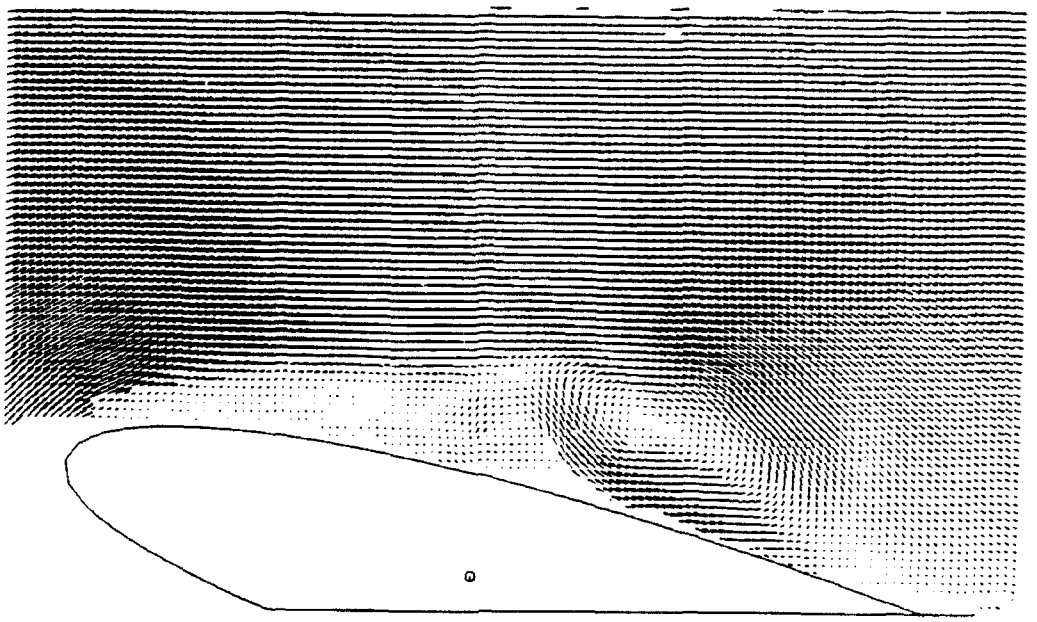

Instantaneous Velocity

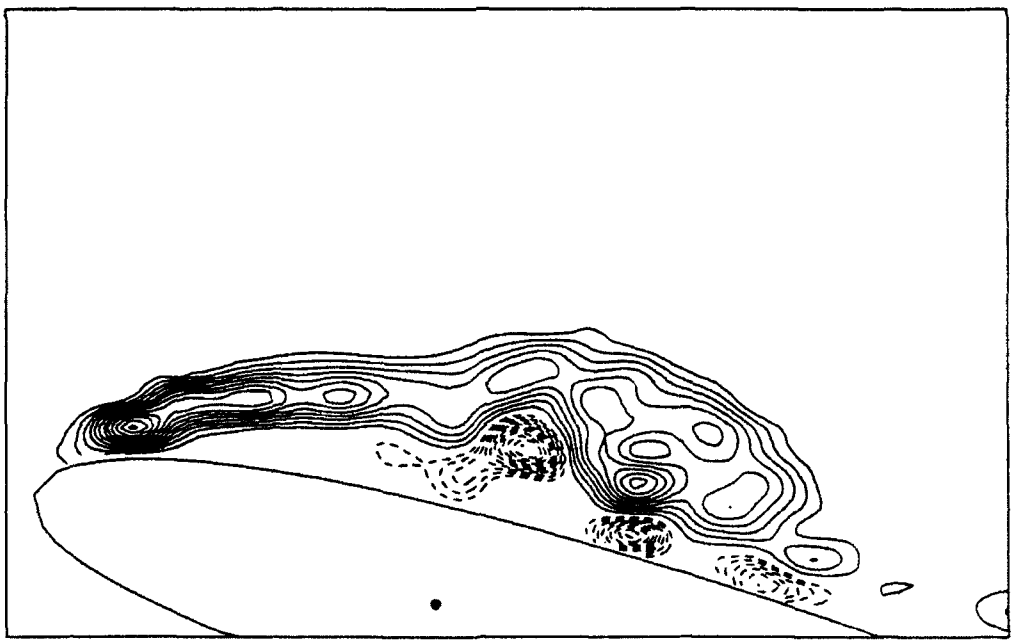

Instantaneous Vorticity

(d) $t^+=3.38$, $\alpha=15.4^\circ$

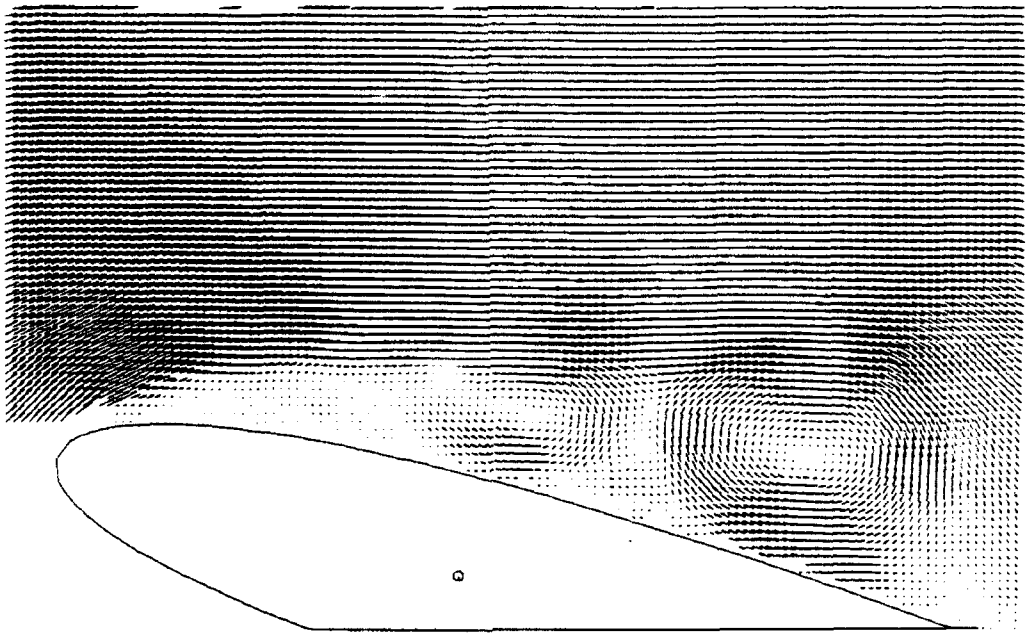

Instantaneous Velocity

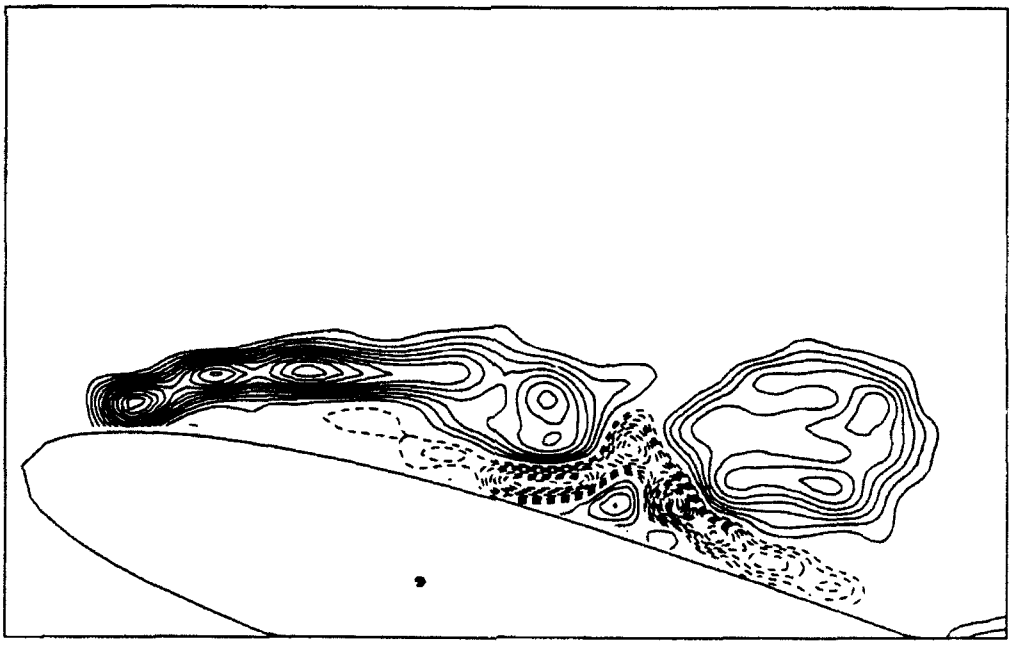

Instantaneous Vorticity

(e) $t^+=3.55$, $\alpha=16.1^\circ$

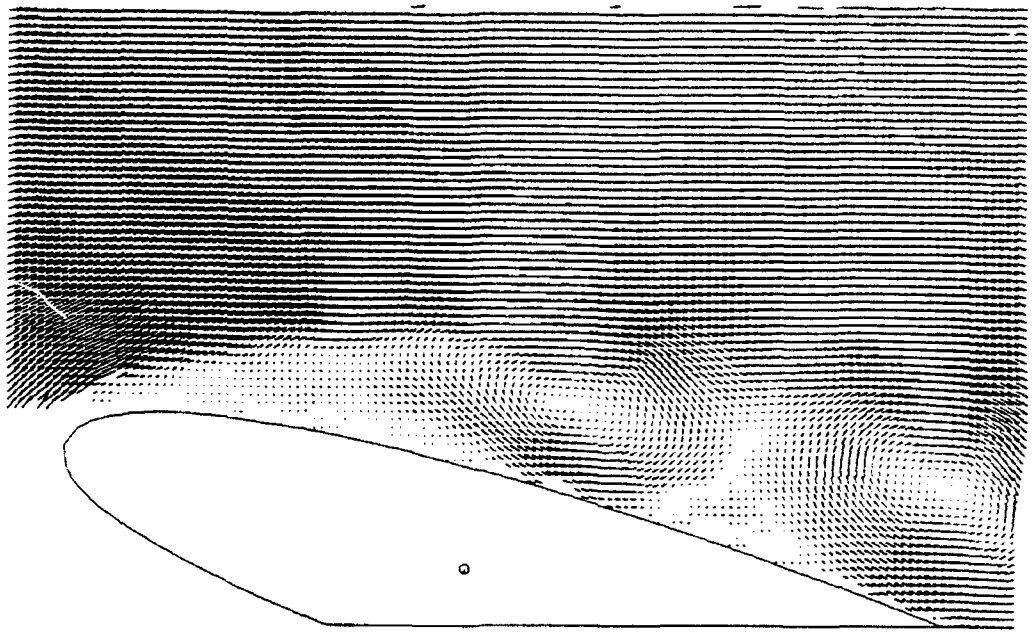

Instantaneous Velocity

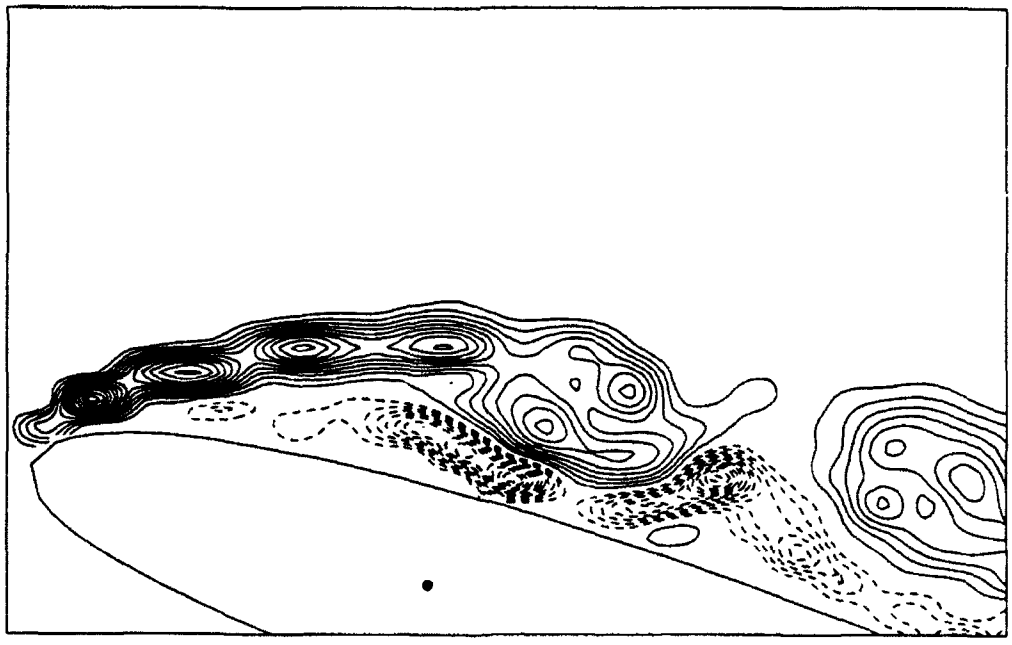

Instantaneous Vorticity

(f) $t^+=3.72$, $\alpha=16.9^\circ$

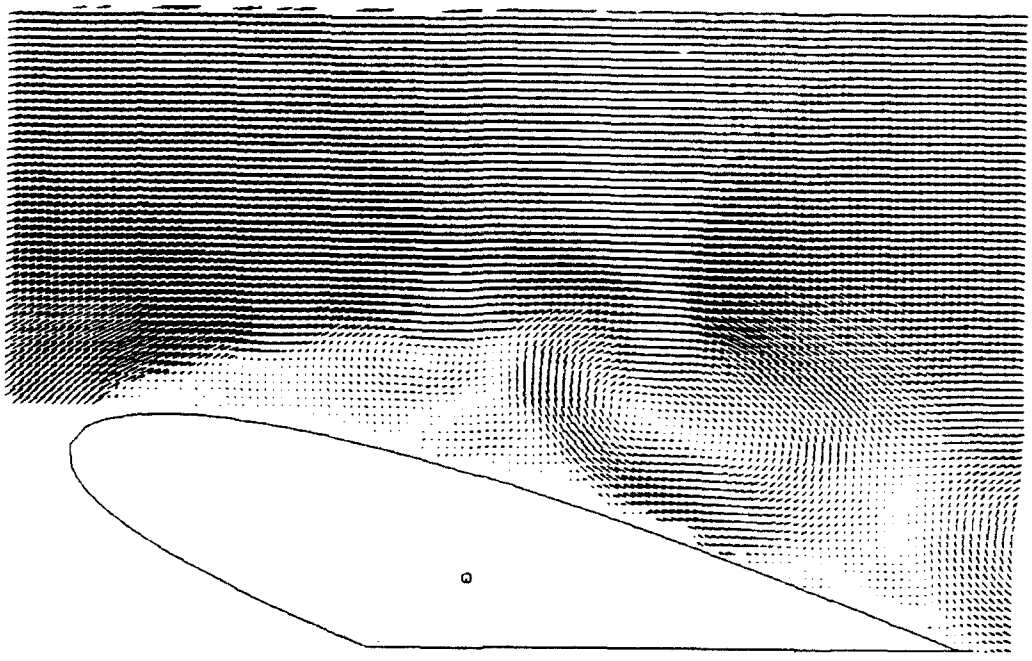

Instantaneous Velocity

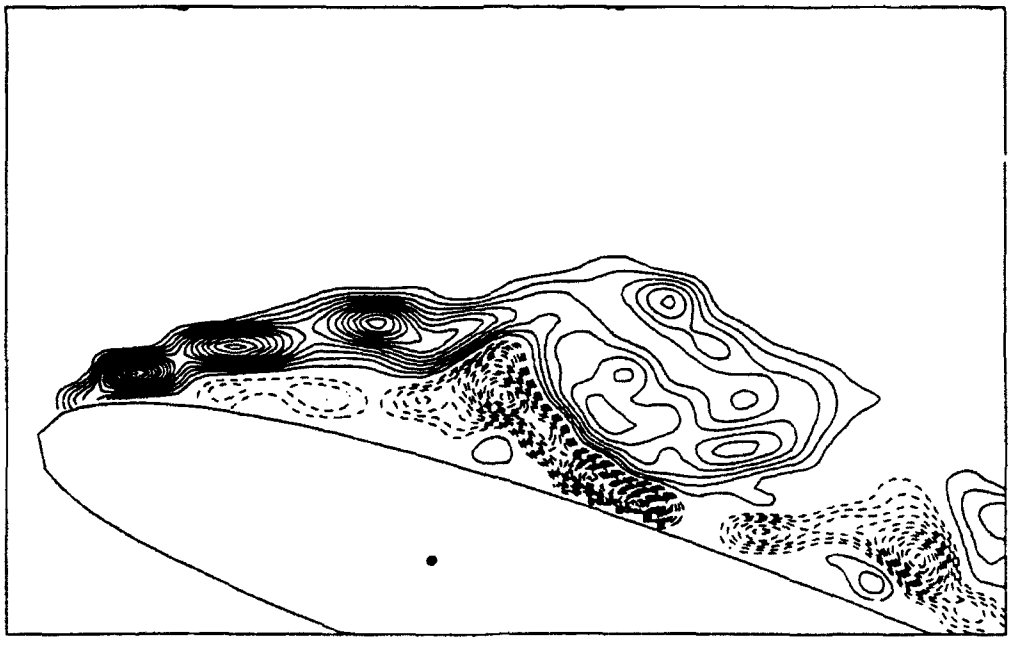

Instantaneous Vorticity

(g) $t^+=3.89$, $\alpha=17.6^\circ$

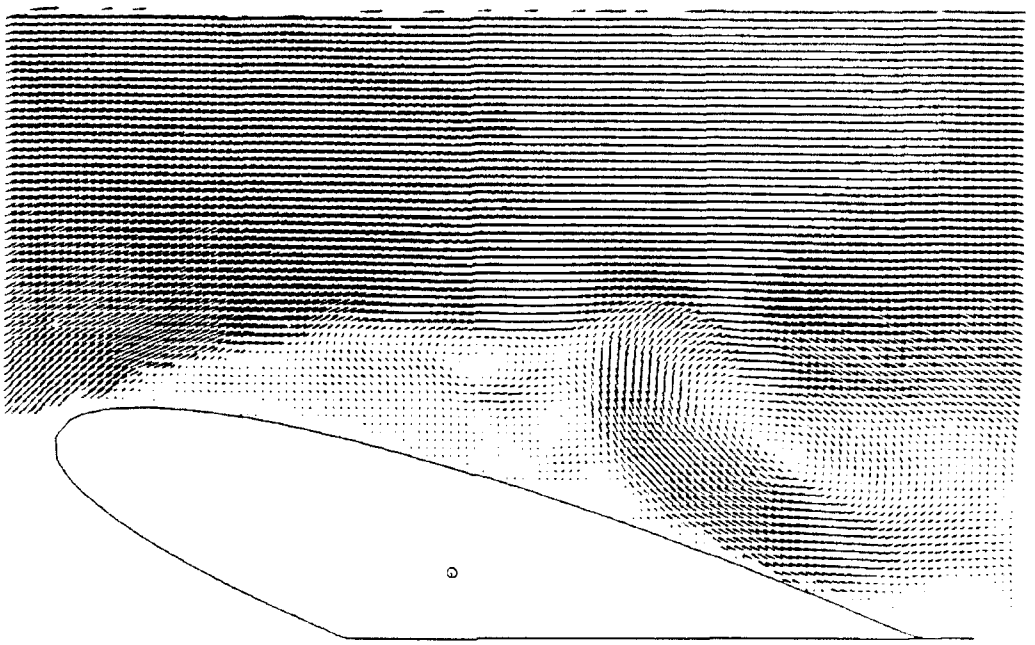

Instantaneous Velocity

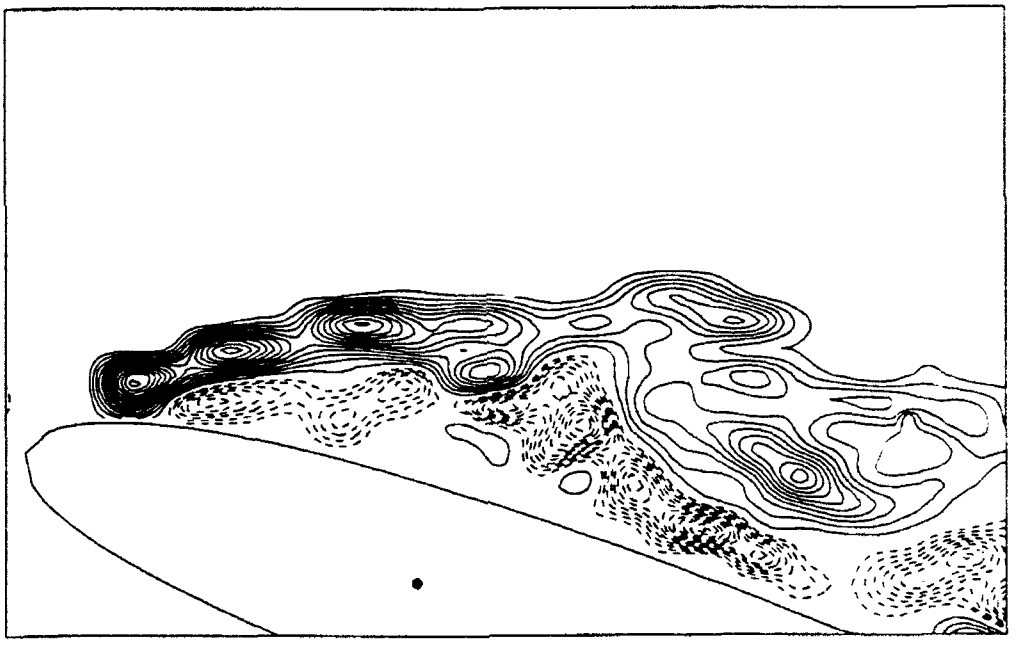

Instantaneous Vorticity

(h) $t^+=4.05$, $\alpha=18.4^o$

Figure 10 Time sequence of the instantaneous velocity and vorticity fields, leading edge region Re=5,000, $\alpha^+=0.08$

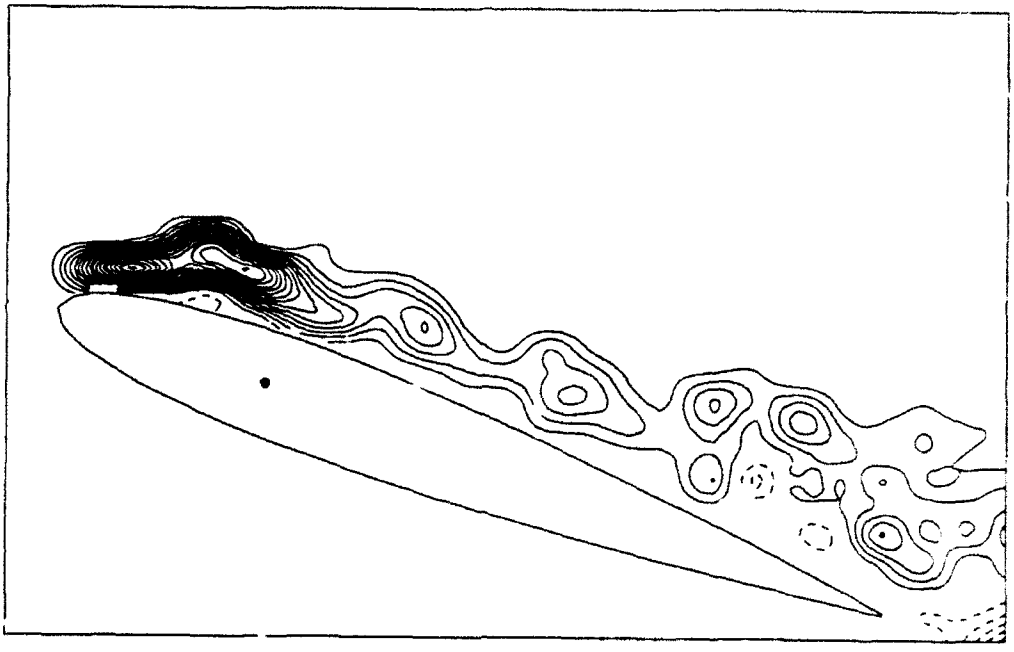

(a) $t^+=3.51$, $\alpha=26.3^\circ$

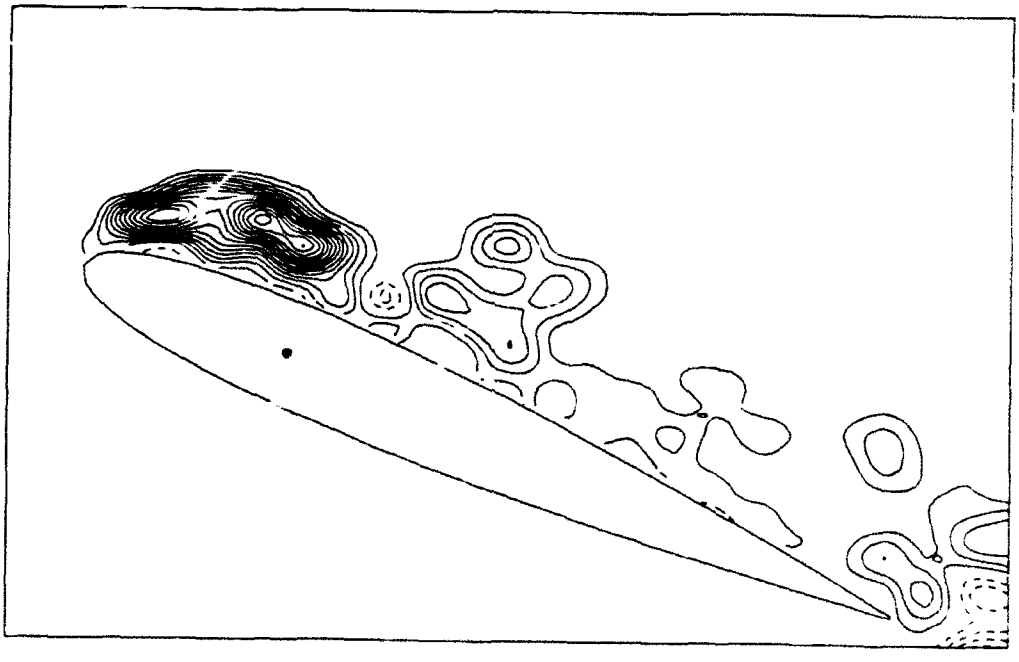

(b) $t^+=3.93$, $\alpha=29.5^\circ$

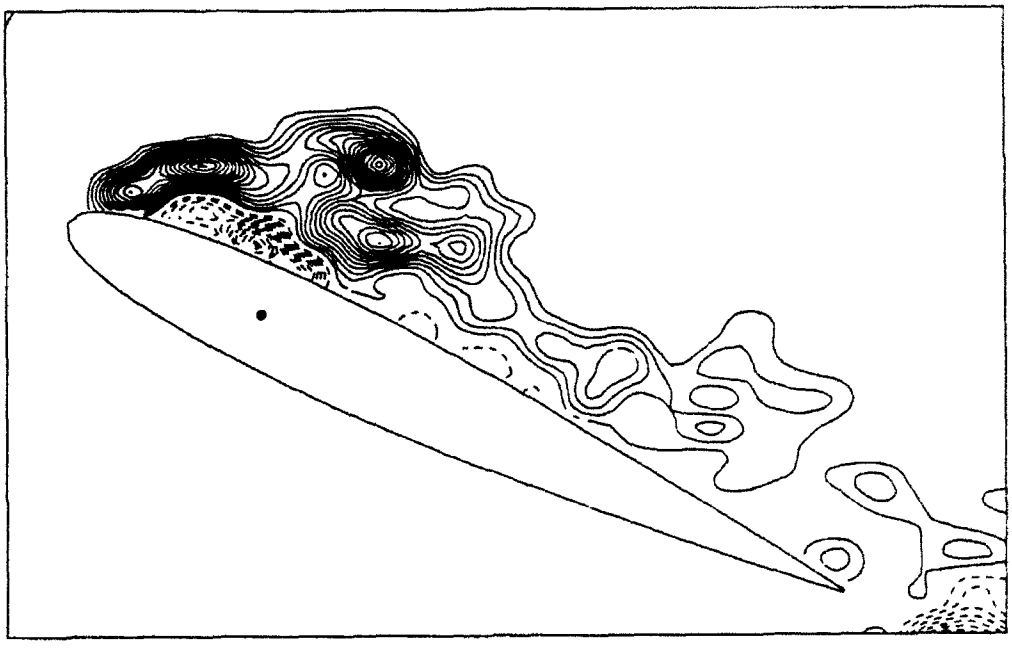

(c) $t^+=4.35$, $\alpha=30.0^\circ$

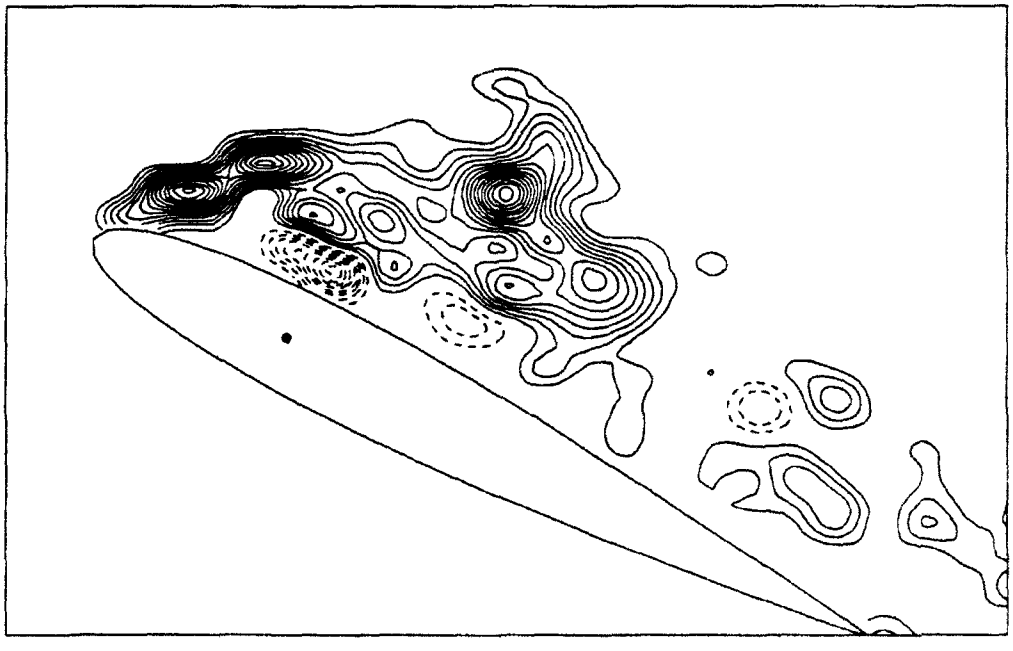

(d) $t^+=4.67$, $\alpha=30.0^\circ$

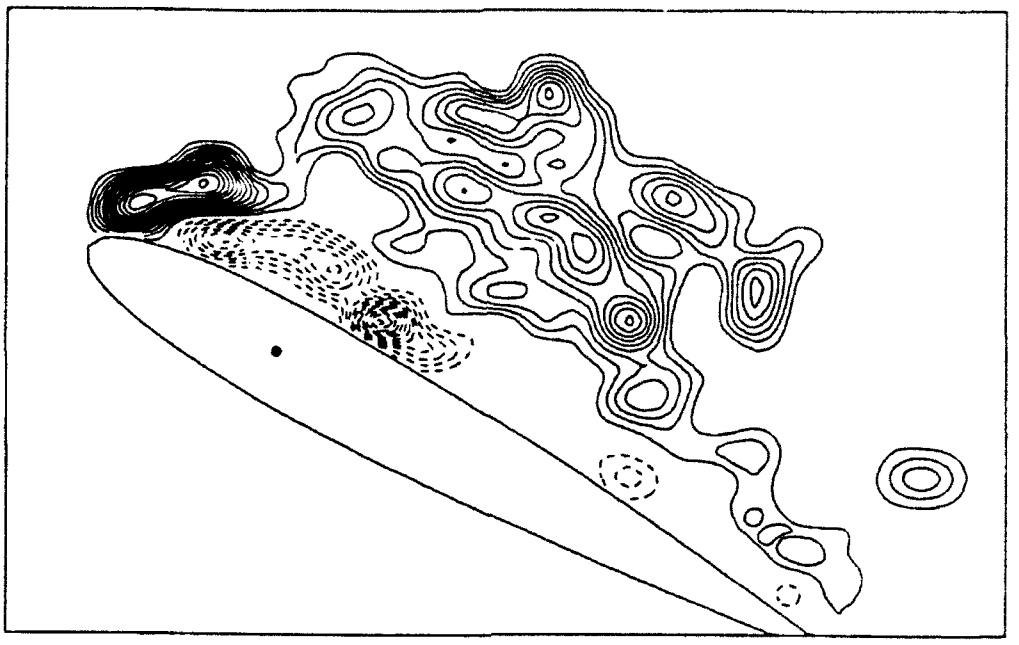

(e) $t^+=4.99$, $\alpha=30.0°$

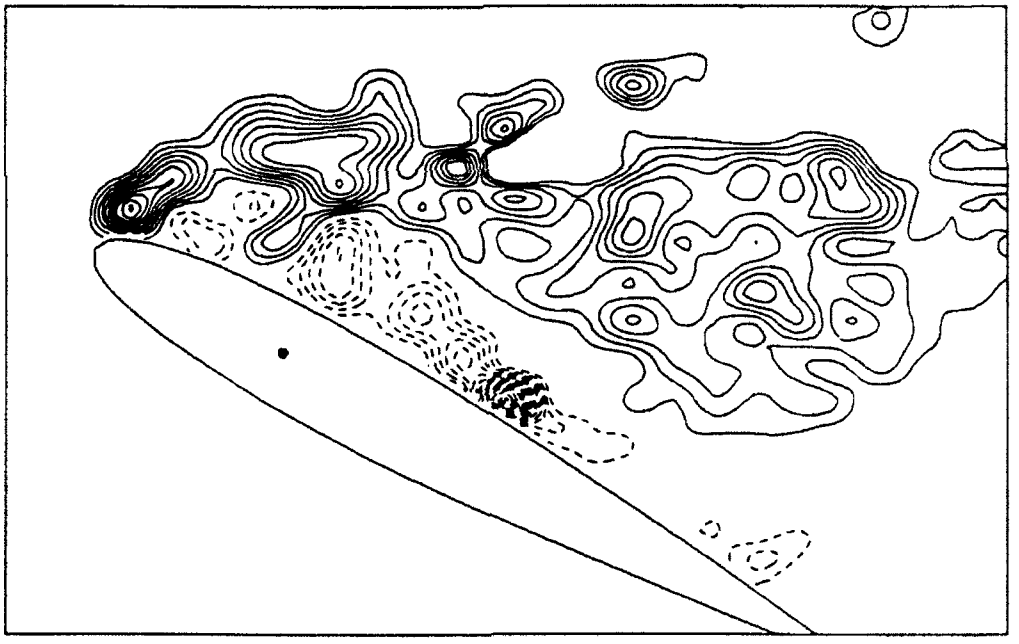

(f) $t^+=5.31$, $\alpha=30.0°$

Figure 11 Time sequence of ths instantaneous vorticity field. Global flow field.

Re=25,000, $\alpha^+=0.131$

Appendix II. Computational Results

First Year

Random-walk vortex simulations of the full Navier-Stokes equations were performed for comparison. In the computations, the flow field was represented by discrete vortex blobs. The diffusion processes were simulated by adding a random component of magnitude $\sqrt{2\nu\Delta t}$ to the vortex motion. In this form, the method approaches the solution of the two-dimensional Navier-Stokes equations in the limit of many vortices, although the rate of convergence is sizably slower than for conventional mesh–based methods.

However, unlike mesh–based methods, no accuracy is lost in describing the strong convection processes typical of unsteady separated flows. Additionally, the computational domain is truly infinite; there are no artificial boundary conditions. But most importantly, since computational elements are only used in the limited regions containing appreciable vorticity, the *resolution*, (the smallest processes the computation can distinguish), is much higher than possible in finite difference procedures or also vortex methods which include a mesh, such as the conventional cloud-in-cell technique.

The fast solution–adaptive Laurent series technique [1] was used to allow a large number of vortex blobs to be included without using a mesh–based fast solver to find the velocity.

The normal wall boundary condition was satisfied by mirror vortices, after a mapping of the airfoil onto a circle. The mapping used was a generalized Von Mises transform:

$$\frac{dZ}{d\zeta} = C \prod_{k=1}^{K} \left(1 - \frac{\zeta_k}{\zeta}\right)^{\gamma_k}$$

The constants C, ζ_k and γ_k are determined from least square mimimization. This mapping procedure is computationally much more efficient than other methods for vortex tracing and exactly produces an airfoil with a slightly blunted trailing edge which is indistinguishable from a NACA 0012.

The no-slip boundary condition was satisfied by the addition of vortices at the wall during each time-step. First all vortices within a distance of $1.27\sqrt{2\nu\Delta t}$ were removed. Then a ring of new vortices was added at a distance $0.675\sqrt{2\nu\Delta t}$ to correct the wall slip to zero. (The distance for adding vortices equals the diffusion distance of the vorticity generated by the wall during the time-step for the true Navier-Stokes equations; the removal distance was chosen based on a statistical study requiring that the scheme handles locally uniform vorticity distributions accurately, not unlike discretization techniques in finite difference procedures). The vortex diameter was rather arbitrarily chosen to be $0.675\sqrt{2\nu\Delta t}$; testing showed that results depended little on the actual value used.

In order to allow piching motion, the equations of vortex motion were developed in an inertial reference frame and subsequently converted to an airfoil based system. This is

required since Kelvin's theorem cannot be used in a rotating coordinate system. In terms of the conformally mapped complex airfoil coordinate ζ, the inviscid vortex motion is then given by

$$\left|\frac{dZ}{d\zeta}\right|^2 \frac{d\zeta^*}{dt} = -CV_0^* + C^*V_0\frac{1}{\zeta^2} + \dot{\beta}\left[\sum_{t=2}^{T}\frac{c_t}{\zeta^t} - iZ^*\frac{dZ}{d\zeta} + \frac{T_2^c}{\zeta^2}\left(1-\frac{\zeta_2}{\zeta}\right)^{\gamma_2} + \frac{T_3^c}{\zeta^2}\left(1-\frac{\zeta_3}{\zeta}\right)^{\gamma_3}\right] + \sum_v g_v\frac{(\eta-\eta_v)+i(\xi-\xi_v)}{(\xi-\xi_v)^2+(\eta-\eta_v)^2+d_v^2} - ig\frac{d^2Z}{d\zeta^2}\Big/2\frac{dZ}{d\zeta}$$

where Z is the complex physical airfoil coordinate, V_0 indicates the velocity of the origin of the airfoil coordinate system and $\dot{\beta}$ its rate of angular rotation, while the star indicates the complex conjugate. In the sum in the second line, the coefficients c_t depend on the airfoil shape and are found from a fast Fourier transform; the final two terms in the second line capture the singular behaviour at the kinks in the contour at the blunted trailing edge. These terms are needed to obtain a computationally efficient convergence of the Fourier series. The sum in the third line represents the interaction between vortex blobs: the sum includes the mirror vortices. It is this sum which is performed using fast summation. The final term represents the self-induced motion of the vortices due to the physical airfoil shape.

The force on the airfoil is found from

$$\frac{F}{\rho} = 2\pi\left(\dot{C}_1 - i\dot{\beta}C_1\right) + A\left(\dot{V}_0 - i\dot{\beta}V_0 - \dot{\beta}^2Z_c - i\ddot{\beta}Z_c\right)$$

and the moment from

$$\frac{M}{\rho} = 2\pi\left(\dot{S} - \Im(C_1V_0^*)\right) + 2(I_c + AZ_cZ_c^*)\ddot{\beta} + A\Im\left(Z_c\dot{V}_0^* + i\dot{\beta}Z_cV_0^*\right)$$

Here

$$\frac{C_1}{C} = -V_0C^* + V_0^*E - \dot{\beta}(T_2^c + T_3^c + c_2) + \sum_v ig_v\left(\frac{1}{\zeta_v^*} - \zeta_v\right)$$

$$S = \sum_v \tfrac{1}{2}g_vZ_vZ_v^*$$

while A is the airfoil area, Z_c the center of area, I_c the polar moment of area and E the coefficient of the $1/\zeta$ term in the asymptotic expansion of Z for large ζ. The sums do not include the mirror vortices.

The actual vortex computations were performed on various supercomputers (ETA 10, Cray YMP), and results were post-processed on the College of Engineering Vax Cluster. In post-processing, fast Fourier transform techniques were used to determine the streamlines. The vorticity was represented in bit-mapped graphics as half tones.

Second Year

Vortex simulations of the Navier-Stokes equations were performed to study unsteady stall from a NACA 0012 airfoil at large angles of attack. In particular the evolution from an initially attached condition to a stalled state was studied [2,3]. The numerical simulations determined the behaviour of lift and drag and vorticity motion, following the development of the Van Dommelen and Shen process. Computations focussing on the formation of the leading edge vortex at the nose were also performed [4]. They were used to assess the effects of suction and wall motion on the separation process.

In the theoretical area, the mechanism of the initial break-up of the boundary layer in general two- and three-dimensional flows was determined using Lagrangian analysis. The results apply to both the incompressible and compressible cases [5,6,7,8]. As a result, a good understanding of the process with which the boundary layer breaks up has been achieved. Such an understanding is important, since it proves that manipulation of the separation process must be performed early in order to be effective.

The question of the next, interactive, stage in the evolution was also addressed [9,10], by the development of an appropriate model which can be analyzed relatively easily, while it still provides a theoretically rigorous description. One apparent result of Navier-Stokes computations which has already been verified is that interaction will enhance, rather than delay the break-up of the boundary layer. This behavior is the opposite of the case of steady stall. However, that profound differences between steady and unsteady stall exist has been long known.

In the area of algorithm development, a first step was token toward the extension of the vortex method to more general flows. A 'redistribution method' was formulated [11,12], and its convergence shown. Like the random-walk procedure, the redistribution is mesh-free, but it is more accurate and more general.

Third Year

The numerical results for stalling wings [13,14,15] showed that at high angles of attack, the first significant flow development is the occurrence of unsteady boundary layer separation. The separation is located near the leading edge and takes the form of a local thickening of the boundary layer according to a Van Dommelen and Shen process. By detailed studies of the flow near the leading edge, it was shown that this separation is distinct from the separation which develops near the trailing edge and which moves upstream from that location.

Previous authors have reported trailing edge separations which would move sufficiently far upstream to reach the leading edge region. However, their definition of 'separation' was based on the streamline picture. It is known that in unsteady flow the streamline picture, including the formation of a 'recirculating wake' or a streamline leaving the wall does not imply a significant departure of most of the boundary layer fluid away from the wall. This was first pointed out independently by Moore [16], Rott [17], and Sears [18] and generalized by Sears and Telionis [19]. The reason is that the particle paths rather than the instantaneous streamlines describe where the boundary layer vorticity ends up.

Sychev [20] and Van Dommelen and Shen [21] were the first authors to derive the flow structures for the unsteady case under different circumstances. The structure derived by Van Dommelen and Shen is the relevant one here. Both analytical structures show that unsteady separation is indeed completely different from the steady case described previously by Sychev and by Smith. Other authors verified and extended the unsteady results, eg, Elliott, Cowley and Smith [22]; other references may be found there and in [5,9].

In particular for the circular cylinder, the numerical evidence is further overwhelming [23-29]. These developments are slow in reaching certain parts of the CFD and experimental communities, which often still use concepts such as unsteady streamlines or zero wall shear in describing 'separation'. The difficulty is that the steady separation is characterized by intuitively 'evident', easily verified criteria (zero wall shear, detachment of the wall streamline, reversed flow), and some practitioners have great difficulty accepting the fact that the unsteady separation criteria become quantititative, and difficult to verify. This leads to the numerous attempts to relate the simple steady criteria to the unsteady boundary layer separation processes, futile since those criteria have already been proven not to have a direct correlation to unsteady separation.

Due to the Van Dommelen and Shen separation process, an extensive dynamic stall vortex develops above the wing. By numerically tracking the vorticity, it was shown conclusively that while this vortex moves downstream out of the leading edge region, the vorticity that it contains does originate from the leading edge. Despite the presence of the dynamic stall vortex, initially the lift does not change significantly from its attached unsteady flow value, and is much higher than the value for attached steady flow. The reason why it is possible to have a quite sizable vortex above the wing without a significant loss of lift is the influence of the vortex on the wing surface below. In fact as long as the vortex stays near the wing surface, it can be shown that the lift is maintained, by using the control volume form of the momentum equations following Wu [30].

The next significant stage occurs when the vortex is convected past the trailing edge; around that time the lift force produced by the wing drops off rapidly. The reduced circulation around the wing cross section allows the flow near the nose to reattach, the lift builds up again, a new Van Dommelen and Shen process develops near the nose, and the cycle repeats itself.

While the lift only collapses when the main vortex leaves the vicinity of the wing surface, experience shows that it is difficult to prevent this loss of wing effectiveness once the vortex has been shed from the leading edge. For that reason, recent work has focussed on eliminating the the vortex altogether. To do that, the Van Dommelen and Shen process must be prevented. Since this process occurs in the middle of the boundary layer, rather than at the wall, it is hard to modify in its final stages. Early recognition and corrective action is therefor essential.

The structure of the Van Dommelen and Shen process provides insight in what procedures can be effective. It is known that the process requires a layer of boundary layer fluid near the wall with vorticity of opposite sense compared to the remaining boundary layer above it. This reversed vorticity is ordinarily associated with reversed flow in the boundary layer. However, it is possible for the process to occur even after the reversed flow has been eliminated by a favorable pressure gradient.

It is also known that the actual boundary layer thickening in the Van Dommelen and Shen process occurs near the line where the lower reversed vorticity layer meets the other boundary layer fluid above. For that reason, a possible procedure to prevent the Van Dommelen and Shen process is to inhibit formation of reversed vorticity. This can be achieved by giving the wing surface near the leading edge a motion in the direction of the flow of the air, so that the surface does not retard the fluid motion in the boundary layer sufficiently to cause separation. In actual applications, a rotating cylinder can be installed at the leading edge [31].

Numerical experiments show that this procedure performs as expected. Without correction, the leading edge vorticity rolls up into a discretized vortex which eventually leads either to the loss of lift for wings with a small leading edge sweep angle or to the lead ing edge vortices for delta wings. With sufficient motion of the wing surface, the vortex formation can be suppressed.

The amount of wall motion is still too high for practical purposes, since a very small cylinder would have to be installed in the leading edge and rotate with an excessive rpm. However, this is in part due to the assumption that the nose shape is unchanged in our computations, leading to an excessively small nose radius and correspondingly small cylinder. It is more appropriate to replace the entire wing leading edge shape by a cylinder of a diameter comparable to the wing thickness. The most important conclusion which can be drawn from our preliminary computations is that wall motion does work, while its practicality still needs further study.

A second procedure is to allow the wing surface to retard the boundary layer fluid, but remove any reversed vorticity which is created by means of suction through the wing surface. This renders the Van Dommelen and Shen process impossible. It is well known that suction is effective for steady separation, which forms the limiting case of unsteady separation, yet there it has never found widespread popularity. The application to rapidly

maneuvering aircraft changes the balance however, since suction needs only be provided for high angles of attack, rather than continuously, and low drag is less important. As a result, the effectiveness of suction must be reevaluated for this application. For example, the suction could be provided by lowering a venturi duct into the flow during the transient maneuver, accepting the resulting drag penalty. Clogging of suction holes is less critical since stall at high altitudes is recoverable.

Figure 1 shows that for a NACA 0012 airfoil without suction, large scale separation occurs. For this particular case, the airfoil was started impulsively at 30 degrees angle of attack; however, other computations show similar separations for travelling wings which pitch up more gradually to high angles of attack. Applying light suction leads to the much smaller separation in figure 2, and stronger suction maintains the attached flow shown in figure 3. The computed lift history demonstrates that with suction the lift is indeed maintained. The suction coefficient describes how much boundary layer fluid is being removed, and should be as small as possible. Figure 2 corresponds to a suction coefficient $c_Q\sqrt{Re} = 1.9$ and figure 3 to 3.8. These values are about the same as values for the steady case at Reynolds numbers in the range of 10^6 [32].

Experimentation showed that the smallest suction coefficients are obtained when continuous suction is applied in the range from the leading edge until 20% of the cord downstream, in agreement with steady flow observations. This good agreement with steady data may in part be due to the fact that continuous suction was applied. It has been suggested that suction should be applied further downstream, to prevent the formation of the secondary vortices induced by the dynamic stall vortex. However, computations shows that this delays, rather than prevents the collapse of the lift for the same amount of suction. In order to maintain lift for longer times, the primary Van Dommelen and Shen process needs to be prevented, rather than its secondary effects.

For transient maneuvers, it is possibly to further reduce the suction volume by applying suction only as needed, less in the initial stages when there is no reversed vorticity yet, and less in the final stages when the angle of attack returns to normal. Preliminary tests have proved to be very encouraging, and are continuing.

Other possibilities to prevent the Van Dommelen and Shen process exist. An example is injection of a jet to energize the boundary layer. Blowing can also applied at the trailing edge; in that case its effects are most likely due to modification of the interaction of the dynamic stall vortex with the trailing edge, rather than to prevent the formation of this vortex. As a result, intermittent blowing might be effective here. Near the trailing edge, the correct strategy is to induce the trailing edge to shed new starting vorticity when the dynamic stall vortex passes it. For manipulation of the flow by blowing, the additional construction weight requires consideration. Another method, which does not require additional weight, is to pitch the plane down and up again when the dynamic stall vortex passes the trailing edge. We have conducted preliminary numerical experiments, but the results are still inconclusive. More study is needed in this area. An approximate

model for the trailing edge flow would be helpful in deciding the optimal airfoil motion.

Further the nose shape may also be altered in order to delay the separation, or allow it to occur at a more favorable location further downstream. However, since the possible gains seem limited, investigations in this area have received low priority. Finally a slat may be used during the transient maneuver. Additional construction weight and the possibility of mechanical failure are considerations here.

Most of the methods above are based on preventing the layer of reversed boundary layer vorticity in the Van Dommelen and Shen process. A different approach now being studied makes use of another property of the Van Dommelen and Shen structure: its instability. The velocity profiles of the process are highly unstable, since the upper part of the boundary layer behaves as a free vortex layer. At high Reynolds numbers, such velocity profiles can only occur in transient flow, in which free stream disturbances have only a limited time to grow. The idea now is to augment the disturbances by selectively forcing the most unstable frequencies. The large perturbations increase the mixing and energize the flow near the surface, to prevent separation. The effect is similar to the reduction in drag coefficient of blunt bodies when the separation turns turbulent. Advantages of this procedure is that the perturbations can be provided by a variety of methods, and rapid response times are possible.

A significant amount of promise still exists for further developments in this area, but current emphasis has shifted towards three-dimensional and compressible flows. Yet one graduate student is still pursuing these areas further even without outside funding.

References

1 Van Dommelen, L.L. and Rundensteiner, E.A., "Fast solution of the two-dimensional Poisson equation with point-wise forcing", *Journal of Computational Physics*, Vol. 83, 1989, pp. 126-147.

2. Lourenco, L.M., Van Dommelen, L.L., Shih, C., and Krothapalli, A., "Unsteady Flow Past an Airfoil at Constant Pitch Rate", Workshop on Physics of Forced Unsteady Separation, NASA-Ames Research Center, April 17-19, 1990.

3. Shih, C., Lourenco, L., Krothapalli, A., & Van Dommelen, L., "Unsteady Flow Past An Airfoil Pitched at Constant Rate" International Symposium on Nonsteady Fluid Dynamics, ASME Meeting, Toronto, Canada 1990.

4. Wang, S. and Van Dommelen, L.L., "Manipulation of leading edge stall of thin wings", 44th Annual Meeting Div. Fluid Dynamics, *Bulletin of the American Physical Society*, Vol. 36, No. 10, 1991.

5. Van Dommelen, L.L. & Cowley, S.J., "On the Lagrangian description of unsteady boundary layer separation. Part 1. General theory", *Journal of Fluid Mechanics*, Vol 210, 1990, 593-

626. Also NASA TM 102026, ICOMP-89-8.

6. Van Dommelen, L.L., "On the Lagrangian description of unsteady boundary layer separation. Part 2. The spinning sphere", *Journal of Fluid Mechanics*, Vol 210, 1990, 627-645. Also NASA TM 102027, ICOMP-89-9.

7. Van Dommelen, L.L., "Generalized tructures for 3-D unsteady separation", 42th Annual Meeting Div. Fluid Dynamics, *Bulletin of the American Physical Society*, Vol. 34, No. 10, 1989.

8. Van Dommelen, L.L., "Lagrangian Methods For Unsteady Separation", AMS-SIAM Summer Seminar, Seattle, WA, June 18-29, 1990.

9. Cowley, S.J., Van Dommelen, L.L. and Lam, S.T. "On the use of Lagrangian variables in unsteady boundary–layer separation", *Phil. Trans. R. Soc. Lond.* A**333**, 1990, 343-378. Also ICASE Report 90-47, 1990.

10. Cowley, S.J., and Van Dommelen, L.L., "Unsteady separation", Workshop on Analytical Methods In Unsteady Separation, Columbus, OH, Jan 25-26, 1990.

11. Van Dommelen, L.L., "Some experiments on a vortex redistribution method", American Mathematical Society regional meeting, Hoboken, NJ, Oct 21-22, 1989.

12. Van Dommelen, L.L. and Lourenco, L.M., "A mesh-free redistribution technique", 44th Annual Meeting Div. Fluid Dynamics, *Bulletin of the American Physical Society*, Vol. 36, No. 10, 1991.

13. C. Shih, L. Lourenco, L. Van Dommelen and A. Krothapalli, "Unsteady flow past an airfoil pitching at a constant rate", *AIAA Journal*, Vol. 30, No. 5, May 1992, 1153-1161.

14. Van Dommelen, L.L., "Manipulation of Separated Flows", presented at the *Symposium and Banquet in Honor of Professor Shan-fu Shen*, May 2, 1992, Cornell University, Ithaca, NY 14853.

15. Van Dommelen, L.L., "Discussion, Quasi-Two-Dimensional Flow Structure, Numerical and Analytical", *AFOSR Workshop on Supermaneuverability: Physics of Unsteady Flows Past Lifting Surfaces at High Angle of Attack*, April 9-10, 1992, Lehigh University, Bethlehem, PA.

16. Moore, F.K. 1958 On the separation of the unsteady laminar boundary layer. In *Boundary-Layer Research*, ed. H.G. Gortler. Springer.

17. Rott, N. 1956 Unsteady viscous flows in the vicinity of a separation point. *Q. Appl. Math.* **13**, 444-451.

18. Sears, W.R. 1956 Some recent developments in airfoil theory. *J. Aeronaut. Sci.* **23**, 490-499.

19. Sears, W.R. & Telionis, D.P. 1975 Boundary-layer separation in unsteady flow. SIAM *J. Appl. Math.* **23**, 215.

20. Sychev, V.V. 1979 Asymptotic theory of non-stationary separation. Izv. Akad. Nauk. SSSR, *Mekh. Zhid. i Gaza*, No. 6, 21-32. Also *Fluid Dynamics* **14**, 829-838.

21. Van Dommelen, L.L. & Shen, S.F. 1982 The genesis of separation. In *Numerical and Physical Aspects of Aerodynamic Flows*, ed. T. Cebeci. Springer-Verlag.

22. Elliott, J.W., Cowley, S.J. & Smith, F.T. 1983 Breakdown of boundary layers:, i. on moving surfaces, ii. in semi-similar unsteady flow, iii. in fully unsteady flow. *Geophys. Astrophys. Fluid Dynamics* **25**, 77-138.

23. Cowley, S.J. 1983 Computer extension and analytic continuation of Blasius' expansion for impulsive flow past a circular cylinder. *J. Fluid Mech.* **135**, 389-405.

24. Ece, M.C., Walker, J.D.A. & Doligalski, T.L. 1984 The boundary layer on an impulsively started rotating and translating cylinder. *Phys. Fluids* **27**, 1077-1089.

25. Henkes, R.A.W.M. & Veldman, A.E.P. 1987 On the breakdown of the steady and unsteady interacting boundary-layer description. *J. Fluid Mech.* **179**, 513-530.

26. Ingham, D.B. 1984 Unsteady separation. *J. Comp. Phys.* **53**, 90-99.

27. Van Dommelen, L.L. & Shen, S.F. 1980a The spontaneous generation of the singularity in a separating laminar boundary layer. *J. Comp. Phys.* **38**, 125-140.

28. Vasantha, R. & Riley, N. 1988 On the initiation of jets in oscillatory viscous flows. *Proc. R. Soc. Lond.* A**419**, 363-378.

29. Puppo, Gabriella 1990 PhD Thesis, Courant Institute, New York.

30. Wu, J.C., 1981 "Theory for Aerodynamic Force and Moment in Viscous Flows," *AIAA J.*, Vol. 19, pp. 432-441.

31. Modi, V. J., Mokhtarian, F., Fernando, M. S. U. K., and Yokomizo, T., "Moving Surface Boundary-Layer Control as Applied to Two-Dimensional Airfoils", *J. Aircraft*, Vol 19, no 2, pp. 104-112

32. Schlichting, H., 1979 *Boundary Layer Theory*, 7th Ed., McGraw-Hill.

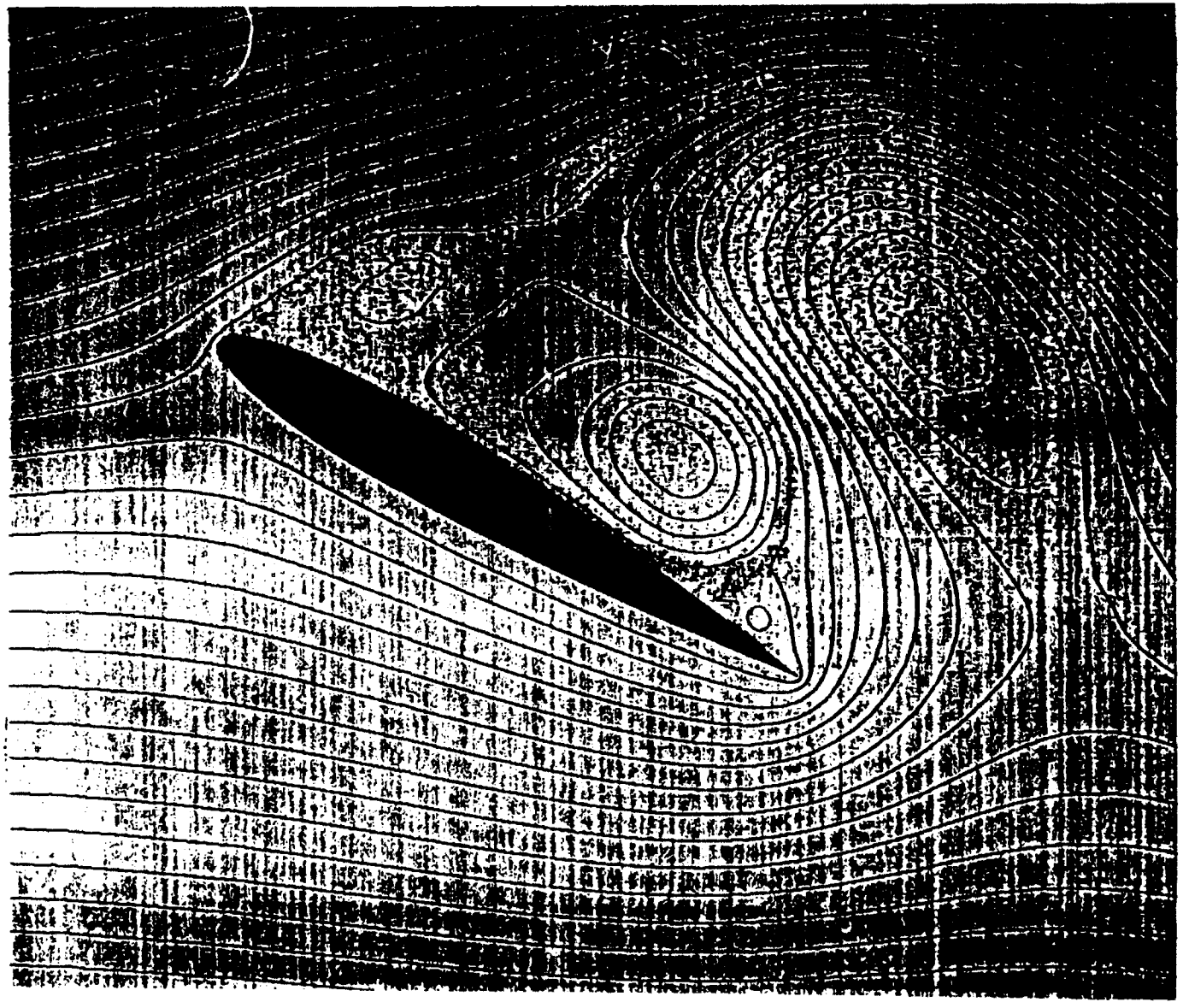

Figure 1 Impulsively started airfoil, Re=5,000, α=30deg., t^{+}=4.0, no control

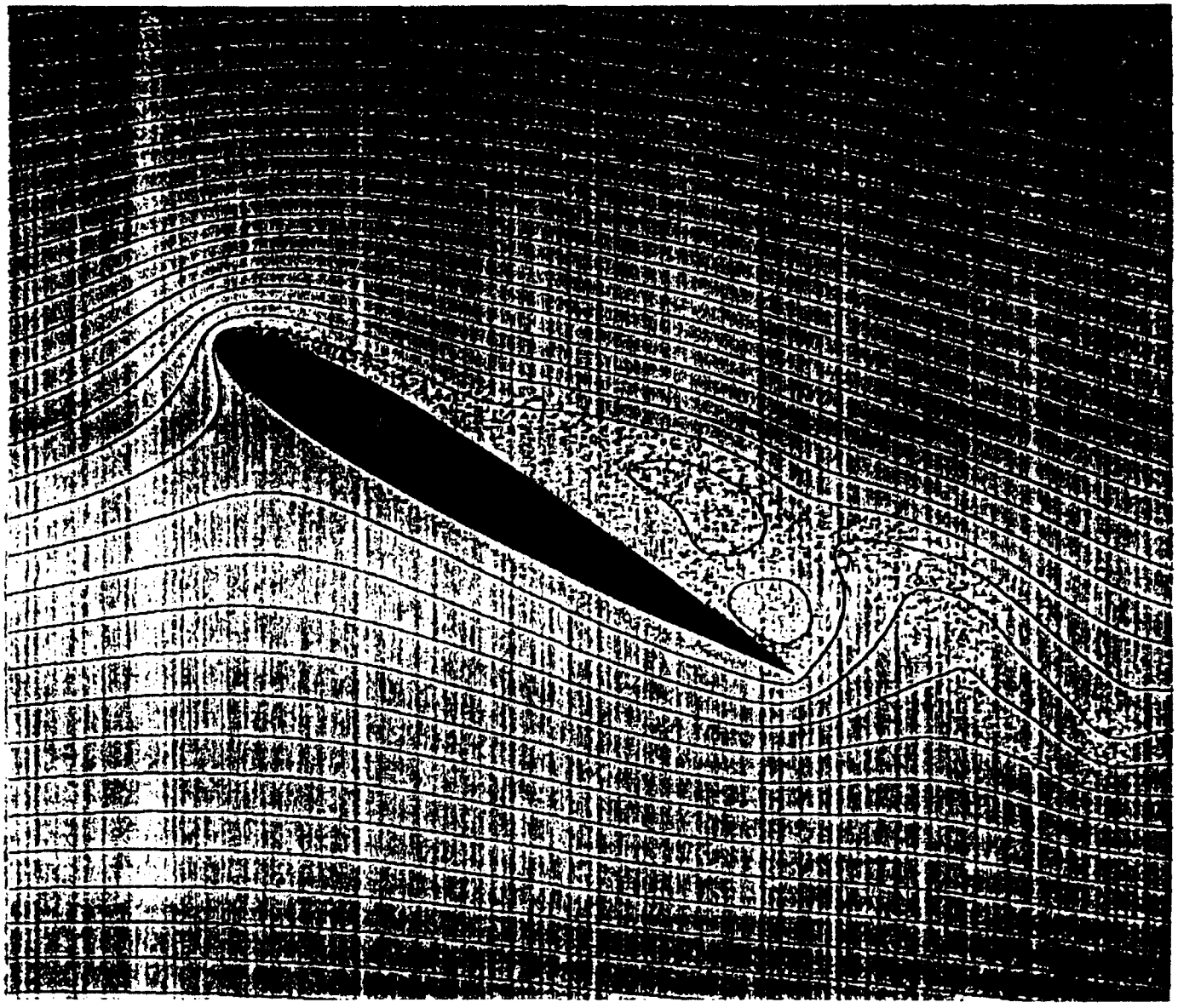

Figure 2 Impulsively started airfoil, Re=5,000, α=30 deg., t^{+}=4.0, light control

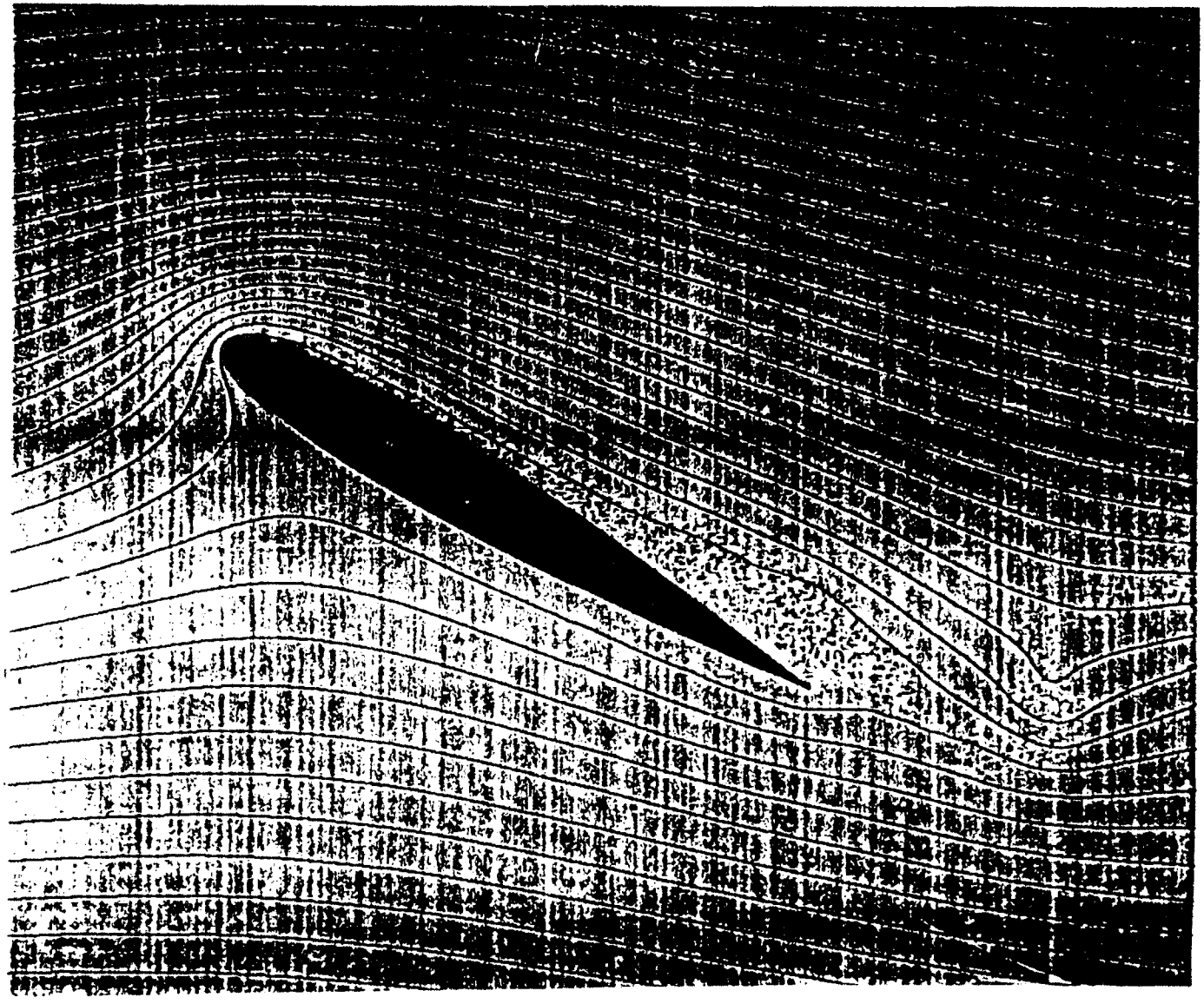

Figure 3 Impulsively started airfoil, Re=5,000, α=30 deg., t^{+}=4.0, strong control